

Advances in reconstructing past atmospheric oxidation chemistry
using the oxygen isotope composition of nitrate and sulfate in ice cores

Shelley A. Kunasek

A dissertation
submitted in partial fulfillment of the
requirements for the degree of

Doctor of Philosophy

University of Washington

2009

Program Authorized to Offer Degree:
Department of Earth and Space Sciences

University of Washington
Graduate School

This is to certify that I have examined this copy of a doctoral dissertation by

Shelley A. Kunasek

and have found that it is complete and satisfactory in all respects,
and that any and all revisions required by the final
examining committee have been made.

Co-Chairs of the Supervisory Committee:

Eric J. Steig

Becky Alexander Suess

Reading Committee:

Eric J. Steig

Becky Alexander Suess

Joel A. Thornton

Date: _____

In presenting this dissertation in partial fulfillment of the requirements for the doctoral degree at the University of Washington, I agree that the Library shall make its copies freely available for inspection. I further agree that extensive copying of the dissertation is allowable only for scholarly purposes, consistent with "fair use" as prescribed in the U.S. Copyright Law. Requests for copying or reproduction of this dissertation may be referred to ProQuest Information and Learning, 300 North Zeeb Road, Ann Arbor, MI 48106-1346, 1-800-521-0600, or to the author.

Signature: _____

Date: _____

University of Washington

Abstract

Advances in reconstructing past atmospheric oxidation chemistry
using the oxygen isotope composition of nitrate and sulfate in ice cores

Shelley A. Kunasek

Chair of the Supervisory Committee:
Professor Eric J. Steig
Department of Earth and Space Sciences

Atmospheric oxidants determine the lifetimes of reduced trace gases that act as greenhouse gases and pollutants. There has thus been great interest in deducing past variability in oxidant concentrations from ice cores. Ice core measurements of $\Delta^{17}\text{O}$ of nitrate and sulfate ($\Delta^{17}\text{O}(\text{NO}_3^-)$ and $\Delta^{17}\text{O}(\text{SO}_4^{2-})$ ($\Delta^{17}\text{O} \approx \delta^{17}\text{O} - 0.52 \times (\delta^{18}\text{O})$) provide a means of reconstructing past changes in the oxidation chemistry of nitrate and sulfate production. This dissertation describes improvements to methods for $\Delta^{17}\text{O}(\text{NO}_3^-)$ and $\Delta^{17}\text{O}(\text{SO}_4^{2-})$ analysis and contributes new snow and ice core records of $\Delta^{17}\text{O}(\text{NO}_3^-)$ and $\Delta^{17}\text{O}(\text{SO}_4^{2-})$ in Greenland and Antarctica, respectively. Measurements of sulfur isotopes of sulfate ($\delta^{34}\text{S}$, $\Delta^{33}\text{S}$, $\Delta^{36}\text{S}$) provide complementary information on sources of atmospheric sulfate.

Methods are presented for automated, simultaneous analysis of $\Delta^{17}\text{O}(\text{NO}_3^-)$ and $\Delta^{17}\text{O}(\text{SO}_4^{2-})$ at micromole levels and for $\Delta^{17}\text{O}(\text{NO}_3^-)$ analysis at submicromole levels. The automation of simultaneous $\Delta^{17}\text{O}(\text{NO}_3^-)$ and $\Delta^{17}\text{O}(\text{SO}_4^{2-})$ analysis will expand

environmental applications of these complementary isotopic measurements. Reduced sample size requirements will improve the temporal resolution of ice core analysis.

We present measurements of seasonal changes in $\Delta^{17}\text{O}(\text{NO}_3^-)$ from a snowpit at Summit, Greenland, and compare them with calculations from an atmospheric chemical box model. The box model underestimates summer $\Delta^{17}\text{O}(\text{NO}_3^-)$, suggesting several important influences on nitrate isotopic composition that are not accounted for in our box model: Non-zero $\Delta^{17}\text{O}$ of OH over polar regions, stratospheric influence on surface O_3 at Summit, participation of BrO in nitrate production, and tropospheric transport of nitrate. A box model sensitivity study shows that annual mean $\Delta^{17}\text{O}(\text{NO}_3^-)$ at Summit is most sensitive to changes in the ratio of $[\text{O}_3]/([\text{HO}_2]+[\text{RO}_2])$ in summer.

Ice core measurements of $\Delta^{17}\text{O}$, $\delta^{34}\text{S}$, $\Delta^{33}\text{S}$, and $\Delta^{36}\text{S}$ of sulfate over the past 230 years from the West Antarctic Ice Sheet (WAIS) Divide are also presented. Sulfur isotope measurements suggest stronger influence of volcanogenic and/or stratospheric sulfate in West relative to East Antarctica. The lack of change in $\Delta^{17}\text{O}$ of non-sea salt sulfate from the mid-1800s to early 2000s ($2.4\text{-}2.6\pm 0.2\text{‰}$) is consistent with atmospheric chemistry model estimates indicating preindustrial to industrial increases in O_3 as high as 50% and decreases in OH of 20% in the southern polar troposphere, as long as H_2O_2 concentrations also increase by over 50%.

TABLE OF CONTENTS

	<u>Page</u>
List of Figures	iii
List of Tables	iv
Chapter 1: Introduction.....	1
1.1 Motivation	1
1.2 Background.....	4
1.2.1 Atmospheric $\Delta^{17}\text{O}$ of Nitrate and Sulfate	4
1.2.2 Analysis of $\Delta^{17}\text{O}$ of Nitrate and Sulfate.....	7
1.3 Dissertation Goals and Synopsis.....	8
Chapter 2: Automated Methods for $\Delta^{17}\text{O}$ Analysis of Nitrate and Sulfate at Micromole and Submicromole Levels	13
2.1 Summary.....	13
2.2 Introduction	14
2.3 Methods.....	17
2.3.1 Silver Salt Preparation System.....	17
2.3.2 Oxygen Isotope Analysis of Silver Salts	19
2.3.2.1 System Configuration.....	19
2.3.2.2 System Operation.....	22
2.3.3 $\Delta^{17}\text{O}$ Calculation and Reference Materials.....	23
2.4 Results and Discussion.....	24
2.4.1 Micromole-Level Sample Analysis (TCEA-IRMS).....	24
2.4.1.1 Precision and Accuracy	24
2.4.1.2 Size Limit	25
2.4.2 Submicromole-Level Sample Analysis (TCEA-GB-IRMS).....	26
2.4.2.1 Blank Correction.....	26
2.4.2.2 Quartz Capsules and Isotopic Exchange Correction....	27
2.4.2.3 Precision and Accuracy	28
2.4.2.4 Size Limit	29
2.4.3 Further Work.....	29
2.5 Conclusions	30
Chapter 3: Measurements and Modeling of $\Delta^{17}\text{O}$ of Nitrate from Snowpits at Summit, Greenland.....	42
3.1 Summary.....	42
3.2 Introduction	43
3.3 Chemistry and Isotopic Composition of Nitrate in Polar Regions	45
3.4 Laboratory Methods.....	49
3.5 Box Model: $\Delta^{17}\text{O}$ of Nitrate.....	51
3.5.1 Boundary Conditions	52
3.5.2 $\Delta^{17}\text{O}$ of Nitrate Calculation.....	53
3.5.3 Model Limitations	55
3.6 Greenland Observations and Box Model Results.....	57

3.7 Measurement-Model Comparison	59
3.7.1 $\Delta^{17}\text{O}$ of Oxidants	59
3.7.2 Stratospheric Influence on Snowpack Nitrate.....	62
3.7.3 Reactive Halogen Chemistry.....	63
3.7.4 Tropospheric Transport of Nitrate.....	65
3.8 Sensitivity of $\Delta^{17}\text{O}$ of Nitrate to Oxidation Chemistry.....	67
3.9 Conclusions	70
Chapter 4: Sulfate Sources and Oxidation Chemistry Over the Past ~230 Years from Sulfur and Oxygen Isotopes of Sulfate in a West Antarctic Ice Core	79
4.1 Summary.....	79
4.2 Introduction	80
4.3 Controls on Isotopic Composition of Atmospheric Sulfate	82
4.4 Methods.....	85
4.5 Ice Core Observations and Model Results	88
4.6 Sulfur Isotopes and Source Partitioning.....	90
4.6.1 $\delta^{34}\text{S}$ and Sulfur Sources	90
4.6.2 $\Delta^{33}\text{S}$ and Stratospheric Sulfur Sources.....	94
4.7 Oxygen Isotopes and Oxidation Chemistry.....	95
4.7.1 Ice Core Variations in $\Delta^{17}\text{O}$ of Sulfate	95
4.7.2 Model Interpretation of Ice Core $\Delta^{17}\text{O}$ of Sulfate (1837-2005)..	96
4.7.2.1 Assumptions in Calculation of $\Delta^{17}\text{O}$ Change	97
4.7.2.2 Calculation of Preindustrial to Industrial Change in Tropospheric $\Delta^{17}\text{O}$ of Sulfate	98
4.7.2.3 Uncertainties in Calculation of $\Delta^{17}\text{O}$ Change.....	102
4.8 Conclusions	103
Chapter 5: Conclusions.....	109
5.1 Summary of Findings and Implications.....	109
5.2 Further Research.....	113
References.....	119
Vita	137

LIST OF FIGURES

	<u>Page</u>
Figure 1.1 Chemistry of nitrate formation.....	11
Figure 1.2 Chemistry of sulfate formation from SO ₂	12
Figure 2.1 Overview of method for Δ ¹⁷ O analysis of nitrate and sulfate	35
Figure 2.2 Flow diagram of silver salt preparation system (IC-CX-FC)	36
Figure 2.3 Flow diagram of system for oxygen isotope analysis of silver salts, including (a) TCEA-IRMS and (b) TCEA-GB-IRMS in an integrated system.....	37
Figure 2.4 Δ ¹⁷ O of nitrate versus amount for USGS-35 nitrate measured using the TCEA-IRMS system.....	38
Figure 2.5 Memory effect test for (a) TCEA-IRMS using 5 μmol O ₂ sample size and (b) TCEA-GB-IRMS using 200 nmol O ₂ sample size.....	39
Figure 2.6 Blank-corrected Δ ¹⁷ O of nitrate measured by TCEA-GB-IRMS in quartz capsules versus accepted values of USGS-35, NIT-A, and an equal parts mixture of both standards	40
Figure 2.7 Fully corrected Δ ¹⁷ O of nitrate versus amount for USGS-35 nitrate measured using the TCEA-GB-IRMS system	41
Figure 3.1 Chemistry of nitrate formation in box model calculations	75
Figure 3.2 Local versus regional oxidation chemistry reflected in Δ ¹⁷ O of nitrate	76
Figure 3.3 (a) 2001 and 2006 snowpit δ ¹⁸ O of water versus depth, and (b) 2001 and 2006 snowpit Δ ¹⁷ O of nitrate versus time	77
Figure 3.4 Sensitivity of Δ ¹⁷ O of nitrate to various oxidation pathways.....	78
Figure 4.1 (a) Literature summary of reported δ ³⁴ S ranges of sulfur sources (b) Summary of measured background δ ³⁴ S _{nss} ranges from Antarctic ice cores	107
Figure 4.2 Timeseries of WAIS Divide ice core measurements	108

LIST OF TABLES

	<u>Page</u>
Table 2.1 Timing of gas bench method.....	33
Table 2.2 $\Delta^{17}\text{O}$ of USGS-35 nitrate analyzed by TCEA-GB-IRMS and corrected for blank and isotopic exchange.....	34
Table 3.1 Box model reactions and rate constants	72
Table 3.2 Calculation of partition ratios in box model	73
Table 3.3 Comparison of box model inputs with reported observations.....	74
Table 4.1 Raw and non-sea salt $\delta^{34}\text{S}$ and $\Delta^{17}\text{O}$ of sulfate from WAIS Divide	106

ACKNOWLEDGEMENTS

My advisors, Eric Steig and Becky Alexander, have provided critical support both professionally and personally. I thank Eric for sharing his contagious enthusiasm for scientific exploration, for entertaining any and all questions and discussion, and for offering me many opportunities for both personal and professional development. I thank Becky for her unwavering confidence in me as a scientist and professional, for her infinite patience with me during difficult times, and for the extraordinary amount of time (both in and out of business hours) that she made herself available to assist me. I also thank my committee members, Joel Thornton, Lyatt Jaegle, and Steve Emerson, for their abundantly helpful comments and support, and my hosts at Laboratoire de Glaciologie et Géophysique de l'Environnement in Grenoble, Joël Savarino, Samuel Morin, and Joseph Erbland, for many insightful conversations during the writing process.

I owe deep thanks to many other colleagues associated with the University of Washington Stable Isotope Lab (Isolab). Meredith Hastings was a great mentor and role model, encouraging and overseeing my first steps in labwork and providing excellent discussions during the writing of my first paper. Andrew Schauer's enthusiasm and expertise in the laboratory exponentially increased my enjoyment of labwork; I cannot thank him enough for making many brainstorming and troubleshooting sessions not only successful but fun. I thank my fellow graduate students Julia Jarvis, Eric Sofen, and Dan Almington for many supportive and insightful conversations. I also owe so many thanks to undergraduate students Dan Gleason, Helen Amos, Peter Neff, and Janet Bautista who were responsible for serious legwork in the freezer and the lab.

Lastly, the completion of this work would not have been possible without the personal support of my friends and family. Thanks to fellow graduate student friends who supported me to the end: Dan Morgan, Jessica Drees Lundin, Kat Huybers, Carrie Lee, Rob Elleman, Kevin Rennert, Justin Wettstein, Kristin Ludwig, Emily Fischer, Aaron Wech, Sanjoy Som, Darci Snowden. To Kelsey McDuffee, Dan VanderElst, Wren McNally and Phil Capp: thanks for the delightful distractions, so many enlightening conversations, and unstoppable laughs. Thanks to Mom, Bob, and Shawn for empowering me with love and support, no matter what I choose. And most of all thanks to Mike, for supporting this work on every level.

Chapter 1

Introduction

1.1 Motivation

Closing the budget of atmospheric species requires quantitative constraints on atmospheric abundance as well as fluxes (sources and sinks). While ice core reconstructions indicate strong correlations between past greenhouse gas abundance (e.g., CO₂, CH₄) and climate [Brook, 2005; Loulergue *et al.*, 2008], the bio- and geochemical mechanisms causing natural variability remain an open area of research. Atmospheric oxidants (e.g., O₃, OH, HO₂) are the primary sink for many reduced trace gases, including methane, the second most important anthropogenic greenhouse gas. The global abundance of OH, the most powerful atmospheric oxidant, is commonly referred to as the “oxidizing capacity” of the atmosphere [Lawrence *et al.*, 2001] as it provides a metric for the efficiency of trace gas removal by oxidation. Tropospheric oxidants such as O₃, H₂O₂, and peroxy radicals (RO₂, where R is a hydrogen atom or hydrocarbon chain) also influence the oxidizing capacity of the atmosphere, both through direct oxidation reactions and through regeneration of OH in the presence of reactive nitrogen oxides (NO_x = NO+NO₂). Constraints on past changes in the atmospheric abundances of these oxidants are necessary for quantitative interpretation of reduced trace gas budgets from ice core concentration records.

Estimates of past changes in the oxidizing capacity of the atmosphere primarily come from atmospheric photochemical models that are constrained by ice core reconstructions of past abundances in CH₄ and CO₂ [i.e., Thompson *et al.*, 1993]. Model results suggest a global increase in the abundance of O₃ as a result of industrialization

(25% to over 60% increase), while estimates of preindustrial-industrial change in OH concentration vary in sign (+6% to -33%) [*Martinerie et al.*, 1995; *Wang and Jacob*, 1998; *Mickley et al.*, 1999; *Lelieveld and Dentener*, 2000; *Grenfell et al.*, 2001; *Hauglustaine and Brasseur*, 2001; *Lelieveld et al.*, 2002; *Shindell et al.*, 2003; *Lamarque et al.*, 2005]. Model reconstructions also suggest a global increase in O₃ abundance from the Last Glacial Maximum (LGM) to preindustrial time (15-30%), while estimates of LGM-preindustrial OH concentration changes vary more widely (-30 to +30%) [*Thompson et al.*, 1993; *Karol et al.*, 1995; *Martinerie et al.*, 1995; *Valdes et al.*, 2005; *Kaplan et al.*, 2006]. Coupling of ice core reconstructions of methane abundance with vegetation modeling [*Chappellaz et al.*, 1993; *Thompson et al.*, 1993; *Kaplan*, 2002] and methane isotope studies [*Fischer et al.*, 2008] provide indirect evidence that global OH abundance was greater in the LGM than in the preindustrial Holocene. While ice core reconstructions of past oxidant concentrations have been sought to provide independent validation of atmospheric photochemical model estimates, early attempts to reconstruct oxidant abundance using H₂O₂ and HCHO [*Sigg & Neftel*, 1991; *Staffelbach et al.*, 1991] were complicated by post-depositional alteration of these species prior to preservation in the ice at depth [*Hutterli et al.*, 2003].

Recently, ice core measurements of the triple oxygen isotope anomaly ($\Delta^{17}\text{O}$) of sulfate and nitrate have shown promise for diagnosing past changes in atmospheric oxidation chemistry [*Alexander et al.*, 2002; *Alexander et al.*, 2004], as the isotopic signatures are largely conserved during snowpack burial [*Alexander et al.*, 2002; *McCabe et al.*, 2005; *Savarino et al.*, 2007]. The $\Delta^{17}\text{O}$ value quantifies the relationship between fractionation in oxygen's two rare isotopes (¹⁷O and ¹⁸O) and is approximated as:

$$\Delta^{17}O = \delta^{17}O - 0.52 \times (\delta^{18}O) \quad (1)$$

where $\delta^xO = ((^xO/^{16}O)_{\text{sample}}/(^xO/^{16}O)_{\text{standard}}) - 1$, with $x = 17$ or 18 and Vienna Standard Mean Ocean Water (V-SMOW) is the standard. (Hereafter, $\Delta^{17}O$ of species X is written as $\Delta^{17}O(X)$). Since different oxidants (e.g., O_3 , OH, HO_2) transfer O-atoms with different $\Delta^{17}O$ to nitrate and sulfate during formation reactions, $\Delta^{17}O(SO_4^{2-})$ and $\Delta^{17}O(NO_3^-)$ reflect the relative importance of different oxidants in their formation [Savarino *et al.*, 2000; Michalski *et al.*, 2003]. Recent ice core $\Delta^{17}O(SO_4^{2-})$ measurements from Vostok, Antarctica have shown that a change in oxidation chemistry occurred during glacial-interglacial climate changes [Alexander *et al.*, 2002]. Measurements of $\Delta^{17}O(NO_3^-)$ and $\Delta^{17}O(SO_4^{2-})$ from central Greenland also indicate a change in oxidation chemistry of the Northern Hemisphere associated with anthropogenic biomass burning changes in the past several centuries [Alexander *et al.*, 2004]. However, quantitative reconstructions of changes in oxidant concentrations from ice core $\Delta^{17}O(NO_3^-)$ and $\Delta^{17}O(SO_4^{2-})$ have not yet been produced. Additionally, labor-intensive laboratory techniques and sample size requirements for $\Delta^{17}O$ analysis of nitrate and sulfate limit both the extent of sampling in the polar environment and the temporal resolution of ice core measurements (i.e., multi-decadal averaging). This dissertation focuses on improving both the measurement and model interpretation of ice core $\Delta^{17}O(NO_3^-)$ and $\Delta^{17}O(SO_4^{2-})$, as well as contributing new records of temporal changes in $\Delta^{17}O(NO_3^-)$ and $\Delta^{17}O(SO_4^{2-})$ in Greenland and Antarctica.

1.2 Background

1.2.1 Atmospheric $\Delta^{17}\text{O}$ of Nitrate and Sulfate

Most physical and chemical processes in the Earth system fractionate oxygen's two rare isotopes (^{17}O and ^{18}O) in a predictable way according to their difference in mass ("mass-dependent fractionation") [Matsuhisa *et al.*, 1978]:

$$\delta^{17}\text{O} \approx 0.52 \times \delta^{18}\text{O} \quad (1)$$

Chemical compounds demonstrating a deviation from mass-dependent isotope ratios are characterized using the $\Delta^{17}\text{O}$ value [Thiemens *et al.*, 1999]. Definitions of the $\Delta^{17}\text{O}$ isotope anomaly vary [e.g., Michalski *et al.*, 2003; Kaiser *et al.*, 2007]. We employ the linear definition here:

$$\Delta^{17}\text{O} = \delta^{17}\text{O} - 0.52 \times (\delta^{18}\text{O}) \quad (2)$$

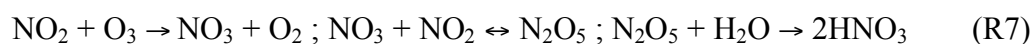
While most terrestrial compounds exhibit $\Delta^{17}\text{O} = 0$, several atmospheric species deviate from mass-dependent isotope ratios (e.g., O_3 , H_2O_2 , NO_3^- , SO_4^{2-}) displaying $\Delta^{17}\text{O} > 0$ [Thiemens *et al.*, 2006]. Atmospheric O_3 , whose formation reaction has been experimentally shown to result in anomalous (non-zero) $\Delta^{17}\text{O}$ [Thiemens and Heidenreich, 1983], is thought to be the origin of non-zero $\Delta^{17}\text{O}$ in other atmospheric compounds [Cliff and Thiemens, 1997; Savarino and Thiemens, 1999; Savarino *et al.*, 2000; Lyons, 2001; Michalski *et al.*, 2003], as the isotope anomaly is transferred from O_3 during oxidation [e.g., Savarino *et al.*, 2000]. Measurements [Schueler *et al.*, 1990; Krankowsky *et al.*, 1995, 2000; Johnston and Thiemens, 1997] and photochemical equilibrium model results [Lyons, 2001] constrain tropospheric $\Delta^{17}\text{O}(\text{O}_3)$ to between 25 - 35‰. Most atmospheric oxidants other than O_3 have been shown to have small $\Delta^{17}\text{O}$ (<2‰). Empirical and modeling studies suggest HO_2 and H_2O_2 have $\Delta^{17}\text{O}$ of 1-2‰

[Savarino and Thiemens, 1999; Lyons, 2001], and $\Delta^{17}\text{O}(\text{OH})$ is thought to be similar to atmospheric water vapor ($\Delta^{17}\text{O}(\text{H}_2\text{O}) = 0\text{‰}$) throughout most of the troposphere due to rapid isotopic exchange [Dubey *et al.*, 1997; Lyons, 2001]. The magnitude of $\Delta^{17}\text{O}(\text{NO}_3^-)$ and $\Delta^{17}\text{O}(\text{SO}_4^{2-})$ is determined by the relative importance of these atmospheric oxidants during nitrate and sulfate formation.

Atmospheric nitrate (HNO_3 +particulate NO_3^-) is predominantly formed through oxidation of NO_x ($=\text{NO}+\text{NO}_2$) (Figure 1.1), which originates from soils, lightning, and combustion. In the presence of sunlight, rapid photochemical cycling occurs between NO and NO_2 :



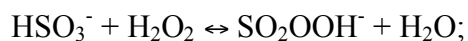
NO_2 is then oxidized to HNO_3 via several possible oxidation pathways:

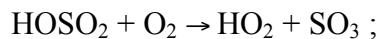
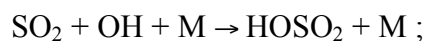


(HC/DMS refers to hydrocarbons and dimethyl sulfide). Other oxidants, including bromine oxides (e.g., BrO), may also play a regionally important role in nitrate formation but are not thought to be significant on a global scale. Most NO_x emitted to the atmosphere achieves isotopic equilibrium with oxidants in NO_x cycling prior to conversion to nitrate [Michalski *et al.*, 2003]. Thus, two of nitrate's three oxygen atoms reflect the transfer of $\Delta^{17}\text{O}$ from oxidants during NO_x cycling (R1-R3), while the third oxygen atom reflects $\Delta^{17}\text{O}$ transferred during the final oxidation of NO_2 to nitrate (R5-R7). The O-atom(s) transferred to oxidation products are assumed to directly reflect the

bulk isotopic composition of the oxidant (e.g., for R2, $\Delta^{17}\text{O}(\text{NO}_2) = \Delta^{17}\text{O}(\text{HO}_2)$) [Alexander *et al.*, 2004; Michalski *et al.*, 2003; Morin *et al.*, 2007; Savarino *et al.*, 2007], with the exception of O_3 . Due to the enrichment of heavy isotopes in the terminal versus central oxygen atom of O_3 (i.e., OOQ versus OQO, respectively, where Q = ^{17}O or ^{18}O) [Janssen, 2005; Bhattacharya *et al.*, 2008] and expected preferential transfer of terminal oxygen atoms from ozone during R1, R6, and R7, an empirical transfer function can be employed to estimate $\Delta^{17}\text{O}$ resulting from these reactions [Savarino *et al.*, 2008]. Tropospheric $\Delta^{17}\text{O}(\text{NO}_3^-)$ measurements largely fall between 22-35‰ [Michalski *et al.*, 2003; Morin *et al.*, 2007; Savarino *et al.*, 2007], reflecting the importance of O_3 in oxidation of NO to NO_2 [Alexander *et al.*, 2009a].

Atmospheric sulfate is formed through oxidation of SO_2 (Figure 1.2), which can be emitted to the atmosphere directly (e.g., fossil fuel combustion, volcanoes, sea salt) or produced through oxidation of biogenic dimethyl sulfide (DMS). Atmospheric SO_2 undergoes rapid isotopic exchange with atmospheric water vapor ($\Delta^{17}\text{O}(\text{H}_2\text{O}) = 0$), erasing any $\Delta^{17}\text{O}$ signature from sources or previous oxidation steps (e.g., DMS oxidation). Thus two of sulfate's four oxygen atoms have an isotopic composition reflecting atmospheric water vapor. The isotopic composition of the additional two oxygen atoms of sulfate depends entirely on the chemistry of SO_2 oxidation to SO_4^{2-} , which is dominated globally by aqueous-phase/in-cloud oxidation of dissolved SO_2 by H_2O_2 and O_3 (R8, R9) and gas-phase oxidation of SO_2 by OH (R10):



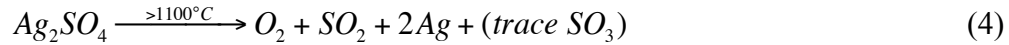
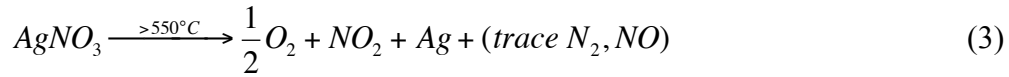


Other SO₂ oxidation pathways that have been shown to be regionally important include oxidation by O₃ on sea salt and dust aerosols and oxidation by O₂ catalyzed by transition metals. Oxidation pathway R9 is highly dependent on partitioning of total dissolved SO₂ as sulfite (i.e., S(IV) ≡ SO₂ • H₂O ↔ HSO₃⁻ ↔ SO₃²⁻) and is limited for pH < 6 [Calvert *et al.*, 1985; Chameides, 1984]. Laboratory studies of Δ¹⁷O transfer during sulfate production suggest transfer of two oxygen atoms from H₂O₂ during R8 and transfer of one oxygen atom from O₃ during R9 [Savarino *et al.*, 2000], resulting in distinctive Δ¹⁷O(SO₄²⁻) for each path under background tropospheric conditions (Δ¹⁷O(H₂O₂) = 1-2‰ and Δ¹⁷O(O₃) = 25-35‰), as shown above. Sulfate produced by SO₂ oxidation by OH (R10) has Δ¹⁷O = 0‰, reflecting the isotopic composition of water vapor and OH. Because O₃ is the only oxidant that imparts a positive Δ¹⁷O(SO₄²⁻) greater than 1‰, an increase in Δ¹⁷O(SO₄²⁻) above 1‰ can be interpreted as an increase in the importance of SO₂ oxidation by O₃ relative to other oxidants in sulfate formation.

1.2.2 Analysis of Δ¹⁷O of Nitrate and Sulfate

Because Δ¹⁷O(NO₃⁻) and Δ¹⁷O(SO₄²⁻) provide complementary information about atmospheric oxidation chemistry [Alexander *et al.*, 2004; Patris *et al.*, 2007], streamlined methods for simultaneous analysis of Δ¹⁷O(NO₃⁻) and Δ¹⁷O(SO₄²⁻) are essential for improving atmospheric and ice core measurement campaigns. Isotopic analysis of the oxygen atoms of both nitrate and sulfate can be achieved following pyrolytic release of

O₂ from salts in silver form (AgNO₃, Ag₂SO₄) [Michalski *et al.*, 2002; Savarino *et al.*, 2001]:



While other approaches exist for the analytical determination of $\Delta^{17}\text{O}(\text{NO}_3^-)$ and $\Delta^{17}\text{O}(\text{SO}_4^{2-})$ [e.g., Kaiser *et al.*, 2007; Bao & Thiemens, 2000], no other approach offers the potential for simultaneous analysis of $\Delta^{17}\text{O}(\text{NO}_3^-)$ and $\Delta^{17}\text{O}(\text{SO}_4^{2-})$. The steps necessary for the determination of $\Delta^{17}\text{O}(\text{NO}_3^-)$ and $\Delta^{17}\text{O}(\text{SO}_4^{2-})$ using the AgNO₃/Ag₂SO₄ pyrolysis approach, include: (1) sample pre-processing to achieve required nitrate and/or sulfate amounts; (2) separation of sample anions using ion chromatography (3) conversion of nitrate and sulfate to silver salts (AgNO₃ and Ag₂SO₄, respectively); (4) drying of silver salts to produce solid AgNO₃ and Ag₂SO₄; (5) pyrolysis of silver salts and trapping of evolved O₂; (6) determination of O₂ isotope ratios (¹⁷O/¹⁶O and ¹⁸O/¹⁶O) using an isotope ratio mass spectrometer. The published methods require sample sizes of >2 μmol nitrate [Michalski *et al.*, 2002; Alexander *et al.*, 2004] and >1 μmol sulfate [Savarino *et al.*, 2001].

1.3 Dissertation Goals and Synopsis

The goals of this dissertation broadly include (1) improving methods for $\Delta^{17}\text{O}(\text{NO}_3^-)$ and $\Delta^{17}\text{O}(\text{SO}_4^{2-})$ analysis, particularly in ice cores, (2) providing new records of atmospheric variability in nitrate and sulfate oxidation chemistry, using ice core $\Delta^{17}\text{O}(\text{NO}_3^-)$ and $\Delta^{17}\text{O}(\text{SO}_4^{2-})$ measurements, and (3) improving the use of ice core

$\Delta^{17}\text{O}(\text{NO}_3^-)$ and $\Delta^{17}\text{O}(\text{SO}_4^{2-})$ measurements for reconstructing atmospheric oxidation pathways using atmospheric chemical modeling approaches.

The first goal is addressed in Chapter 2, where we present automated methods for analysis of $\Delta^{17}\text{O}(\text{NO}_3^-)$ and $\Delta^{17}\text{O}(\text{SO}_4^{2-})$ by silver salt pyrolysis with reduced sample sizes. Separation of aqueous sample anions and conversion to AgNO_3 and Ag_2SO_4 is automated by interfacing an ion chromatograph (IC) with a cation exchange (CX) column and fraction collector (FC). Pyrolysis of AgNO_3 and Ag_2SO_4 , cryofocusing of evolved O_2 , and isotopic analysis of the evolved O_2 are automated using a continuous-flow system including a thermocouple elemental analyzer (TCEA), gas bench (GB), and an isotope ratio mass spectrometer (IRMS). In Chapter 3, we present a new record of seasonal variations in $\Delta^{17}\text{O}(\text{NO}_3^-)$ from snowpits at Summit, Greenland and compare measurements with results of an atmospheric box model. This comparison enables an evaluation of controls on $\Delta^{17}\text{O}(\text{NO}_3^-)$ in the ice core record, which will improve the interpretation of changes in ice core $\Delta^{17}\text{O}(\text{NO}_3^-)$ at Summit on longer timescales (e.g., preindustrial-industrial, glacial-interglacial). In Chapter 4, we present a new record of ice core $\Delta^{17}\text{O}(\text{SO}_4^{2-})$ and sulfur isotopes over the past several centuries from the West Antarctic Ice Sheet (WAIS) Divide. $\Delta^{17}\text{O}(\text{SO}_4^{2-})$ measurements are interpreted using sulfate oxidation path partitioning extracted from previous global chemical transport modeling work, with sulfur isotopes providing complementary constraints on sources of sulfate deposited at WAIS Divide. This work provides critical background for future interpretation of glacial-interglacial ice core $\Delta^{17}\text{O}(\text{SO}_4^{2-})$ measurements. Finally, Chapter 5 presents a summary of advances in ice core $\Delta^{17}\text{O}(\text{NO}_3^-)$ and $\Delta^{17}\text{O}(\text{SO}_4^{2-})$ studies from this dissertation and recommends priorities for future work.

Chapters 2-4 are presented in manuscript form. Chapter 2 is intended for submission to *Rapid Communications in Mass Spectrometry*, Chapter 3 has been published in *Journal of Geophysical Research-Atmospheres*, and Chapter 4 is intended for submission to *Journal of Geophysical Research-Atmospheres*. Because the chapters appear in manuscript form, some introductory information is duplicated. Each chapter also details introductory information uniquely critical for the chapter, such as additional regionally significant nitrate and sulfate oxidation processes, stratospheric influence on $\Delta^{17}\text{O}(\text{NO}_3^-)$ and $\Delta^{17}\text{O}(\text{SO}_4^{2-})$, and controls on atmospheric sulfur isotope signatures (i.e., $\delta^{34}\text{S}$, $\Delta^{33}\text{S}$, $\Delta^{36}\text{S}$), which are omitted from this chapter for clarity and brevity.

Figures

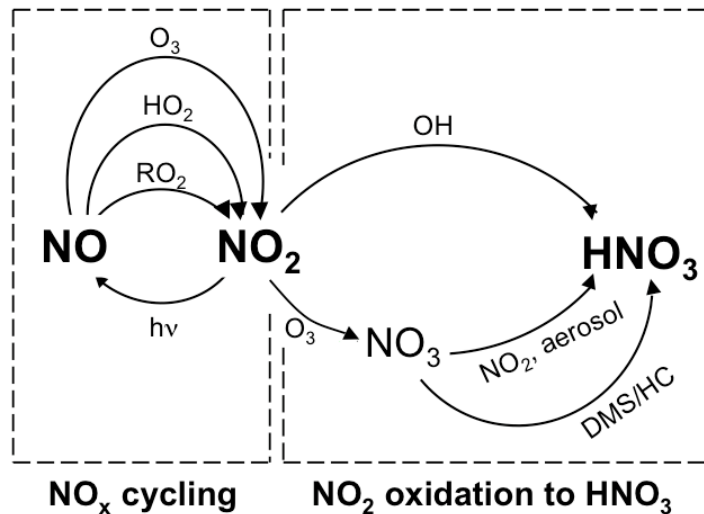


Figure 1.1: Chemistry of nitrate formation. Two oxidation steps include NO_x cycling and NO₂ oxidation to HNO₃. The three oxidation pathways in NO_x cycling are oxidation by O₃, HO₂, and RO₂. The three main oxidation pathways in NO₂ oxidation to HNO₃ are: oxidation via OH; oxidation by O₃ to NO₃, reaction of NO₃ with NO₂, and subsequent hydrolysis of N₂O₅ on water vapor molecules and/or aerosols; and oxidation by O₃ to NO₃, and abstraction of a hydrogen atom from dimethylsulfide or a hydrocarbon.

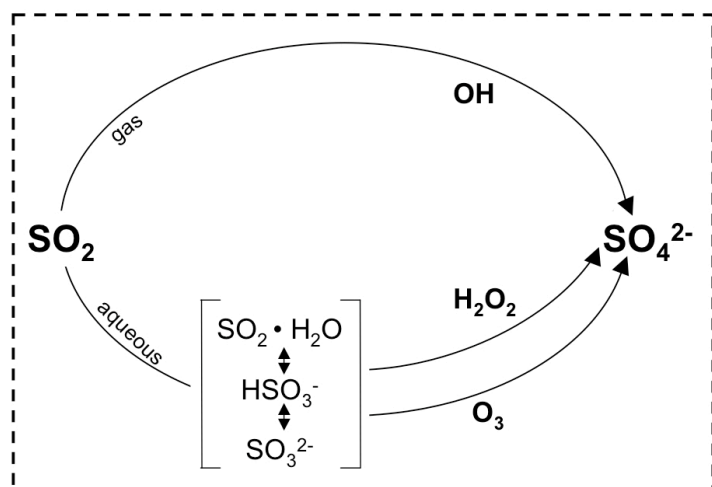


Figure 1.2: Chemistry of sulfate formation from SO_2 . Globally, three oxidation pathways of SO_2 dominate sulfate production: SO_2 is oxidized in the gas-phase by OH and in the aqueous phase by H_2O_2 and O_3 . Aqueous-phase SO_2 oxidation by O_3 is highly dependent on the pH-dependent equilibrium partitioning of total dissolved SO_2 ($\text{SO}_2 \cdot \text{H}_2\text{O}$) as sulfite (SO_3^{2-}).

Chapter 2

Automated methods for analysis of $\Delta^{17}\text{O}$ of nitrate and sulfate at micromole and sub-micromole levels

2.1 Summary

The measurement of the complete oxygen isotope composition ($\Delta^{17}\text{O} \approx \delta^{17}\text{O} - 0.52 \times (\delta^{18}\text{O})$) of nitrate and sulfate in aerosol, rain, and snow samples provides a new means of elucidating the importance of various oxidation pathways in atmospheric nitrate and sulfate formation. We describe the development of automated methods for the analysis of $\Delta^{17}\text{O}$ of nitrate and sulfate at micromole and sub-micromole levels, using pyrolysis of silver salts (AgNO_3 and Ag_2SO_4) in a continuous flow isotope ratio mass spectrometer system. Separation of aqueous sample anions and conversion to AgNO_3 and Ag_2SO_4 is automated using an ion chromatograph (IC) interfaced with a cation exchange (CX) column and fraction collector (FC). Pyrolysis of AgNO_3 and Ag_2SO_4 and isotopic analysis of the evolved O_2 are automated using a thermocouple elemental analyzer (TCEA) coupled with an isotope ratio mass spectrometer (IRMS) with He as the carrier gas. For micromole sample sizes, this method provides precision of $\pm 0.3\%$ for nitrate and $\pm 0.2\%$ (1σ) for sulfate, based on repeated analyses of the international reference standard USGS-35 (NaNO_3 , $\Delta^{17}\text{O} = 21.6\%$) [Böhlke *et al.*, 2003] and inter-lab calibration standards SULF- α and SULF- β (Na_2SO_4 , $\Delta^{17}\text{O} = 0.75\%$, 1.9%). For sub-micromole sample sizes (50 nmol-1 μmol), we further modify the TCEA-IRMS system to include a Gas Bench (GB) that enables cryofocusing of sample O_2 prior to isotopic determination. After correction for a cryofocusing blank and isotopic exchange between the sample and quartz capsules, we find $\Delta^{17}\text{O}(\text{NO}_3^-)$ of USGS-35 for samples ranging

between 50 nmol to 1 μmol O_2 gives 21.6‰, consistent with accepted values; however, due to current blank sizes, sample sizes of ≥ 300 nmol O_2 are necessary to achieve good precision ($\pm 0.6\%$, 1σ). The automated methods for simultaneous analysis of $\Delta^{17}\text{O}$ of nitrate and sulfate and reduction of sample sizes will enable critical improvements in environmental applications.

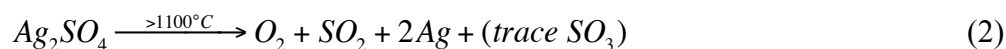
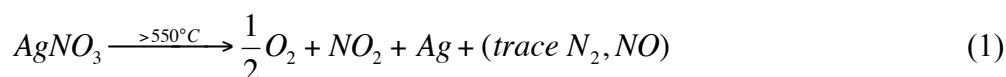
2.2 Introduction

The recent development of techniques to measure the triple isotope composition of oxygen ($\Delta^{17}\text{O} \approx \delta^{17}\text{O} - 0.52 \times (\delta^{18}\text{O})$) in nitrate and sulfate has provided a new tool for investigating atmospheric oxidation chemistry and global geochemical cycling of nitrogen and sulfur [Bao and Thiemens, 2000; Savarino *et al.*, 2001; Michalski *et al.*, 2002; Kaiser *et al.*, 2007]. The magnitude of $\Delta^{17}\text{O}$ in atmospheric nitrate and sulfate (hereafter $\Delta^{17}\text{O}(\text{NO}_3^-)$ and $\Delta^{17}\text{O}(\text{SO}_4^{2-})$) reflects the relative importance of oxidants with distinct $\Delta^{17}\text{O}$ (e.g., O_3 , HO_2 , OH) during nitrate and sulfate formation reactions [Savarino *et al.*, 2000; Michalski *et al.*, 2003]. Measurements of $\Delta^{17}\text{O}(\text{NO}_3^-)$ and $\Delta^{17}\text{O}(\text{SO}_4^{2-})$ in atmospheric and precipitation samples have, thus, been employed to investigate the role of different oxidants during modern atmospheric processes, such as polar O_3 depletion events, as well as during paleoclimate changes, such as glacial-interglacial changes recorded in polar ice cores [e.g., Alexander *et al.*, 2002, 2004, 2005; McCabe *et al.*, 2006, 2007; Morin *et al.*, 2007; Patris *et al.*, 2007; Savarino *et al.*, 2007; Kunasek *et al.*, 2008]. Because $\Delta^{17}\text{O}(\text{NO}_3^-)$ and $\Delta^{17}\text{O}(\text{SO}_4^{2-})$ provide complementary information about atmospheric oxidation chemistry [Alexander *et al.*, 2004; Patris *et al.*, 2007], streamlined methods for simultaneous analysis of $\Delta^{17}\text{O}(\text{NO}_3^-)$ and $\Delta^{17}\text{O}(\text{SO}_4^{2-})$ are essential for

improving environmental measurement campaigns. Reducing sample size requirements to submicromole-levels is also critical for applying $\Delta^{17}\text{O}(\text{NO}_3^-)$ and $\Delta^{17}\text{O}(\text{SO}_4^{2-})$ analysis to environments with low nitrate and sulfate concentrations, such as polar regions.

Several approaches are currently used for the analytical determination of $\Delta^{17}\text{O}(\text{NO}_3^-)$ and $\Delta^{17}\text{O}(\text{SO}_4^{2-})$ [Bao and Thiemens, 2000; Savarino *et al.*, 2001; Michalski *et al.*, 2002; Kaiser *et al.*, 2007]. For $\Delta^{17}\text{O}(\text{NO}_3^-)$ analysis, denitrifying bacteria can be used to convert aqueous nitrate to N_2O gas [Casciotti *et al.*, 2002], which is then quantitatively thermally decomposed to N_2 and O_2 in a gold tube and analyzed for nitrogen and oxygen isotopic composition [Kaiser *et al.*, 2007]. This method enables determination of both the oxygen and nitrogen isotope composition of nitrate with submicromole sample size requirements (minimum 50 nmol nitrate); however, most users must perform duplicate or triplicate analyses due to unreliable bacteria behavior. $\Delta^{17}\text{O}(\text{SO}_4^{2-})$ can be measured by generating O_2 from BaSO_4 (barite) via CO_2 -laser fluorination in a BrF_5 atmosphere [Bao and Thiemens, 2000]. This method requires a costly and hazardous fluorinating agent, is difficult to interface with automated continuous-flow isotopic analysis systems, and requires large sulfate samples (minimum 17 μmol), which is practical only for terrestrial (not atmospheric or ice core) samples. Neither the bacterial denitrification method [Kaiser *et al.*, 2007] nor the barite laser fluorination method [Bao and Thiemens, 2000] have been adapted for simultaneous determination of $\Delta^{17}\text{O}(\text{NO}_3^-)$ and $\Delta^{17}\text{O}(\text{SO}_4^{2-})$. A third approach, employing pyrolytic release of O_2 from salts in silver form (AgNO_3 , Ag_2SO_4) [Savarino *et al.*, 2001; Michalski *et al.*, 2002], is the only current approach amenable to simultaneous determination of $\Delta^{17}\text{O}(\text{NO}_3^-)$ and $\Delta^{17}\text{O}(\text{SO}_4^{2-})$.

Figure 2.1 shows the steps necessary for the determination of $\Delta^{17}\text{O}(\text{NO}_3^-)$ and $\Delta^{17}\text{O}(\text{SO}_4^{2-})$ using the $\text{AgNO}_3/\text{Ag}_2\text{SO}_4$ pyrolysis approach, including: (1) sample pre-processing to achieve required nitrate and/or sulfate amounts; (2) separation of sample anions using ion chromatography (3) conversion of nitrate and sulfate to silver salts (AgNO_3 and Ag_2SO_4 , respectively); (4) drying of silver salts to produce solid AgNO_3 and Ag_2SO_4 ; (5) pyrolysis of silver salts and trapping of evolved NO_2/SO_2 ; (6) determination of evolved O_2 isotope ratios ($^{17}\text{O}/^{16}\text{O}$ and $^{18}\text{O}/^{16}\text{O}$) using an isotope ratio mass spectrometer. Pyrolysis of silver salts (AgNO_3 , Ag_2SO_4) follows the reactions [Michalski *et al.*, 2002; Savarino *et al.*, 2001]:



The deviation of $\delta^{17}\text{O}$ and $\delta^{18}\text{O}$ from mass-dependent relationships ($\delta^{17}\text{O} = 0.52 \times (\delta^{18}\text{O})$) [Matsuhisa *et al.*, 1978] is calculated using the linear relationship $\Delta^{17}\text{O} = \delta^{17}\text{O} - 0.52 \times (\delta^{18}\text{O})$. Because environmental samples contain trace amounts of organic material that react with the O_2 produced in (1) and (2) and reduce O_2 yields, fractionation of $\delta^{17}\text{O}$ and $\delta^{18}\text{O}$ may occur during sample analysis. However, fractionation of oxygen isotopes during sample analysis is expected to follow mass-dependent relationships, resulting in no alteration of $\Delta^{17}\text{O}$. While the silver pyrolysis methods employ only non-hazardous inorganic chemicals (no bacteria or fluorinating agents) and can be used for simultaneous $\Delta^{17}\text{O}(\text{NO}_3^-)$ and $\Delta^{17}\text{O}(\text{SO}_4^{2-})$ analysis, the published techniques are manual and time-consuming and require minimum sample sizes of 1 μmol for sulfate [Savarino *et al.*, 2001] and 2 μmol or more for nitrate [Alexander *et al.*, 2004; Michalski *et al.*, 2003].

We address these limitations by automating techniques for analysis of $\Delta^{17}\text{O}(\text{NO}_3^-)$ and $\Delta^{17}\text{O}(\text{SO}_4^{2-})$ by pyrolysis of AgNO_3 and Ag_2SO_4 and reducing sample size limits. We automate the separation of anions and conversion to silver salts (Figure 2.1, steps 2-3) by interfacing an ion chromatograph (IC) with a cation exchange membrane (CX) and fraction collector (FC) (IC-CX-FC system). We automate the pyrolysis of silver salts and subsequent isotope analysis (Figure 2.1, steps 5-6) with a continuous-flow system interfacing a thermocouple elemental analyzer (TCEA) and an isotope ratio mass spectrometer (IRMS) (TCEA-IRMS system). We also present a modified system that employs a gas bench to cryofocus sample O_2 prior to isotope analysis (TCEA-GB-IRMS), enabling the detection and analysis of submicromole samples.

2.3 Method

2.3.1 Silver Salt Preparation System

Figure 2.2 shows the automated ion chromatography-cation exchange-fraction collection (IC-CX-FC) system used to separate major anions (e.g., Cl^- , NO_3^- , SO_4^{2-}) and convert nitrate and sulfate to AgNO_3 and Ag_2SO_4 . We use a Dionex ion chromatograph (IC) with an IonPac® AG15 column (4 x 50 mm) for anion preconcentration, IonPac® AG19 guard column (4 x 50 mm), IonPac® AS19 separation column (4 x 250 mm), ASRS-Ultra II suppressor (4 mm), and Dionex conductivity detector. The aqueous sample (<50 ml) is first pumped at a rate less than 1 ml/min through the IC six-way valve in “Load” position (see Figure 2.2), retaining and concentrating sample anions on the preconcentration column. The six-way valve is then switched to the “Inject” position (see Figure 2.2) to elute anions from the pre-concentration column and pass them through

the guard and separation columns, the suppressor, and the conductivity detector. Anions elute from the IC suppressor in acid form, with chloride eluting first, followed by nitrate, then sulfate. To optimize peak separation and minimize eluted anion fraction volumes, the starting eluant concentration of 7 mM KOH undergoes a step increase to 10 mM between chloride and nitrate peak elution and to 15 mM between nitrate and sulfate peak elution. The first anions to elute from the IC (e.g., organic compounds and chloride) flow to waste. Detection of the chloride peak end then triggers a pneumatic three-way valve to switch the eluent flow in-line with a Dionex AMMS III (4 mm) cation exchange column (CX) and Teledyne ISCO Foxy Jr. fraction collector (FC). The remaining acidified nitrate (HNO_3) and sulfate (H_2SO_4) fractions are converted to AgNO_3 and Ag_2SO_4 by cation exchange with Ag_2SO_4 regenerant (2.5 mM), which flows continuously through the cation exchange column from a regenerant bottle pressurized with compressed N_2 gas. The fraction collector begins collection of AgNO_3 or Ag_2SO_4 when the IC conductivity detector triggers a peak start ($>100 \mu\text{S}$ conductivity) and ends collection one minute after peak end detection ($<20 \mu\text{S}$ conductivity). This delay accounts for the volume and flow rate between the IC conductivity detector trigger and the fraction collector. Samples containing 1 μmol each of nitrate and sulfate generally yield 5-10 ml for each anion fraction, which is collected in 13 x 100 mm test tubes.

Sample AgNO_3 and Ag_2SO_4 from the IC-CX-FC system are transferred and dried in capsules in successive steps using a miVac Duo centrifuging concentrator at 45°C . For micromole-level samples, AgNO_3 is transferred to Costech 5 x 9 mm silver capsules, while Ag_2SO_4 is transferred to 100 μl custom-made quartz capsules. For submicromole-level samples quartz capsules are used for both AgNO_3 and Ag_2SO_4 . To transfer sample

from test tubes to capsules, the aqueous sample fractions are dried to solid in test tubes, redissolved in a small volume of 18 M Ω water (100 μ l for quartz capsules, 150 μ l for silver capsules), sonicated for 10 minutes, then transferred to capsules and again dried to solid. To maximize yields, roughly 5 ml of 18 M Ω water is added to the empty fraction test tube and these steps are repeated twice for transfer of AgNO₃ or three times for transfer of Ag₂SO₄ (due to the lower solubility of Ag₂SO₄ (0.57 versus 122 g/100 mL H₂O)).

2.3.2 Oxygen Isotope Analysis of Silver Salts

2.3.2.1 System Configuration

The TCEA-IRMS and TCEA-GB-IRMS methods are integrated in a single continuous flow system to allow easy transitions between methods (Figure 2.3a and 2.3b, respectively). We use a Finnigan Thermocouple Elemental Analyzer (TCEA), a Finnegan Conflo III interface or a ThermoFisher Gas Bench II interface with cryofocusing traps (GB), and a Finnigan MAT 253 Isotope Ratio Mass Spectrometer (IRMS) with He as the carrier gas. Prior to introduction into the TCEA, the He carrier gas is scrubbed of any trace O₂ using a large trap (70 cm, 1/4" OD) filled with molecular sieve (5A, 80-100 mesh) that is frozen in liquid nitrogen ("He-Scrub Trap", not shown in Figure 2.3). For both methods, the TCEA autosampler introduces sample capsules into an empty quartz pyrolysis tube heated to 550°C for nitrate or 1100°C for sulfate. The standard quartz pyrolysis tube (18 mm OD x 45 cm) is altered with several pinches that are custom-made to catch sample capsules at the maximum temperature of the furnace (30 cm from top) but also permit carrier gas flow. To minimize gas leaks in the TCEA,

the standard autosampler lid O-ring (5.5 mm cross-section, 165 ID) is replaced with a larger O-ring (6 mm cross-section, 164 ID) and the rubber seal at the base of the pyrolysis tube is replaced with a Teflon ferrule (18 mm). Following the TCEA pyrolysis chamber, we employ a trap (empty 1/8" ID x 100 cm stainless steel tubing) ("Cleanup Trap") maintained at liquid nitrogen temperature to remove pyrolysis byproducts other than O₂ (i.e., NO₂, SO₂). A three-way valve following the Cleanup Trap allows venting of trapped pyrolysis byproducts from the thawed trap at the end of each day. A manual four-way valve following the Cleanup Trap enables the user to choose whether or not samples are cryofocused using the Gas Bench prior to IRMS analysis. The branch of the system not in use may also receive He flow via this four-way valve.

For the TCEA-IRMS method, sample leaving the Cleanup Trap flows directly to a packed 5A molecular sieve gas chromatography column (GC) at 35°C (80-100 mesh, 0.6 m x 1/4" x 4.0 mm, stainless steel) contained within the TCEA housing, then through the open split of a Conflo II interface, and finally into the IRMS for isotopic analysis. The sample oxygen peak is detected 100-150 seconds after sample pyrolysis. Injections of O₂ reference gas (1 bar, 50 sec), plumbed through the Conflo II interface split (not shown in Figure 2.3a), are made twice before and once after sample peak detection. IRMS Faraday cups detect masses (m/z) 32 (¹⁶O₂), 33 (¹⁶O¹⁷O), and 34 (¹⁶O¹⁸O) and employ resistors of 10⁹, 10¹², and 10¹¹ Ω, respectively, to maximize signal.

In the TCEA-GB-IRMS method, sample leaving the Cleanup trap flows to the Gas Bench (Figure 2.3b) that is automated with the timing shown in Table 2.1. In the Gas Bench, the sample O₂ coming from the TCEA is first concentrated by freezing on molecular-sieve in 1/16" OD tubing (stainless steel, ~60 cm) at liquid nitrogen

temperature (“Concentrating Trap”) (Figure 2.3b, valve ports 2 to 6) with the Gas Bench Valco® valve in “Load” position (see Figure 2.3b). In “Load” position, flow through the Concentrating Trap and out the Valco® valve vent (1/16” OD s.s. tubing) (Figure 2.3B, valve port 5) has a rate of ~20 ml/min. After 4.5 minutes, the Valco® valve is switched to “Inject” position (see Figure 2.3b), reversing He flow through the Concentrating Trap and placing it in line with a capillary molecular sieve-filled trap (~60 cm, from Varian capillary GC below) that is lowered into liquid nitrogen (“Cryofocusing Trap”) (Figure 2.3b, port 3). In “Inject” position, He loss through the Valco® valve vent is reduced to 7 ml/min due to backpressure from capillary tubing between Valco® valve ports 4 and 8. When the Cryofocusing Trap is frozen (30 seconds), the Concentrating Trap is thawed and the released O₂ is transferred to the Cryofocusing Trap where it freezes again. After 5 minutes, the Cryofocusing trap is thawed and the released O₂ continues to a capillary GC at 35°C (Varian 5A molecular sieve-coated silica, 30 m x 0.32 mm ID) housed in the Gas Bench, then through the Gas Bench open split, and to the IRMS for isotopic analysis. For samples greater than 200 nmol O₂, the quantity of sample entering the IRMS source is reduced by a factor of 10 using the Gas Bench open split to avoid saturating IRMS detectors. The sample oxygen peak is detected roughly 800 seconds after sample pyrolysis. Injections of O₂ reference gas (1 bar, 50 sec), plumbed through the Gas Bench interface (not shown in Figure 2.3b), are made before sample peak detection (see Table 2.1). The IRMS focus and detectors are configured identically for both methods (TCEA-IRMS and TCEA-GB-IRMS). However, the IRMS inlet employs a separate needle valve for each method, so the sample flow of the method in use is isolated from backgrounds of the second method.

2.3.2.2 System Operation

The linearity of the IRMS tune is tested and refined regularly, such that $\Delta^{17}\text{O}$ of the O_2 reference gas is constant ($\pm 0.15\%$) for varying peak areas down to 15 Vs. Prior to sample analysis using either the TCEA-IRMS or TCEA-GB-IRMS system, the GC and (if applicable) Concentrating and Cryofocusing Traps are baked out at 180°C , such that background levels of H_2O are less than 1 mV (TCEA-IRMS) or 2 mV (TCEA-GB-IRMS), as measured on cup 1 ($10^9 \Omega$ resistor). (Differing background levels of the two methods are due to differences between the Conflo and Gas Bench interfaces.) We also precondition the IRMS source by exposure to O_2 reference gas overnight prior to sample analysis. During sample analysis, a memory effect is observed, likely due to non-laminar flow in the TCEA pyrolysis tube that results in tailing of the evolved O_2 gas peak. We reduce memory effects by allowing a total of 24 minutes to elapse between pyrolysis of samples. During the delay between sample analyses (14 min for TCEA-IRMS, 7 min for TCEA-GB-IRMS), O_2 reference gas injections are performed to maintain source conditioning. For the TCEA-GB-IRMS system, the Gas Bench Valco® valve is maintained in the “Load” position between sample analyses to eliminate the influence of a small memory effect associated with valve changes. The He-Scrub Trap and Cleanup Trap are frozen in liquid nitrogen for the duration of sample analyses, and liquid nitrogen levels for the Concentrating and Cryofocusing Traps are maintained at a constant level when the Gas Bench is in use. At the end of a day of sample analyses, the two-way valve following the Cleanup Trap (see Figure 2.3) is opened and the He-Scrub and Cleanup traps are thawed to vent trapped gases (i.e., NO_2 , SO_2) so they do not flow through the

GC and IRMS. Also, when the TCEA-GB-IRMS system is not in use, the Valco® valve is left in the “Inject” position to minimize He losses via the Valco® valve vent (flow rate 7 ml/min). The pyrolysis tube is removed and emptied after every 50 samples in silver capsules or 12 samples in quartz capsules, such that new samples introduced into the tube always fall within the hot zone of the TCEA furnace.

2.3.3 $\Delta^{17}\text{O}$ Calculation & Reference Materials

Raw isotope ratios from the IRMS ($^{17}\text{O}/^{16}\text{O}$ and $^{18}\text{O}/^{16}\text{O}$) are converted to delta-notation ($\delta^x\text{O} = ((^x\text{O}/^{16}\text{O})_{\text{sample}} / (^x\text{O}/^{16}\text{O})_{\text{standard}}) - 1$, where $x = 17$ or 18), from which raw $\Delta^{17}\text{O}$ is calculated via $\Delta^{17}\text{O} = \delta^{17}\text{O} - 0.52 \times (\delta^{18}\text{O})$. The standard used in calculation of $\delta^{17}\text{O}$ and $\delta^{18}\text{O}$ is an ultra-pure O_2 reference gas whose isotopic composition on the VSMOW scale ($\delta^{17}\text{O} = 13.441\text{‰}$, $\delta^{18}\text{O} = 26.295\text{‰}$ vs. VSMOW) was predetermined by inter-laboratory comparison with the Stable Isotope Laboratory at University of California, San Diego (UCSD).

Several nitrate international reference materials are used to validate the methods presented including two international reference materials, USGS-35 (NaNO_3 , $\delta^{18}\text{O} = 57.5\text{‰}$, $\delta^{17}\text{O} = 51.5\text{‰}$, $\Delta^{17}\text{O} = 21.6\text{‰}$) and IAEA-N3 (KNO_3 , $\delta^{18}\text{O} = 25.6\text{‰}$, $\delta^{17}\text{O} = 13.2\text{‰}$, $\Delta^{17}\text{O} = 0\text{‰}$) [Böhlke *et al.*, 2003], and two off-the-shelf working standards, NIT-A (AgNO_3 , Fisher Scientific, $\Delta^{17}\text{O} = 0\text{‰}$) and NIT-B (NaNO_3 , Fisher Scientific, $\Delta^{17}\text{O} = 0\text{‰}$). Because USGS-35 is the only nitrate reference material with non-zero $\Delta^{17}\text{O}$, we primarily employ measurements of USGS-35 and a mix of NIT-A:USGS-35 to validate our methods. Net yields are determined by comparison of IRMS peak areas of

potassium- and sodium-form standards (USGS-35, IAEA-N3, NIT-B) with the nitrate working standard in silver form (NIT-A) that does not undergo IC-CX-FC preparation.

For sulfate, an international reference material with non-zero $\Delta^{17}\text{O}$ is not available. We thus validate our methods through inter-laboratory comparison of several sulfate standards prepared at the University of Washington. The sulfate standards were prepared by dissolving off-the-shelf NaSO_3 in ^{17}O -enriched water (Cambridge Isotope Laboratories), allowing oxygen isotope exchange to occur overnight, then oxidizing SO_3^{2-} to SO_4^{2-} by addition of excess H_2O_2 . Two different dilutions of ^{17}O -enriched water were employed to produce standards with different $\Delta^{17}\text{O}(\text{SO}_4^{2-})$. The two sulfate standards produced (SULF- α and SULF- β) were measured at UCSD and Louisiana State University (LSU) following published methods [*Bao and Thiemens, 2000; Savarino et al., 2001*]. In addition to these sulfate standards of non-zero $\Delta^{17}\text{O}$, we employ a sulfate working standard in silver form (SULF-A)($\text{Ag}_2\text{SO}_4^{2-}$, EM Science, $\Delta^{17}\text{O} = 0\text{‰}$) to determine method yields.

2.4 Results and Discussion

2.4.1 Micromole-Level Sample Analysis (TCEA-IRMS)

2.4.1.1 Precision & Accuracy

We report sample sizes for nitrate and sulfate as $\mu\text{mol O}_2$ due to the differing pyrolysis chemistry of AgNO_3 and Ag_2SO_4 (e.g., 2 μmol nitrate gives 1 $\mu\text{mol O}_2$, while 1 μmol sulfate gives 1 $\mu\text{mol O}_2$)(see equations 1-2). Yields of AgNO_3 and Ag_2SO_4 from reference standards processed by IC-CX-FC are greater than 90%. For nitrate samples producing greater than 1 $\mu\text{mol O}_2$ (e.g., $> 2 \mu\text{mol NO}_3^-$), repeated measurements of

USGS-35 by TCEA-IRMS produce $\Delta^{17}\text{O}(\text{NO}_3^-) = 21.6 \pm 0.3\text{‰}(1\sigma)(n = 52)$ (see Figure 2.4), which agrees directly with the internationally accepted $\Delta^{17}\text{O}$ value ($21.6 \pm 0.1\text{‰}$) [Michalski *et al.*, 2002; Böhlke *et al.*, 2003] and requires no isotopic correction. When a delay is used between sample analyses (see Section 2.3.2.2), we observe no systematic memory effect for $\Delta^{17}\text{O}(\text{NO}_3^-)$ analysis of samples of between 2-5 $\mu\text{mol O}_2$, as indicated by repeated switching between analysis of high (= 21.6‰: USGS-35) and low (= 0‰: NIT-B, IAEA-N3) $\Delta^{17}\text{O}(\text{NO}_3^-)$ (see Figure 2.5a; not all results shown). For micromole-level sulfate samples, measurements of SULF- α and SULF- β by TCEA-IRMS give $\Delta^{17}\text{O}(\text{SO}_4^{2-})$ of $0.9 \pm 0.1(1\sigma)(n = 6)$ and $1.7 \pm 0.2(1\sigma)(n = 4)$, respectively.

Measurements at UCSD and LSU University using published methods [Bao and Thiemens, 2000; Savarino *et al.*, 2001] give $\Delta^{17}\text{O}(\text{SO}_4^{2-})$ of $0.76 \pm 0.05(1\sigma)(n = 3)$ and $0.76 \pm 0.05(1\sigma)(n = 2)$ for SULF- α and $1.83 \pm 0.05(1\sigma)(n = 3)$ and $2.01 \pm 0.01(1\sigma)(n = 2)$ for SULF- β . Memory effects in consecutive $\Delta^{17}\text{O}(\text{SO}_4^{2-})$ analyses are expected to be negligible as for $\Delta^{17}\text{O}(\text{NO}_3^-)$ analysis, since system flow rates are identical for analysis of both species. The good agreement of TCEA-IRMS measurements of $\Delta^{17}\text{O}(\text{NO}_3^-)$ and $\Delta^{17}\text{O}(\text{SO}_4^{2-})$ at micromole-levels with results from previously published methods validates the use of the automated IC-CX-FC and TCEA-IRMS systems for micromole-level analysis of $\Delta^{17}\text{O}(\text{NO}_3^-)$ and $\Delta^{17}\text{O}(\text{SO}_4^{2-})$ without the need for any isotopic corrections.

2.4.1.2 Size Limit

Previously published methods for analysis of $\Delta^{17}\text{O}(\text{NO}_3^-)$ by pyrolysis of AgNO_3 found a blank occurring for samples $< 5 \mu\text{mol O}_2$ [Michalski *et al.*, 2002], whereas we

find no deviation of $\Delta^{17}\text{O}(\text{NO}_3^-)$ from accepted values for samples as small as $1\ \mu\text{mol O}_2$. *Michalski et al.* [2002] converted reference standards (e.g., USGS-35) to silver form by neutralization of HNO_3 with Ag_2O , which may have resulted in trace Ag_2O contamination and caused the observed blank. By contrast, our reference standards are converted to silver form via cation-exchange (IC-CX-FC system), which likely reduces silver oxide contamination and explains the lower size limit we report for the TCEA-IRMS system ($1\ \mu\text{mol O}_2$). We suggest the minimum sample size of $1\ \mu\text{mol O}_2$ for the TCEA-IRMS system is due largely to the design of the Conflo III interface, which must restrict the amount of sample from the TCEA that enters the IRMS due to the different flow rates of the two components ($\sim 80\ \text{ml/min}$ and $\sim 0.3\ \text{ml/min}$, respectively). Samples of less than $1\ \mu\text{mol O}_2$ produce small peak areas ($< 20\ \text{Vs}$) on the TCEA-IRMS system, and thus are outside the range for which IRMS $\Delta^{17}\text{O}$ analysis is constant with respect to sample size.

2.4.2 Submicromole-Level Sample Analysis (TCEA-GB-IRMS)

2.4.2.1 Blank Correction

When the TCEA-GB-IRMS method is used for measurement of submicromole sample sizes, raw $\Delta^{17}\text{O}$ values must be corrected for the influence of an O_2 blank from cyrofocusing. Although the He carrier gas stream is scrubbed of O_2 by the He-scrubbing trap prior to entering the TCEA autosampler and pyrolysis chamber, minor imperfections in the TCEA autosampler and pyrolysis tube seals downstream of the He-scrubbing trap result in a small leak of O_2 into the He stream. While insignificant under continuous-flow conditions of the TCEA-IRMS system, this trace O_2 in the He stream is

concentrated along with sample O₂ during cryofocusing by the gas bench, resulting in a blank. The raw $\Delta^{17}\text{O}$ is corrected for the cryofocusing blank following:

$$\Delta^{17}\text{O}_{\text{blk_corr}} = \frac{\Delta^{17}\text{O}_{\text{raw}} - (f_{\text{blk}} \times \Delta^{17}\text{O}_{\text{blk}})}{f_{\text{sample}}} \quad (3)$$

where $\Delta^{17}\text{O}_{\text{blk}}$ is assumed to be 0‰, and f_{sample} and f_{blk} indicate the relative fractions of sample and blank in the measured O₂, as determined by a comparison of sample peak area with peak areas of blanks analyzed before and after the sample. By improving the seals on the TCEA autosampler lid and pyrolysis tube bottom (see Section 2.3.2), we reduced the blank size that to less than 20% of the total O₂ analyzed for samples of greater than 200 nmol O₂, resulting in a maximum 3.9‰ correction of $\Delta^{17}\text{O}(\text{NO}_3^-)$ in our USGS-35 analyses (see Table 2.2).

2.4.2.2 Quartz Capsules & Isotopic Exchange Correction

We use quartz rather than silver capsules for submicromole $\Delta^{17}\text{O}(\text{NO}_3^-)$ analysis by TCEA-GB-IRMS because empty silver capsules introduced into the pyrolysis tube were found to react with up to 15 nmol O₂, as deduced from a reduction in the cryofocusing blank size. While this reaction would have negligible influence on micromole-level samples analyzed by TCEA-IRMS (i.e., size reductions of maximum 1.5%), the reaction has stronger influence on smaller samples (i.e., size reduction of 30% for 50 nmol samples) and makes it difficult to correct for the cryofocusing O₂ blank due to greater size variability. No reduction in O₂ yield was observed for quartz capsules. However, as suggested by related work [Revesz & Böhlke, 2002], we find significant oxygen isotope exchange between sample and quartz capsules during AgNO₃ pyrolysis. This leads to micromole-level samples (>1 μmol O₂) of USGS-35 analyzed in quartz

capsules by TCEA-IRMS giving $\Delta^{17}\text{O}(\text{NO}_3^-)$ over 3‰ lower (18.5‰) than when silver capsules are used (21.6‰). Submicromole-level samples of USGS-35 (200 nmol to 1 μmol) analyzed in quartz capsules by the TCEA-GB-IRMS method and corrected for the cryofocusing O_2 blank indicate isotopic exchange consistent with the measurements made by TCEA-IRMS (mean $\Delta^{17}\text{O} = 18.2\text{‰}$)(see Table 2.2). Thus, for analysis of $\Delta^{17}\text{O}(\text{NO}_3^-)$ using the TCEA-GB-IRMS method, the blank-corrected $\Delta^{17}\text{O}$ value ($\Delta^{17}\text{O}_{\text{corr1}}$) must also be corrected for isotopic exchange between AgNO_3 and quartz capsules during pyrolysis. Based on analyses of USGS-35, NIT-A, and a mixture of equal parts USGS-35:NIT-A in quartz capsules (see Figure 2.6), we use an empirical relationship to correct for isotopic exchange with quartz capsules:

$$\Delta^{17}\text{O}_{\text{chg_corr}} = 1.1675(\Delta^{17}\text{O}_{\text{blk_corr}}) + 0.8175 \quad (R^2 = 0.990) \quad (4)$$

No isotopic exchange correction is necessary for micromole-level $\Delta^{17}\text{O}(\text{NO}_3^-)$ analysis by TCEA-IRMS when silver capsules are used. Also, analysis of micromole-level sulfate inter-laboratory calibration standards by silver pyrolysis in quartz capsules [Savarino *et al.*, 2001; this work] produces $\Delta^{17}\text{O}(\text{SO}_4^{2-})$ within error of results from barite laser fluorination methods [Bao & Thiemens, 2001] (see Section 2.4.2.1) with no isotopic exchange correction. This suggests that isotopic exchange occurs during AgNO_3 decomposition, and not between evolved O_2 and quartz.

2.4.2.3 Precision & Accuracy

When corrected for both cryofocusing blank and isotopic exchange with quartz (see Table 2.2), we find $\Delta^{17}\text{O}(\text{NO}_3^-)$ of USGS-35 for samples of 50 nmol – 1 μmol O_2 has a mean of 21.6‰ (Figure 2.7), consistent with the accepted value. Precision is best for

samples greater than 300 nmol O₂ ($\pm 0.6\%$, 1σ). No systematic memory effect is observed for $\Delta^{17}\text{O}(\text{NO}_3^-)$ analysis of samples of 200 nmol O₂ by TCEA-GB-IRMS (Figure 2.5b), when a delay is used between sample analyses (see Section 2.3.2.2). Even when switching between analyses of the lowest (= 0‰: NIT-A) and the highest (= 21.6‰: USGS-35) $\Delta^{17}\text{O}(\text{NO}_3^-)$ or vice versa, the first sample of a series of identical composition is not significantly different from the others.

2.4.2.4 *Size Limit*

The reduced sample size limit of the TCEA-GB-IRMS system relative to the TCEA-IRMS system results from the lower flow rate of gas leaving the Gas Bench relative to the Conflo interface (see Section 2.3.2.1). This allows a greater fraction of sample to enter the IRMS when the Gas Bench is used, resulting in peak sizes for samples as small as 50 nmol O₂ that are within the range for which IRMS $\Delta^{17}\text{O}$ analysis is constant with respect to sample size (i.e., > 20 Vs). Cryofocusing of sample O₂ by the Gas Bench is also critical, as it ensures that sample O₂ flowing from the large volume of the TCEA pyrolysis chamber (i.e., 18 mm O.D.) is quantitatively transferred as a small volume “plug” into the capillary tubing that interfaces with the IRMS. This step sharpens the sample peak detected by the IRMS (~150 seconds width), which would otherwise be too broad for analysis.

2.4.3 *Further Work*

Refinements to the TCEA-GB-IRMS system may improve the precision and accuracy of $\Delta^{17}\text{O}(\text{NO}_3^-)$ analysis of submicromole samples and further reduce sample

size limits (i.e., <300 nmol O₂). Gas-tight seals on the TCEA will likely be further improved (see Section 2.3.2) by optimization during ongoing use. Improving TCEA seals will further reduce the cryofocusing blank, improving precision and accuracy of $\Delta^{17}\text{O}(\text{NO}_3^-)$ analysis by TCEA-GB-IRMS for smaller samples (i.e., 50-100 nmol O₂). The TCEA-GB-IRMS method will also be tested for application to $\Delta^{17}\text{O}(\text{SO}_4^{2-})$ analysis. Because of the similarities in AgNO₃ and Ag₂SO₄ pyrolysis and the success of the TCEA-IRMS method for micromole-level $\Delta^{17}\text{O}(\text{SO}_4^{2-})$ analysis, we expect that submicromole-level analysis of $\Delta^{17}\text{O}(\text{SO}_4^{2-})$ using the TCEA-GB-IRMS method will also be successful. We plan to test $\Delta^{17}\text{O}(\text{SO}_4^{2-})$ analysis by TCEA-GB-IRMS over a range of submicromole sample sizes (50-1000 nmol O₂), quantify any possible isotopic exchange with quartz capsules, and test whether any memory effects occur. We also plan to test the TCEA-IRMS system for memory effects in consecutive analyses of $\Delta^{17}\text{O}(\text{SO}_4^{2-})$, although we expect they will be negligible as in $\Delta^{17}\text{O}(\text{NO}_3^-)$ analysis.

2.5 Conclusion

We present automated methods for the analysis of $\Delta^{17}\text{O}(\text{NO}_3^-)$ and $\Delta^{17}\text{O}(\text{SO}_4^{2-})$ by pyrolysis of silver salts (AgNO₃ or Ag₂SO₄) for micromole- and submicromole-level sample sizes. We use an automated IC-CX-FC system for preparation of AgNO₃ and Ag₂SO₄, and obtain yields greater than 90%. We describe modifications to a continuous flow TCEA-IRMS system to enable automation of the pyrolysis of silver salts and subsequent oxygen isotope analysis. The standard TCEA-IRMS set-up is modified for the analysis of $\Delta^{17}\text{O}(\text{NO}_3^-)$ and $\Delta^{17}\text{O}(\text{SO}_4^{2-})$ by including a custom quartz pyrolysis tube, to catch samples within the hot zone of the furnace without introducing a reactive

packing, and a liquid nitrogen trap between the TCEA pyrolysis tube and the IRMS, to trap pyrolysis byproducts (e.g., NO₂, SO₂) other than the O₂ desired for isotopic analysis. Our measurements of $\Delta^{17}\text{O}(\text{NO}_3^-)$ of the international standard USGS-35 using the TCEA-IRMS method agree with accepted values [Böhlke *et al.*, 2003] for sample sizes as little as 1 μmol O₂ (2 μmol NO₃⁻) and have a precision of $\pm 0.3\text{‰}$ (1 σ). Our $\Delta^{17}\text{O}(\text{SO}_4^{2-})$ measurements by TCEA-IRMS of two new inter-laboratory calibration standards, SULF- α and SULF- β , agree well with those made using other published methods [Bao & Thiemens, 2000; Savarino *et al.*, 2001] for sample sizes as little as 1 μmol O₂ (1 μmol SO₄²⁻) and have a precision of $\pm 0.2\text{‰}$ (1 σ).

For submicromole-level sample analysis, we include a further modification of the TCEA-IRMS system, employing a Gas Bench to cryofocus sample O₂ on molecular sieve prior to isotopic analysis (TCEA-GB-IRMS system). Due to the gas bench interface with the IRMS, over an order of magnitude more sample gas reaches the IRMS in the TCEA-GB-IRMS versus the TCEA-IRMS system. Thus, while submicromole-level samples analyzed with the TCEA-IRMS method fall outside the range for which IRMS $\Delta^{17}\text{O}$ analysis is constant with respect to sample size, the peak area of submicromole-level samples analyzed with the TCEA-GB-IRMS method are well within IRMS instrumental limits. Submicromole-level samples analyzed using the TCEA-GB-IRMS system must be corrected for a blank due to cryofocusing of trace O₂ in the He carrier gas stream. An additional correction is applied for submicromole analysis of $\Delta^{17}\text{O}(\text{NO}_3^-)$ due to oxygen isotope exchange between sample and quartz capsules during pyrolysis. When corrected for cryofocusing blank and isotopic exchange with quartz, we find $\Delta^{17}\text{O}(\text{NO}_3^-)$ of USGS-35 of 21.6‰ for samples ranging between 50 nmol to 1 μmol O₂; however, analytical

precision is best ($\pm 0.6\%$, 1σ) for samples producing ≥ 300 nmol O_3 . We find no significant memory effects for either the TCEA-IRMS or TCEA-GB-IRMS systems, when delaying the time between consecutive analyses by 24 minutes.

The TCEA-IRMS and TCEA-GB-IRMS methods offer several critical benefits to the atmospheric and ice core $\Delta^{17}O(NO_3^-)$ and $\Delta^{17}O(SO_4^{2-})$ research communities, including: (1) fully automated sample preparation and oxygen isotope analysis; (2) simultaneous analysis of $\Delta^{17}O(NO_3^-)$ and $\Delta^{17}O(SO_4^{2-})$, which provide complementary information about atmospheric oxidation chemistry; (3) the capacity to measure a wide range of sample sizes (i.e., 300 nmol to $1\mu\text{mol } O_2$ for TCEA-GB-IRMS; 1-5 $\mu\text{mol } O_2$ for TCEA-IRMS); (4) elimination of the need to work with hazardous chemicals, such as fluorinating agents, or bacteria, which can behave inconsistently; (5) sample size limits for $\Delta^{17}O(NO_3^-)$ analysis by TCEA-GB-IRMS (300 nmol NO_3^-) comparable with the lowest limits suggested for the bacterial denitrification methods described by *Kaiser et al.* [2007] (50 nmol NO_3^-), given that most users of the latter depend on duplicate or triplicate measurements in light of inconsistent bacterial behavior. The automation of methods and reduction of sample sizes for simultaneous analysis of $\Delta^{17}O(NO_3^-)$ and $\Delta^{17}O(SO_4^{2-})$ will greatly expand their use in investigating environments with low nitrate and sulfate concentrations.

Tables

Table 2.1: Timing of Gas Bench Method

Time (seconds)	TCEA Autosampler	Valco® Valve	Concentrating Trap	Cryofocusing Trap	O ₂ Reference Gas
Pre-Run	Off	Load	Up	Up	On
0	-	-	Down	-	Off
10	On	-	-	-	-
12	Off	-	-	-	-
270	-	Inject	-	Down	On
300	-	-	Up	-	Off
570	-	-	-	Up	-
870	-	Load	-	-	-
1000	Sample Method End				

Table 2.2: $\Delta^{17}\text{O}$ of USGS-35 Nitrate Analyzed by TCEA-GB-IRMS and Corrected for the Cryofocusing Blank (“blk_corr”) and Isotopic Exchange with Quartz (“xchg_corr”)

Size	Peak Area	Peak-Blank Area	Blank Fraction	$\Delta^{17}\text{O}$ raw	$\Delta^{17}\text{O}_{\text{blk_corr}}$	$\Delta^{17}\text{O}_{\text{xchg_corr}}$
<i>nmol O₂</i>	<i>V_s</i>	<i>V_s</i>		<i>‰</i>	<i>‰</i>	<i>‰</i>
139	212.55	181.50	0.15	14.7	17.3	21.0
199	290.50	278.54	0.04	15.7	16.3	19.9
199	302.43	277.25	0.08	16.0	17.4	21.1
201	313.94	280.67	0.11	15.3	17.1	20.8
173	294.66	236.02	0.20	15.4	19.3	23.3
234	371.83	334.08	0.10	15.9	17.1	21.5
182	312.87	251.03	0.20	15.4	19.2	23.3
195	298.56	272.29	0.09	17.3	18.9	22.9
330	89.99	82.45	0.08	17.1	18.6	22.6
497	137.29	127.63	0.07	17.3	18.6	22.5
499	139.42	128.00	0.08	16.6	18.1	22.0
724	203.12	188.78	0.07	17.7	19.1	23.1
738	207.43	192.50	0.07	17.4	18.8	22.7
787	218.40	205.79	0.06	16.5	17.6	21.3
935	262.56	245.46	0.07	17.6	18.9	22.8
1008	276.08	265.20	0.04	16.8	18.0	21.8

*see Sections 2.4.2.1 and 2.4.2.2 for details on corrections

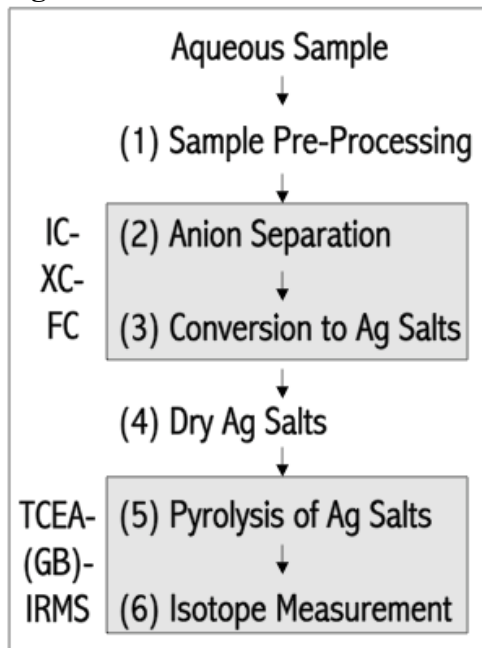
Figures

Figure 2.1: Overview of method for $\Delta^{17}\text{O}$ analysis of nitrate and sulfate. Steps 2 and 3 are automated by the Ion Chromatography-Cation Exchange-Fraction Collector System (IC-CX-FC). Steps 5 and 6 are automated by a Thermocouple Elemental Analyzer-Isotope Ratio Mass Spectrometer System (TCEA-IRMS) or a further modified system that uses a Gas Bench to cryofocus the sample before introduction into the IRMS (TCEA-GB-IRMS).

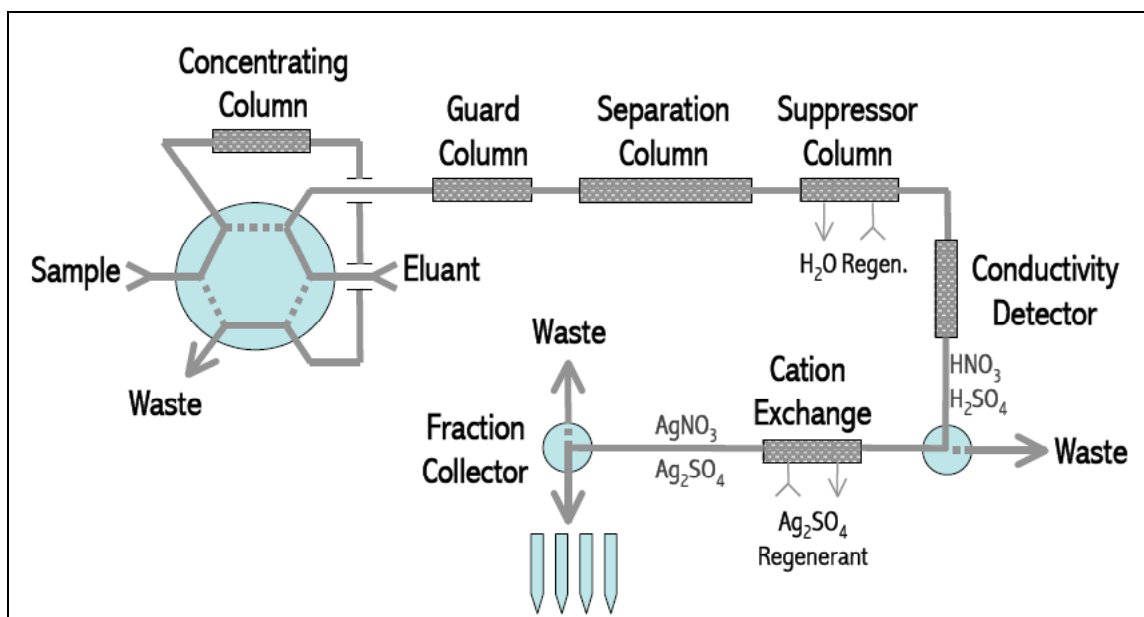


Figure 2.2: Flow diagram of silver salt preparation system (IC-XC-FC). Thick solid lines represent the flow of sample and KOH eluent, dashed lines indicate alternate flow of valve switches, and thin solid lines indicate the flow of regenerant through the suppressor and cation exchange columns. In the IC six-way valve (top left) solid lines show “Load” position, while dotted lines indicate “Inject” position.

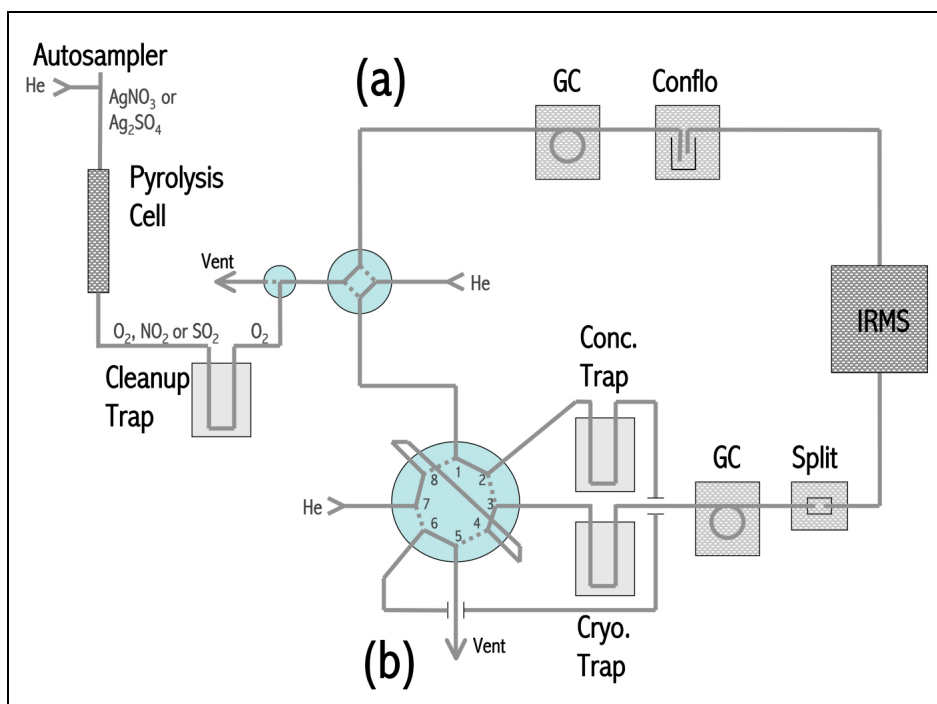


Figure 2.3: Flow diagram of system for oxygen isotope analysis of silver salts, including (a) TCEA-IRMS and (b) TCEA-GB-IRMS in an integrated system. Solid lines represent the flow of sample and He-carrier gas, while dotted lines indicate alternate flow of valves. Manual four-way method valve (center) is shown in position for TCEA-IRMS method. Gas Bench eight-way Valco® valve (bottom center) solid lines show “Load” position, while dotted lines indicate “Inject” position.

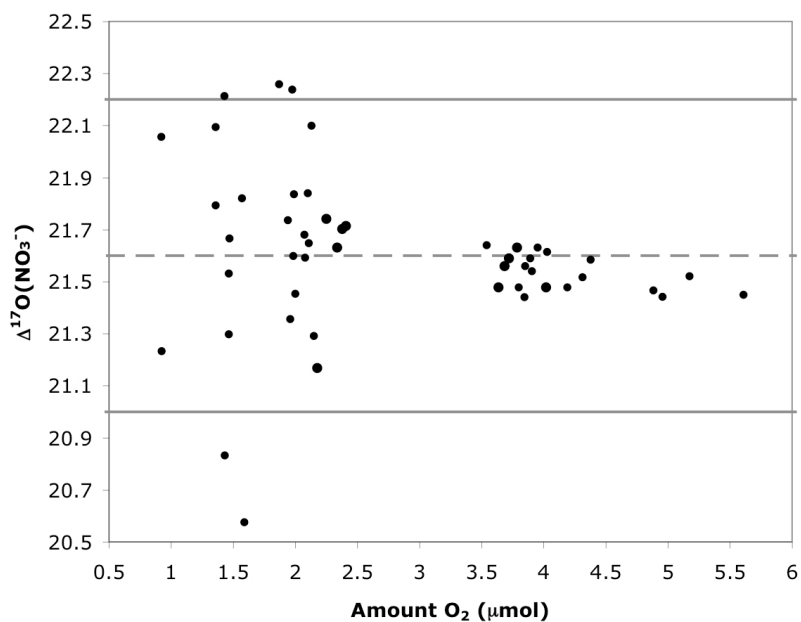


Figure 2.4: $\Delta^{17}\text{O}(\text{NO}_3^-)$ versus amount O₂ for USGS-35 nitrate measured using the TCEA-IRMS system. $\Delta^{17}\text{O}$ is shown in per mil. Dashed line indicates internationally accepted value of $\Delta^{17}\text{O}(\text{NO}_3^-)$ of USGS-35; solid lines indicate 2σ analytical uncertainty ($\pm 0.6\text{‰}$).

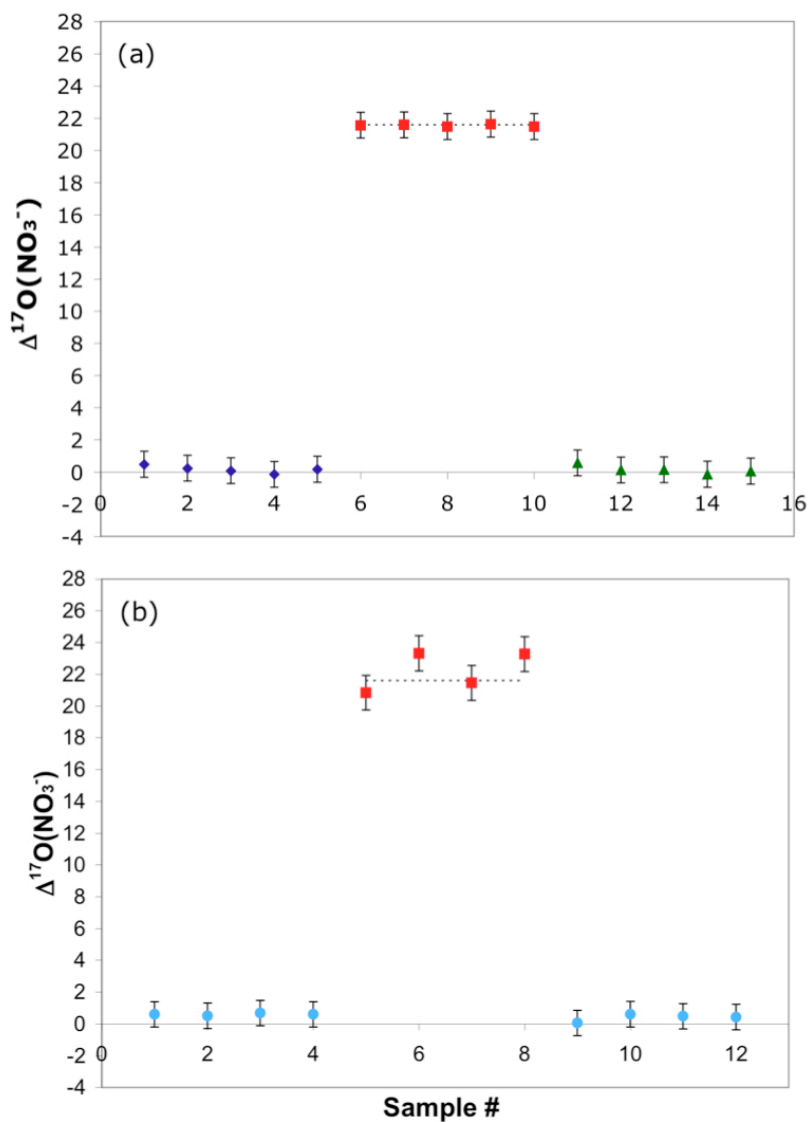


Figure 2.5: Memory effect test for (a) TCEA-IRMS system using $\sim 5 \mu\text{mol O}_2$ sample size and (b) TCEA-GB-IRMS system using $\sim 200 \text{ nmol O}_2$ sample size. Nitrate reference materials used include NIT-B (dark blue diamonds), USGS-35 (red squares), IAEA-N3 (green triangles), and NIT-A (light blue circles). Values shown in panel (b) have been corrected for both blank and isotopic exchange effects ($\Delta^{17}\text{O}_{\text{xchg_corr}}$, see 2.4.2.1-2.4.2.2).

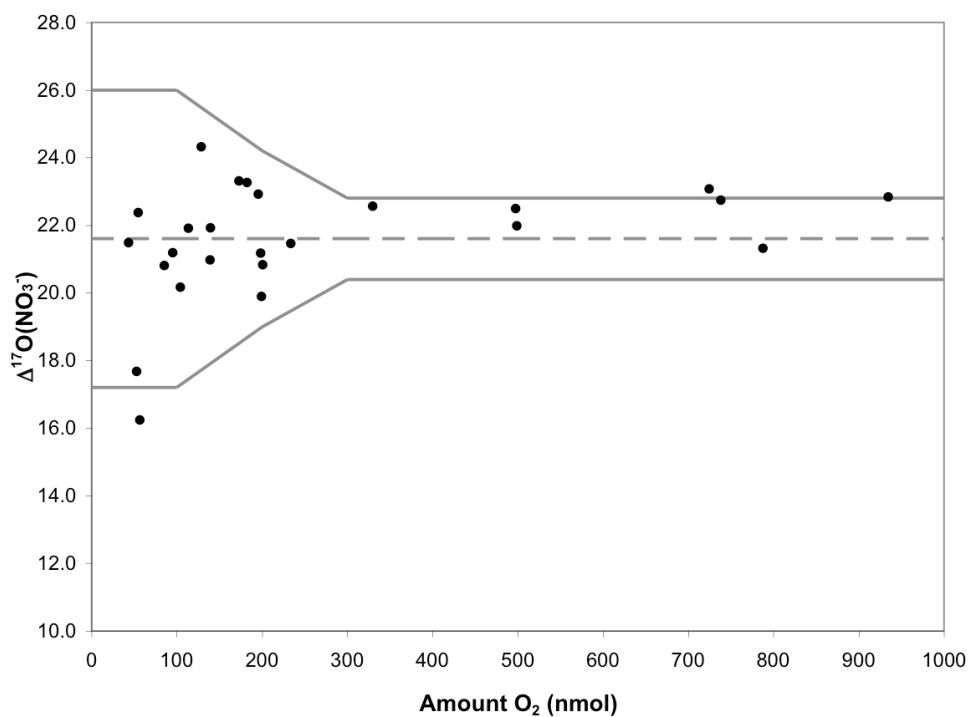


Figure 2.7: Fully corrected $\Delta^{17}\text{O}$ ($\Delta^{17}\text{O}_{\text{xchg_corr}}$, see Section 2.4.2.1-2.4.2.2) versus amount O_2 for USGS-35 nitrate measured using the TCEA-GB-IRMS system. $\Delta^{17}\text{O}$ is shown in per mil. Dashed line indicates internationally accepted value of $\Delta^{17}\text{O}(\text{NO}_3^-)$ of USGS-35; solid lines indicate 2σ analytical uncertainty for samples of each size group.

Chapter 3

Measurements and Modeling of $\Delta^{17}\text{O}$ of Nitrate in Snowpits from Summit, Greenland

[Kunasek, S. A., B. Alexander, E. J. Steig, M. G. Hastings, D. J. Gleason, and J. C. Jarvis (2008), Measurements and modeling of $\Delta^{17}\text{O}$ of nitrate in snowpits from Summit, Greenland, *J. Geophys. Res.-Atmos.*, 113(D24302), doi:10.1029/2008JD010103.]

3.1 Summary

We quantify controls on seasonal changes of the oxygen isotope anomaly of nitrate ($\Delta^{17}\text{O}(\text{NO}_3^-)$, where $\Delta^{17}\text{O} \approx \delta^{17}\text{O} - (0.52 \times \delta^{18}\text{O})$) in snow at Summit, Greenland in an effort to enable quantitative reconstructions of paleoatmospheric oxidant concentrations from ice core $\Delta^{17}\text{O}(\text{NO}_3^-)$. Measurements of $\Delta^{17}\text{O}(\text{NO}_3^-)$ from a snowpit at Summit are compared to calculations from an atmospheric chemical box model. Measured values of $\Delta^{17}\text{O}(\text{NO}_3^-)$ covering three seasonal cycles (Jan - Dec 2000, Jul 2003 - Mar 2006) range from 22.4‰ in summertime to 33.7‰ in wintertime, while model results show a larger range (18.9 - 31.5‰). Agreement between observed and modeled results is excellent for winter, when O_3 oxidation of nitrogen oxides dominates nitrate production (winter averages agree within 0.3‰). The 2 - 7‰ discrepancy between summertime box model results and measurements of $\Delta^{17}\text{O}(\text{NO}_3^-)$ may result from several influences not accounted for by our box model, including: Non-zero $\Delta^{17}\text{O}$ of OH over polar regions, stratospheric influence on surface O_3 at Summit, participation of BrO in nitrate production, and tropospheric transport of nitrate. A box model sensitivity study shows that annual mean $\Delta^{17}\text{O}(\text{NO}_3^-)$ is most sensitive to changes in the ratio of $[\text{O}_3]/([\text{HO}_2]+[\text{RO}_2])$ in summer.

3.2 Introduction

Atmospheric oxidants (e.g., O₃, OH, HO₂) are the primary sink for most reduced trace gases (e.g., CH₄, CO) that contribute to air pollution and climate change. Global mean concentrations of OH, the most powerful atmospheric oxidant, along with its precursor O₃, provide a metric for assessing the efficiency of trace gas removal by oxidation. Global mean OH concentration is commonly referred to as the “oxidizing capacity” of the atmosphere [Lawrence *et al.*, 2001 and references therein]. Modern human activities (e.g., fossil fuel and biomass burning) co-emit OH precursors and sink reactants, thereby buffering the atmospheric oxidizing capacity [Wang and Jacob, 1998]. However, as air pollution and greenhouse gas mitigation strategies alter anthropogenic emissions, a new balance between OH source and sink reactions could alter the atmospheric oxidizing capacity [Prinn, 2003]. Such changes could alter trace gas lifetimes, resulting in a feedback that amplifies the effect of emissions changes on climate and atmospheric pollution [Thompson *et al.*, 1993].

Reconstructions of past changes in the oxidizing capacity of the atmosphere have been sought to elucidate the relationship between oxidant levels and climate change. Due to inadequate or unavailable preindustrial measurements of O₃ and OH, estimates of past changes in the oxidizing capacity of the atmosphere come from photochemical transport modeling. While models agree on the sign of preindustrial-industrial change in O₃ concentration (25% to over 100% increase, depending on the metric used) [Volz and Kley, 1988; Levy *et al.*, 1997; Wang and Jacob, 1998; Lelieveld and Dentener, 2000; Grenfell *et al.*, 2001; Hauglustaine and Brasseur, 2001; Valdes *et al.*, 2005; Kaplan *et al.*, 2006], estimates of changes in OH concentration vary in both sign and magnitude

[*Martinerie et al.*, 1995; *Wang and Jacob*, 1998; *Grenfell et al.*, 2001; *Lelieveld et al.*, 2002]. Reconstructing oxidation chemistry through glacial-interglacial climate changes presents an even greater challenge due to more limited constraints on paleoatmospheric composition. Again, models agree on the change in O₃ from the Last Glacial Maximum (LGM) to preindustrial time (15 - 30% increase), while estimates of LGM-preindustrial OH concentration changes vary more widely (-30 to +30%) [*Thompson et al.*, 1993; *Karol et al.*, 1995; *Martinerie et al.*, 1995; *Valdes et al.*, 2005; *Kaplan et al.*, 2006].

Development of ice core reconstructions of paleoatmosphere oxidant concentrations would offer independent validation of models on preindustrial-industrial and glacial-interglacial timescales. Early ice core reconstructions of oxidation chemistry from H₂O₂ concentration [*Sigg and Nefel*, 1991] and the HCHO/CH₄ ratio [*Staffelbach et al.*, 1991] were complicated by post-depositional alteration of H₂O₂ and HCHO concentrations in the upper snowpack prior to preservation in the ice at depth [*Hutterli et al.*, 2003]. More recently, measurements of the oxygen isotope anomaly ($\Delta^{17}\text{O} \approx \delta^{17}\text{O} - (0.52 \times \delta^{18}\text{O})$ where $\delta^x\text{O} = ((^x\text{O}/^{16}\text{O})_{\text{sample}} / (^x\text{O}/^{16}\text{O})_{\text{standard}}) - 1$, with x = 17 or 18 and Vienna Standard Mean Ocean Water (V-SMOW) is the standard) of nitrate and sulfate in ice cores has shown promise as a conserved proxy for oxidant concentrations [*Alexander et al.*, 2002, 2003, 2004]. (Hereafter: $\Delta^{17}\text{O}$ of species X is written as $\Delta^{17}\text{O}(\text{X})$). The relative importance of different oxidants (e.g., O₃, OH, HO₂) in the production of nitrate and sulfate is reflected in $\Delta^{17}\text{O}(\text{NO}_3^-)$ and $\Delta^{17}\text{O}(\text{SO}_4^{2-})$, respectively, since the oxidants transfer different $\Delta^{17}\text{O}$ to oxidation products [*Savarino et al.*, 2000; *Michalski et al.*, 2003]. Available ice core $\Delta^{17}\text{O}(\text{NO}_3^-)$ and $\Delta^{17}\text{O}(\text{SO}_4^{2-})$ measurements provide evidence that changes in oxidation chemistry occurred during glacial-interglacial climate changes

as well as during the preindustrial-industrial transition [*Alexander et al.*, 2002, 2003, 2004]. However, the sensitivity of $\Delta^{17}\text{O}(\text{NO}_3^-)$ and $\Delta^{17}\text{O}(\text{SO}_4^{2-})$ to the many variables affecting oxidation pathways has not yet been quantified, preventing direct quantification of past oxidant concentrations.

In this study, we present measurements of seasonal changes in $\Delta^{17}\text{O}(\text{NO}_3^-)$ through three annual cycles from two snowpits at Summit, Greenland (72.6°N, 38.5°W). We use a box model to predict $\Delta^{17}\text{O}(\text{NO}_3^-)$ by quantifying the importance of local oxidation pathways producing nitrate. We also examine the sensitivity of box model $\Delta^{17}\text{O}(\text{NO}_3^-)$ to changes in specific oxidation pathways in nitrate production. The results of these studies are used to assess the potential for reconstructing paleoatmospheric oxidant concentrations from ice core $\Delta^{17}\text{O}(\text{NO}_3^-)$.

3.3 Chemistry and Isotopic Composition of Nitrate in Polar Regions

Most physical and chemical processes in the Earth system fractionate the two rare isotopes of oxygen (^{17}O and ^{18}O) in a predictable way according to their difference in mass (“mass-dependent fractionation”) [*Matsuhisa et al.*, 1978]:

$$\delta^{17}\text{O} \approx 0.52 \times \delta^{18}\text{O} \quad (1)$$

Chemical compounds demonstrating a deviation from mass-dependent isotope ratios are characterized using the $\Delta^{17}\text{O}$ value [*Farquhar et al.*, 2000]. Definitions of the $\Delta^{17}\text{O}$ isotope anomaly vary [e.g., *Farquhar et al.*, 2000; *Michalski et al.*, 2003; *Kaiser et al.*, 2007], and we employ the linear definition here:

$$\Delta^{17}\text{O} = \delta^{17}\text{O} - (0.52 \times \delta^{18}\text{O}) \quad (2)$$

Chemical constituents displaying mass-dependent behavior have $\Delta^{17}\text{O} = 0$. *Thiemens and Heidenreich* [1983] first showed that an isotope anomaly is produced during the ozone formation reaction. Positive $\Delta^{17}\text{O}$ observed in other atmospheric constituents, such as N_2O , H_2O_2 , SO_4^{2-} , NO_3^- , is thought to derive from mass transfer of O-atoms during formation reactions involving oxidation by O_3 or $\text{O}(^1\text{D})$ (an O_3 photolysis product) [*Cliff and Thiemens*, 1997; *Savarino and Thiemens*, 1999; *Savarino et al.*, 2000; *Lyons*, 2001; *Michalski et al.*, 2003].

Atmospheric nitrate (HNO_3 +particulate NO_3^-) is predominantly formed through oxidation of NO_x ($=\text{NO}+\text{NO}_2$), which originates from soils, lightning, and combustion. Nitrate is then deposited to the surface through wet and dry deposition. Figure 3.1 details oxidation reactions in nitrate production. Of the oxidants involved in nitrate formation (O_3 , HO_2 , OH , and RO_2 , where R represents a hydrocarbon chain), O_3 demonstrates the largest $\Delta^{17}\text{O}$. Photochemical equilibrium model results suggest that tropospheric $\Delta^{17}\text{O}(\text{O}_3) \approx 35 \pm 3\text{‰}$, and stratospheric $\Delta^{17}\text{O}(\text{O}_3)$ is roughly 5‰ higher than in the troposphere [*Lyons*, 2001]. These estimates are at the high end of the range of tropospheric $\Delta^{17}\text{O}(\text{O}_3)$ measurements, with mean $\Delta^{17}\text{O}(\text{O}_3)$ measurements for different locations varying between 25 - 35‰ [*Schueler et al.*, 1990; *Krakovsky et al.*, 1995, 2000; *Johnston and Thiemens*, 1997]. Tropospheric oxidants other than O_3 have very small or zero $\Delta^{17}\text{O}$. Throughout most of the troposphere, $\Delta^{17}\text{O}(\text{OH}) = 0\text{‰}$ due to rapid isotopic exchange with water vapor [*Dubey et al.*, 1997; *Lyons*, 2001]. Empirical [*Savarino and Thiemens*, 1999] and modeling studies [*Lyons*, 2001] suggest $\Delta^{17}\text{O}(\text{HO}_2) \sim 1\text{‰}$. Because O_3 is the only oxidant with a strongly positive $\Delta^{17}\text{O}$, the 22 - 33‰ range observed in mid-latitude atmospheric $\Delta^{17}\text{O}(\text{NO}_3^-)$ [*Michalski et al.*, 2003] primarily

reflects changes in the relative importance of oxidation by O_3 versus other oxidants in nitrate formation.

At a polar site such as Summit, $\Delta^{17}O(NO_3^-)$ should have strong seasonal variability. In summer, 24-hour sunlight drives photolytic production of OH and destruction of NO_3 and N_2O_5 [Stroud *et al.*, 2003], reducing the importance of O_3 in NO_2 oxidation pathways, and hence the magnitude of $\Delta^{17}O(NO_3^-)$ (see also Figure 3.1). Conversely, in the 24-hour darkness of winter, O_3 will be the dominant oxidant in nitrate production. Thus, $\Delta^{17}O(NO_3^-)$ will have a minimum in summer and a maximum in winter.

In addition to season, $\Delta^{17}O(NO_3^-)$ deposited to the snow surface may reflect the location of nitrate formation (Figure 3.2). For example, for nitrate in the Summit snowpack to bear $\Delta^{17}O(NO_3^-)$ indicative of local oxidants, local oxidation of NO_x must be the primary source of snowpack nitrate. On the other hand, if the nitrate deposited to the snowpack originates from transport of nitrate produced in neighboring regions, $\Delta^{17}O(NO_3^-)$ will reflect the oxidation chemistry of the region in which the nitrate was produced. The amount of NO_x transported to Summit may be small compared to the amount of nitrate transported, due to the distance of Summit from NO_x sources and the relatively short lifetime of NO_x (maximum of ~ 3 days in the wintertime mid-troposphere [Levy *et al.*, 1999]). However, thermal decomposition of peroxyacetyl nitrate (PAN) ($CH_3C(O)OONO_2$), which is transported in the mid- and upper-troposphere from continental areas to the Arctic, has been investigated as a potentially important source of NO_x and/or snowpack nitrate to Summit [Munger *et al.*, 1999; Dassau *et al.*, 2002; Ford *et al.*, 2002]. If PAN decomposes to NO_x and is oxidized to nitrate in the atmosphere

near Summit, the nitrate deposited would reflect local oxidant concentrations. It has also been suggested that PAN may decompose to nitrate on snowgrains [Ford *et al.*, 2002; Dassau *et al.*, 2004]. The chemical mechanism and role of local oxidants in this process remain unknown. The regional versus local oxidation signature of $\Delta^{17}\text{O}$ of nitrate originally deposited to the snowpack thus depends on the relative contributions to snowpack nitrate from nitrate transport versus PAN decomposition, as well as the mechanism of PAN decomposition.

Alteration of nitrate in the surface snow after deposition is not expected to directly alter $\Delta^{17}\text{O}(\text{NO}_3^-)$, but may affect the regional versus local oxidation chemistry signal of $\Delta^{17}\text{O}(\text{NO}_3^-)$ at Summit (Figure 3.2). Post-depositional loss of nitrate from the sunlit snowpack provides a source of HONO and NO_x to the local atmosphere [Honrath *et al.*, 1999, 2000, 2002; Munger *et al.*, 1999; Zhou *et al.*, 2001; Dibb *et al.*, 2002; Yang *et al.*, 2002]. However, nitrate concentrations deposited to the snow surface are found to be mostly conserved at Summit (maximum 25% loss) [Burkhart *et al.*, 2004; Dibb *et al.*, 2007]. This suggests that if considerable nitrate is photolyzed from the Summit snowpack, much of the released NO_x is re-oxidized locally to nitrate, which is then re-deposited to the snowpack [Hastings *et al.*, 2004]. Experimental studies suggest that alteration of snowpack $\Delta^{17}\text{O}(\text{NO}_3^-)$ due to post-depositional nitrate loss (e.g., photolysis) is not much greater than analytical uncertainties of measurements [McCabe *et al.*, 2005]. However, because post-depositional processing of snowpack nitrate (e.g., loss as NO_x , re-oxidation, and re-deposition as nitrate) involves oxidation by local oxidants, this process is expected to result in $\Delta^{17}\text{O}(\text{NO}_3^-)$ reflecting local oxidant concentrations. Thus, even if

$\Delta^{17}\text{O}(\text{NO}_3^-)$ in surface snow originally reflects regional oxidation, extensive post-depositional processing could effectively remove that signature.

3.4 Laboratory Methods

1-meter and 2-meter snowpits were sampled at Summit, Greenland, in August 2001 and May 2006, respectively. Sampling and sample dating of the 2001 snowpit is described in detail in *Hastings et al.* [2004]. Measurement of $\Delta^{17}\text{O}(\text{NO}_3^-)$ for the 2001 samples was performed at Princeton University in 2005 using the bacterial denitrifier method described by *Kaiser et al.* [2007]. Briefly, denitrifying bacteria are used to convert NO_3^- to N_2O , which is then quantitatively thermally decomposed in a gold tube to N_2 and O_2 . The O_2 isotopes are then measured online by an Isotope Ratio Mass Spectrometer (IRMS). Isotopic corrections for blank, isotopic exchange with water, and fractionation follow *Kaiser et al.* [2007]. Sample concentrations for the 2001 snowpit, determined by ion chromatography on a Dionex DX500 instrument (with Dionex AS4A column), were used to determine the volume of sample for $\Delta^{17}\text{O}(\text{NO}_3^-)$ analysis. Of the eight samples (see Figure 3.3), four with nitrate concentrations less than $3\ \mu\text{M}$ were analyzed for $\Delta^{17}\text{O}(\text{NO}_3^-)$ with 30 nmol of nitrate (i.e., ~10 - 15 ml of melted snow), while four samples with nitrate concentrations of 3 - $6\ \mu\text{M}$ were analyzed for $\Delta^{17}\text{O}(\text{NO}_3^-)$ with 50 nmol of nitrate (i.e., 16 - 9 ml of melted snow). As reported by *Kaiser et al.* [2007], for a sample size of 50 nmol this method has a 1σ error of 0.5‰ for $\Delta^{17}\text{O}(\text{NO}_3^-)$. The 1σ error for 30 nmol samples was 0.7‰, based on repeated measurements of the international standard USGS-35 reference material (NaNO_3) [*Böhlke et al.*, 2003].

The 2006 snowpit was sampled for 4 L of snow at ~10 cm resolution. Samples were stored frozen in pre-cleaned Kapak polyester bags. They were then thawed in 4 L beakers in a class 100 clean hood. A 10 ml aliquot was analyzed for nitrate anion concentrations using a Dionex Ion Chromatograph with an IonPac® AS11-HC column (2 x 250 mm) and a KOH eluent gradient from 20 mM to 45 mM. Concentration data was used to determine the volume of melted snow necessary to obtain 5 - 6 μmoles of nitrate in each sample. Another 10 ml aliquot was analyzed for $\delta^{18}\text{O}$ of snow using standard CO_2 equilibration techniques [e.g., *Craig*, 1961] with a Micromass Aquaprep system. $\delta^{18}\text{O}_{\text{snow}}$ values were used to estimate the seasonal timing of each sample, following the well-established temperature- $\delta^{18}\text{O}$ relationship [*Jouzel et al.*, 1997]. The remaining volume of sample was evaporated to ~ 50 mL in a clean hood in order to concentrate the ions before further sample preparation for $\Delta^{17}\text{O}(\text{NO}_3^-)$ analysis.

For measurement of $\Delta^{17}\text{O}(\text{NO}_3^-)$, we adapt and automate previously developed techniques [*Savarino et al.*, 2001; *Michalski et al.*, 2002]. For each sample, isolation of nitrate and conversion to silver nitrate is performed using an automated system including ion chromatographic separation, ion-exchange, and a fraction collector. A Dionex Ion Chromatograph with an IonPac® AS19 column (4 x 250 mm) and a multi-step eluent concentration gradient of 7 mM/10 mM/15 mM KOH is used to separate nitrate and sulfate fractions. Fractions then flow directly through an AMMS® III ion-exchange membrane (4 mm) with 2.5 mM Ag_2SO_4 regenerant for conversion to silver salts (e.g., AgNO_3) prior to separate collection by the fraction collector. Silver nitrate fractions are then transferred and dried in Costech 5 x 9 mm silver capsules in multiple successive steps by a miVac Duo centrifuging concentrator at 45°C.

Analysis of oxygen isotopes of nitrate is performed using a Finnigan Thermocouple Elemental Analyzer (TC/EA) in-line with a continuous flow Finnigan MAT 253 IRMS with He as the carrier gas. The TC/EA autosampler drops samples into an empty quartz pyrolysis tube at 550°C. The pyrolysis tube is pretreated by soaking in 7 M HNO₃, etching for 10 minutes in 10% HF, followed by rinsing with ultraclean (18 mΩ) water and annealing at 900°C for 24 hours. In the pyrolysis tube, pyrolysis of AgNO₃ samples proceeds via $\text{AgNO}_3 \rightarrow \frac{1}{2} \text{O}_2 + \text{NO}_2 + \text{Ag(s)} + (\text{N}_2, \text{NO in trace amounts})$. NO₂ and other by-products are removed by a liquid N₂ trap before the pyrolysis products flow through a molecular sieve 5A gas-chromatograph column and into the IRMS. Evolved O₂ is measured for ¹⁶O¹⁶O, ¹⁶O¹⁷O, and ¹⁶O¹⁸O, from which Δ¹⁷O is calculated. Our measurements of the international standard USGS-35 reference material (NaNO₃) result in Δ¹⁷O(NO₃⁻) = 21.5 ± 0.4‰ (1σ error) for samples of 2 - 5 μmol O₂ (4-10 μmol nitrate), which shows excellent agreement with accepted standard values (Δ¹⁷O(NO₃⁻) = 21.6 ± 0.2‰) [Böhlke *et al.*, 2003; Michalski *et al.*, 2003]. A size calibration during each IRMS sample sequence is used to identify any samples displaying yields outside of this size range (2 – 5 μmol O₂), and Δ¹⁷O(NO₃⁻) values for these samples are not reported.

3.5 Box Model: Nitrate Δ¹⁷O

Our atmospheric chemical box model of Δ¹⁷O(NO₃⁻) employs a mass-transfer approach similar to Michalski *et al.* [2003]. Figure 3.1 shows a schematic of the box model. Full reactions and reaction rates are listed in Table 3.1. The box model first determines the partitioning between oxidation pathways in NO₂ and NO₃⁻ formation by

comparison of formation rates. $\Delta^{17}\text{O}(\text{NO}_3^-)$ is then calculated based on the transfer of the isotopic enrichment from O_3 to NO_x and HNO_3 . The box model formulation implicitly assumes entirely local production of nitrate.

3.5.1 Boundary Conditions

Because monthly average concentrations have not yet been measured for most applicable atmospheric species for Summit, Greenland, we use output from the 3-D global chemical transport model GEOS-Chem for box model boundary conditions (www.as.harvard.edu/chemistry/trop/geos/). This includes: concentrations of NO , NO_2 , NO_3 , OH , HO_2 , DMS (dimethylsulfide), HC (hydrocarbons: CH_3CHO , $> \text{C}_2$ aldehydes, and $\geq \text{C}_4$ alkanes); HNO_3 production rates via N_2O_5 hydrolysis; and monthly average temperature and number density of air. Because GEOS-Chem average summer OH concentrations are a factor of 4 - 6 lower than estimates based on summer measurements ($4 - 6.2 \times 10^6$ molecules/ cm^3) [Zhou *et al.*, 2001; Dassau *et al.*, 2002; Grannas *et al.*, 2002; Yang *et al.*, 2002; Sjostedt *et al.*, 2007] (See Table 3.3), we increase GEOS-Chem OH concentrations by a factor of four for all months in our box model. We also employ monthly O_3 concentration observations from NOAA-ESRL (www.esrl.noaa.gov/gmd/) in place of GEOS-Chem values, which are 12 - 26% lower than observations. For consistency with the higher observed O_3 concentrations, we linearly scale GEOS-Chem-derived NO_3 concentration and HNO_3 production rates via N_2O_5 hydrolysis. The factor of four adjustment of box model OH concentrations alters box model $\Delta^{17}\text{O}(\text{NO}_3^-)$ by less than our measurement uncertainty. The use of direct O_3 observations in place of GEOS-Chem values alters box model $\Delta^{17}\text{O}(\text{NO}_3^-)$ by a maximum of 1.2‰ (in summer). The

Model Limitations section below details additional comparisons of model inputs with available observations.

A constant $\Delta^{17}\text{O}$ value of 35‰ is assumed for tropospheric O_3 , based on model estimates of the mean tropospheric surface value [Lyons, 2001] and consistent with early modeling of $\Delta^{17}\text{O}(\text{NO}_3^-)$ [Michalski *et al.*, 2003]. We assume all other oxidants, including OH, HO_2 , and RO_2 , have $\Delta^{17}\text{O} = 0\text{‰}$, as in Michalski *et al.* [2003]. Although measurements suggest that $\Delta^{17}\text{O}(\text{HO}_2) \sim 1\text{‰}$ [Savarino and Thiemens, 1999], the assumption of $\Delta^{17}\text{O}(\text{HO}_2 \& \text{RO}_2) = 0$ affects $\Delta^{17}\text{O}(\text{NO}_3^-)$ by less than our measurement uncertainty and simplifies our analysis. We examine the implications of these assumptions for our results in Section 6.1.

3.5.2 $\Delta^{17}\text{O}$ of Nitrate Calculation

The $\Delta^{17}\text{O}$ of NO_2 and nitrate are calculated in the box model using partition ratios, as in Michalski *et al.* [2003]. A partition ratio is calculated as the ratio of the production rate of the oxidation product by the individual oxidation pathway versus the total production rate of all oxidation pathways. For example, A is the partition ratio of NO oxidation to NO_2 by O_3 given as:

$$A = \frac{\left(\frac{d[\text{NO}_2]}{dt}\right)_{\text{O}_3\text{path}}}{\left(\frac{d[\text{NO}_2]}{dt}\right)_{\text{total}}} = \frac{k_1[\text{O}_3][\text{NO}]}{k_1[\text{O}_3][\text{NO}] + k_2[\text{HO}_2][\text{NO}] + k_3[\text{RO}_2][\text{NO}]} \quad (3)$$

where reaction rates k_1 , k_2 , and k_3 are shown in Table 3.1 and R represents a hydrocarbon chain. In addition to A , which characterizes the strength of O_3 oxidation in NO_2 production, we calculate three partition ratios to characterize oxidation pathways of NO_2 oxidation to NO_3^- . B is the ratio of NO_3^- formation by OH to total NO_3^- formation; C is

the ratio of NO_3^- formation by H-abstraction from DMS and hydrocarbons to total NO_3^- formation; D is the ratio of NO_3^- formation by N_2O_5 hydrolysis to total NO_3^- formation. Table 3.2 details the calculation of partition ratios for all applicable oxidation pathways (see also Figure 3.1).

A few simplifying assumptions are used in the calculation of partition ratios (Table 3.2). First, in the calculation of $d[\text{NO}_2]_{total}/dt$ (the denominator of A) shown above, we approximate the rate of NO_2 formation via RO_2 oxidation (third term of the denominator) as $\frac{1}{2}$ the rate via HO_2 formation ($k_3[\text{RO}_2][\text{NO}] \approx 0.5 \times k_2[\text{HO}_2][\text{NO}]$) rather than account for individual peroxy radical reactions. For most of the year, this approximation agrees within a factor of two with GEOS-Chem calculations of the rate of NO_2 formation via RO_2 oxidation. Second, the calculation of $d[\text{HNO}_3]_{\text{N}_2\text{O}_5\text{path}}/dt$ (the numerator of D) is output directly from GEOS-Chem, rather than calculated explicitly within the box model. GEOS-Chem calculates the production rate of HNO_3 via N_2O_5 hydrolysis as:

$$\frac{d[\text{HNO}_3]}{dt} = 2k[\text{N}_2\text{O}_5], \quad \text{where} \quad (4)$$

$$k = \left(\frac{a}{D_g} + \frac{4}{v\gamma} \right)^{-1} A \quad (5)$$

In equation 5, a is the aerosol particle radius, D_g is the gas-phase molecular diffusion coefficient of N_2O_5 in air, v is the mean molecular speed of N_2O_5 in the gas phase, A is the aerosol surface area per unit volume of air, and γ is the reaction probability [Schwartz, 1987]. GEOS-Chem calculates γ as a function of aerosol type (dust, sulfate, black carbon, organic carbon and sea salt), relative humidity, and temperature [Evans and Jacob, 2005].

$\Delta^{17}\text{O}$ of NO_2 and HNO_3 are calculated sequentially. Because NO_x cycling (Table 3.1, X1-X4) is several orders of magnitude faster than nitrate formation and removal (Table 3.1, X5-X12), NO_x rapidly achieves isotopic equilibrium with oxidants (O_3 , HO_2 , RO_2) prior to further oxidation. As a result, $\Delta^{17}\text{O}(\text{NO}_2)$ is first calculated independently of the second oxidation step as:

$$\Delta^{17}\text{O}(\text{NO}_2) = A \times \Delta^{17}\text{O}(\text{O}_3) \quad (6)$$

where A is the partition ratio of O_3 oxidation in NO_2 production and $\Delta^{17}\text{O}(\text{O}_3) = 35\%$. Determining $\Delta^{17}\text{O}(\text{NO}_3^-)$ then requires calculation of net oxygen isotope composition after mass-transfer of an additional O-atom to NO_2 during oxidation to HNO_3 , as shown in equations 7-10 [Michalski *et al.*, 2003]. B , C , and D indicate partition factors for NO_2 oxidation pathways (see also Table 3.2).

$$\Delta^{17}\text{O}(\text{NO}_3^-)_{\text{PathB}} = \frac{2}{3} \Delta^{17}\text{O}(\text{NO}_2) \quad (7)$$

$$\Delta^{17}\text{O}(\text{NO}_3^-)_{\text{PathC}} = \frac{2}{3} \Delta^{17}\text{O}(\text{NO}_2) + \frac{1}{3} \Delta^{17}\text{O}(\text{O}_3) \quad (8)$$

$$\Delta^{17}\text{O}(\text{NO}_3^-)_{\text{PathD}} = \frac{1}{3} \Delta^{17}\text{O}(\text{NO}_2) + \frac{1}{2} \left(\frac{2}{3} \Delta^{17}\text{O}(\text{NO}_2) + \frac{1}{3} \Delta^{17}\text{O}(\text{O}_3) \right) \quad (9)$$

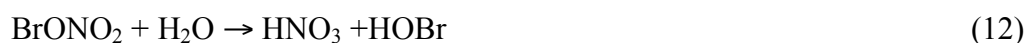
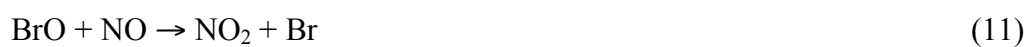
$$\Delta^{17}\text{O}(\text{NO}_3^-)_{\text{net}} = B \left(\Delta^{17}\text{O}(\text{NO}_3^-)_{\text{PathB}} \right) + C \left(\Delta^{17}\text{O}(\text{NO}_3^-)_{\text{PathC}} \right) + D \left(\Delta^{17}\text{O}(\text{NO}_3^-)_{\text{PathD}} \right) \quad (10)$$

3.5.3 Model Limitations

Table 3.3 shows a detailed comparison of box model inputs derived from GEOS-Chem versus reported measurements at Summit and nearby locations, primarily from summer measurement campaigns. (Wintertime observations of most species are not available.) GEOS-Chem-derived monthly average concentrations of NO and NO_2 are nearly a factor of 5 lower than reported observations of summer averages [Dibb *et al.*,

2002; *Ford et al.*, 2002; *Yang et al.*, 2002]. Summer average observations of peroxy radicals ($\text{HO}_2 + \text{RO}_2$) [*Sjostedt et al.*, 2007] differ by only 10% from the summer average GEOS-Chem-derived box model input ($\text{HO}_2 + \text{RO}_2$), where $\text{RO}_2 = \frac{1}{2}\text{HO}_2$ is assumed. GEOS-Chem-derived DMS abundance in June is nearly a factor of 10 greater than most measurements, which frequently fall below detection limits of 1 pptv [D. R. Blake, pers. comm.]. GEOS-Chem-derived abundances of CH_3CHO and $> \text{C}_2$ alkanes in April are 60% and 50% less than observations from Alert, Canada, respectively [*Boudries et al.*, 2002]. GEOS-Chem-derived abundances of $\geq \text{C}_4$ alkanes for Summit are at the low end of the range of reported measurements for the North Atlantic [*Hopkins et al.*, 2002], consistent with Summit's inland, high-altitude location. As previously mentioned, box model inputs of OH and O_3 concentrations are altered to more accurately reflect observational constraints, due to the known importance of changes in OH and O_3 abundances for the seasonal cycle of $\Delta^{17}\text{O}(\text{NO}_3^-)$ (Section 2.0). The implications of uncertainties in box model inputs is discussed in Section 7.0, where the sensitivity of $\Delta^{17}\text{O}(\text{NO}_3^-)$ to box model inputs is detailed.

Reactive halogen chemistry (e.g., BrO, HOBr) is not included in our box model. This chemistry is expected to be most important during early springtime close to sea-ice [*Wagner and Platt*, 1998]. During springtime ozone depletion events in coastal Arctic sites, reactive bromine chemistry has been shown to play a role both in gas-phase NO oxidation (equation 11) and in heterogeneous NO_2 oxidation (equation 12) [*Hanson et al.*, 1996; *Sander et al.*, 1999].



Although Summit's inland location (~ 400 km from the coast) suggests limited influence of halogen chemistry outside of springtime, several indirect lines of evidence have suggested a non-negligible contribution of BrO and HOBr to oxidation chemistry at Summit during summer months [*Peterson and Honrath, 2001; Grannas et al., 2007* and references therein; *Sjostedt et al., 2007*]. Recent BrO measurements during early summer at Summit frequently found concentrations higher than expected (1 - 3 ppt) [*Huey et al., 2007*]. Implications of BrO chemistry for our box model results are discussed in Section 6.1.

Lastly, in the box model, we assume that during oxidation by O₃, NO and NO₂ display equal probability of reacting with ozone's three oxygen atoms [e.g. *Michalski et al., 2003*], resulting in transfer of the bulk $\Delta^{17}\text{O}$ isotope anomaly of O₃ to reaction products. It is known that heavy oxygen atoms are not stochastically distributed in O₃, but that there is an enrichment of heavy isotopes in the terminal versus the central oxygen atom position (i.e., OOQ versus OQO, respectively, where Q = ¹⁷O or ¹⁸O) [*Janssen, 2005; Bhattacharya et al., 2008*]. While early studies suggested a roughly even probability of transfer of terminal and central oxygen atoms of O₃ during reaction with NO (reaction X1, Table 3.1) [*van den Ende and Stolte, 1984*], recent studies suggest that the terminal oxygen atom is preferred [*Savarino et al., 2008*]. We address the implications of these reaction dynamics for our box model results in Section 6.2.

3.6 Greenland Observations and Box Model Results

Figure 3.3 shows $\delta^{18}\text{O}(\text{H}_2\text{O})$ and $\Delta^{17}\text{O}(\text{NO}_3^-)$ measurements for the 2001 and 2006 snowpits. The $\delta^{18}\text{O}(\text{H}_2\text{O})$ measurements (Figure 3.3a) are used to establish a depth-

age relationship from which the timing of $\Delta^{17}\text{O}(\text{NO}_3^-)$ measurements (Figure 3.3b) is determined. The 2006 snowpit samples cover nearly three years (July 2003-May 2006) and have $\Delta^{17}\text{O}(\text{NO}_3^-)$ ranging from 24.7 to 33.0‰ from summer to winter, respectively (annual mean $\Delta^{17}\text{O}(\text{NO}_3^-) = 27.7\text{‰}$). The 2001 snowpit samples cover just over one year (April 2000-August 2001) and have $\Delta^{17}\text{O}(\text{NO}_3^-)$ ranging from 22.4 to 33.7‰ from summer to winter, respectively. Nitrate concentrations for the 2001 snowpit vary between $0.8 - 5.9 \pm 0.2 \mu\text{M}$, and are published elsewhere [Hastings *et al.*, 2004]. Nitrate concentrations for the 2006 snowpit vary between $0.6 - 5.2 \pm 0.2 \mu\text{M}$, consistent with previous studies [Davidson *et al.*, 1989; Whitlow *et al.*, 1992; Yang *et al.*, 1995; Hastings *et al.*, 2004; Dibb *et al.*, 2007].

Box model calculations of $\Delta^{17}\text{O}(\text{NO}_3^-)$, also shown in Figure 3.3, show the same seasonality as measurements, but with a larger range from 18.9‰ in summer to 31.5‰ in winter (annual mean $\Delta^{17}\text{O}(\text{NO}_3^-) = 26.3\text{‰}$). The percentage of NO oxidation by O_3 (vs. HO_2 and RO_2) in NO_x cycling varies between ~80 - 100% from summer to winter, respectively. NO_2 oxidation to nitrate varies between complete domination by OH oxidation in summer (100% of total oxidation) and complete domination by O_3 oxidation pathways in winter, with the DMS/HC oxidation pathway and the N_2O_5 hydrolysis pathway contributing roughly 60% and 40% to total winter oxidation, respectively. Box model $\Delta^{17}\text{O}(\text{NO}_3^-)$ interannual variability is estimated using the standard deviation of monthly $\Delta^{17}\text{O}(\text{NO}_3^-)$ from 2001 and 2004 (Figure 3.3, shaded region). We also propagate uncertainties of all reaction rates used in the box model (reported in Table 3.1 references) to estimate $\pm 2\sigma$ box model uncertainty (roughly $\pm 2.5\text{‰}$ in summer and winter; Figure 3.3, dotted lines). We propagate a factor 5 error for the rate of nitrate production by N_2O_5

hydrolysis on aerosols, to encompass errors that are difficult to constrain (e.g., aerosol size distribution and reaction probability).

3.7 Measurement-Model Comparison

Both $\Delta^{17}\text{O}(\text{NO}_3^-)$ measurements and box model calculations display the expected seasonality, with minimum values during summer when oxidation by OH dominates nitrate production and maximum values during winter when oxidation by O_3 dominates. Winter $\Delta^{17}\text{O}(\text{NO}_3^-)$ measurements and box model results agree well (winter averages are within 0.3‰), but box model $\Delta^{17}\text{O}(\text{NO}_3^-)$ in summer months is consistently biased low by 2 - 7‰. In the sub-sections that follow, we examine potential causes of this summertime discrepancy. First, we reassess the box model assumptions of $\Delta^{17}\text{O}$ of tropospheric OH and O_3 given conditions at Summit (Section 6.1). Next, we consider the effects of vertical transport of stratospheric O_3 on $\Delta^{17}\text{O}(\text{NO}_3^-)$ (Section 6.2). We next estimate possible impacts of reactive halogen chemistry (e.g., BrO) not included in the box model (Section 6.3). Lastly, we examine the influence of regional transport on $\Delta^{17}\text{O}(\text{NO}_3^-)$ and reassess the box model assumption that snowpack nitrate is produced by local oxidation (see also Figure 3.2) (Section 6.4). In a separate section (7.0), we present the results of a sensitivity study using the box model, and discuss implications for the interpretation of $\Delta^{17}\text{O}(\text{NO}_3^-)$ ice core measurements.

3.7.1 $\Delta^{17}\text{O}$ of Oxidants

In light of a recent review of $\Delta^{17}\text{O}$ of oxidants in the Arctic [Morin *et al.*, 2007], we reassess the box model assumptions of the values of $\Delta^{17}\text{O}(\text{OH}) = 0\text{‰}$ and $\Delta^{17}\text{O}(\text{O}_3) =$

35‰. Although rapid isotopic exchange with atmospheric water vapor ensures $\Delta^{17}\text{O}(\text{OH}) = 0\text{‰}$ throughout most of the troposphere [Dubey *et al.*, 1997; Lyons, 2001], low relative humidity and temperatures in Arctic regions may prevent full isotopic equilibration of OH with water vapor prior to removal [Morin *et al.*, 2007]. In this environment, OH may retain some of the $\Delta^{17}\text{O}$ isotope anomaly produced by OH source reactions (e.g., reaction of water vapor with $\text{O}(^1\text{D})$ from O_3 photolysis). Since NO_2 oxidation by OH dominates nitrate production in the summer, a positive $\Delta^{17}\text{O}(\text{OH})$ could potentially explain the summertime measurement-model $\Delta^{17}\text{O}(\text{NO}_3^-)$ discrepancy.

Morin *et al.* [2007] estimate $\Delta^{17}\text{O}(\text{OH})$ as a function of the original $\Delta^{17}\text{O}$ imparted by OH source reactions ($\Delta^{17}\text{O}(\text{OH})_{\text{prod}}$) and the extent to which that signature is retained due to incomplete isotopic equilibration. Using the calculation outlined by Morin *et al.* [2007] for typical summer CO and CH_4 concentration [Spivakovsky *et al.*, 2000; Yang *et al.*, 2002], temperature, pressure, and relative humidity at Summit (e.g., NOAA-ESRL data archive, www.esrl.noaa.gov/gmd/) and established reaction rates [Dubey *et al.*, 1997; Sander *et al.*, 2006], we estimate ~10% of the original $\Delta^{17}\text{O}(\text{OH})_{\text{prod}}$ is retained due to incomplete isotopic equilibration with water vapor in summer. This is consistent with springtime calculations by Morin *et al.* [2007] for Alert, Canada (82.5° N 62.3° W), which estimate that retention of $\Delta^{17}\text{O}(\text{OH})_{\text{prod}}$ drops from 70% to ~20% over spring (late March – late May). Of the four OH sources treated by Morin *et al.* [2007], the highest possible $\Delta^{17}\text{O}(\text{OH})_{\text{prod}}$ at Summit could be produced by photolysis of HOBr, which would give $\Delta^{17}\text{O}(\text{OH})_{\text{prod}} \approx 35\text{‰}$, assuming that HOBr directly reflects $\Delta^{17}\text{O}(\text{O}_3)$. This suggests maximum summer mean values of $\Delta^{17}\text{O}(\text{OH}) \approx 3.5\text{‰}$ at Summit. In our box model, a value over 50% greater ($\Delta^{17}\text{O}(\text{OH}) = 6\text{‰}$) is necessary to increase summer

$\Delta^{17}\text{O}(\text{NO}_3^-)$ to match our lowest summer snowpit measurement (August 2000). Although non-zero $\Delta^{17}\text{O}(\text{OH})$ cannot alone fully reconcile the summer measurement-model $\Delta^{17}\text{O}(\text{NO}_3^-)$ discrepancy based on this estimate, it may partially explain the discrepancy.

The assumption that $\Delta^{17}\text{O}(\text{O}_3) = 35\text{‰}$ in the troposphere, based on early modeling work [Lyons, 2001], has also been questioned by a recent study [Morin *et al.*, 2007], which employs a range of $\Delta^{17}\text{O}(\text{O}_3) = 25 - 35\text{‰}$ to encompass the lower values of atmospheric measurements. The use of $\Delta^{17}\text{O}(\text{O}_3) = 35\text{‰}$ is consistent with previous interpretation and modeling studies of both $\Delta^{17}\text{O}(\text{NO}_3^-)$ and $\Delta^{17}\text{O}(\text{SO}_4^{2-})$ [Lyons, 2001; Michalski *et al.*, 2003; Alexander *et al.*, 2005] and has been preferred over the use of average measured $\Delta^{17}\text{O}(\text{O}_3)$ values due to potential sampling artifacts from these difficult measurements [Brenninkmeijer *et al.*, 2003; Mauersberger *et al.*, 2003]. Previous $\Delta^{17}\text{O}(\text{NO}_3^-)$ model studies [e.g., Michalski *et al.*, 2003] do not incorporate the recent characterization of $\Delta^{17}\text{O}$ transfer during NO oxidation by O_3 [Savarino *et al.*, 2008], where terminal oxygen atoms of O_3 with $\Delta^{17}\text{O}$ higher than central oxygen atoms [Bhattacharya *et al.*, 2008] are preferentially transferred to NO during oxidation. Improving the earlier model of Michalski *et al.* [2003] to include this $\Delta^{17}\text{O}$ transfer mechanism would result in a systematic overestimation of their atmospheric measurements of $\Delta^{17}\text{O}(\text{NO}_3^-)$, unless the assumed value of $\Delta^{17}\text{O}(\text{O}_3)$ is changed from 35‰ to 25‰. This highlights that the value of tropospheric $\Delta^{17}\text{O}(\text{O}_3)$ remains uncertain. We note, however, that inclusion of updated information on the transfer of $\Delta^{17}\text{O}$ during NO oxidation by ozone and a value of $\Delta^{17}\text{O}(\text{O}_3) = 25\text{‰}$ in our box model would not change our results [Savarino *et al.*, 2008].

3.7.2 Stratospheric Influence on Snowpack Nitrate

The influence of stratospheric air masses, with $\Delta^{17}\text{O}(\text{O}_3)$ up to 5‰ higher than tropospheric ozone [Schueler *et al.*, 1990; Krankowsky *et al.*, 2000; Lyons, 2001; Liang *et al.*, 2006; Zahn *et al.*, 2006], provides another potential explanation for higher than anticipated $\Delta^{17}\text{O}(\text{NO}_3^-)$ observed in summer snow. Vertical mixing of upper troposphere/lower stratosphere air masses was recently shown to influence surface O_3 concentrations at Summit [Dibb *et al.*, 2007; Helmig *et al.*, 2007]. Vertical mixing peaks in summer [Dibb, 2007], consistent with our summer measurement-model $\Delta^{17}\text{O}(\text{NO}_3^-)$ discrepancy. Events bringing high O_3 concentrations from the upper troposphere/lower stratosphere occurred ~ 40% of the time in June 2000 [Helmig *et al.*, 2007]. Assuming 40% mixing of stratospheric air with $\Delta^{17}\text{O}(\text{O}_3)$ of 40‰ [Krankowsky *et al.*, 2000; Lyons, 2001] in summer months, our box model summertime average $\Delta^{17}\text{O}(\text{NO}_3^-)$ (20.9‰) still underestimates the summer average of $\Delta^{17}\text{O}(\text{NO}_3^-)$ measurements (~26.3‰). Because of greater O_3 concentrations in the lower stratosphere/upper troposphere, 40% mixing of air masses may lead to a greater than 40% contribution of stratospheric O_3 to total surface O_3 at Summit. However, we find that to produce model $\Delta^{17}\text{O}(\text{NO}_3^-)$ within error of our lowest summer measurements, 100% stratospheric O_3 with $\Delta^{17}\text{O}(\text{O}_3)$ of 45‰ would be necessary. 100% contribution of stratospheric O_3 to the surface O_3 budget is unlikely, and $\Delta^{17}\text{O}$ of 45‰ for stratospheric O_3 is higher than most model estimates and measurements [Krankowsky *et al.*, 2000; Lyons, 2001; Liang *et al.*, 2006]. While the influence of stratospheric O_3 alone cannot fully explain the summer $\Delta^{17}\text{O}(\text{NO}_3^-)$ measurement-model discrepancy based on our current understanding, it may partially explain the discrepancy.

3.7.3 Reactive Halogen Chemistry

BrO has recently been suggested to have high $\Delta^{17}\text{O}$ [Morin *et al.*, 2007], as it is only produced via reaction of Br with O_3 . Recent measurements indicating BrO concentrations often as high as 1 - 3 pptv [Huey *et al.*, 2007] during early summer at Summit suggest that reactive bromine chemistry may be important for nitrate production during the summer season, not only during the well-studied springtime ozone depletion events [Calvert and Lindberg, 2003; Evans *et al.*, 2003]. To examine the impact of the observed summer BrO abundance on $\Delta^{17}\text{O}(\text{NO}_3^-)$, we incorporate bromine chemistry (equations 11 and 12) into our box model for summer months. We assume $\Delta^{17}\text{O}(\text{BrO}) = 35\text{‰}$, an average summer BrO concentration of 3 pptv, and that the oxygen atom transferred to nitrate during BrONO_2 hydrolysis originates from BrO [Gane *et al.*, 2001; McNamara and Hillier, 2001].

The incorporation of bromine chemistry into our box model requires calculation of production rates of NO_2 and HNO_3 via reactive bromine chemistry (equations 11 and 12, respectively) and consequent alteration of the partition factors described in Section 4.0. The production rate of NO_2 from reaction of BrO and NO (equation 11) is determined as $P_{\text{NO}_2} = k_{\text{BrO}+\text{NO}}[\text{BrO}][\text{NO}]$, with $k_{\text{BrO}+\text{NO}}$ taken from Sander *et al.* [2006]. Partition factor A , the ratio of the rate of NO_2 production via O_3 versus the total rate of NO_2 production, is then altered to reflect this additional NO_2 production path (i.e., P_{NO_2} is added to the denominator of A ; see Table 3.2). Additionally, another partition factor, A_2 , is used to quantify the ratio of NO_2 production via BrO versus total NO_2 production. $\Delta^{17}\text{O}(\text{NO}_2)$ is then calculated as $\Delta^{17}\text{O}(\text{NO}_2) = [A \times \Delta^{17}\text{O}(\text{O}_3)] + [A_2 \times \Delta^{17}\text{O}(\text{BrO})]$. The production rate of HNO_3 (P_{HNO_3}) from hydrolysis of BrONO_2 (equation 12) is determined

as in *Morin et al.* [2007], based on concentrations of BrO and NO₂, the kinetic rate constant of the reaction BrO + NO₂ → BrONO₂ ($k_{\text{BrO}+\text{NO}_2}$) [*Sander et al.*, 2006], the heterogeneous removal rate of BrONO₂ (k_{BrONO_2}) [*Ridley and Orlando*, 2003], and the rate constant of BrONO₂ photolysis (J_{BrONO_2}). The latter is calculated for Summit summer conditions using the TUV (Tropospheric Ultraviolet) radiation model [e.g., *Madronich and Flocke*, 1997]. The nitrate production rate via BrONO₂ hydrolysis is added to the total production rate of nitrate in the box model, to update partition factors *B*, *C*, *D* (i.e., P_{HNO_3} is added to the denominator of partition factors *B*, *C*, *D*; see Table 3.2). Also, another partition factor, *E*, is used to quantify the ratio of the rate of HNO₃ production via BrONO₂ hydrolysis to the rate of total nitrate production. This partition factor is then included in the calculation of $\Delta^{17}\text{O}(\text{NO}_3^-)$ from equation 10:

$$\begin{aligned} \Delta^{17}\text{O}(\text{NO}_3^-)_{\text{net}} = & B\left(\Delta^{17}\text{O}(\text{NO}_3^-)_{\text{PathB}}\right) + C\left(\Delta^{17}\text{O}(\text{NO}_3^-)_{\text{PathC}}\right) \\ & + D\left(\Delta^{17}\text{O}(\text{NO}_3^-)_{\text{PathD}}\right) + E\left(\Delta^{17}\text{O}(\text{NO}_3^-)_{\text{PathE}}\right) \end{aligned} \quad (11)$$

where $\Delta^{17}\text{O}(\text{NO}_3^-)_{\text{PathE}} = \frac{2}{3}\Delta^{17}\text{O}(\text{NO}_2) + \frac{1}{3}\Delta^{17}\text{O}(\text{BrO})$.

With these modifications to our box model, we find that production rates of NO₂ and HNO₃ via reactive bromine chemistry do compete with the dominant NO₂ and HNO₃ production pathways in our box model in summer. For the assumed BrO concentrations of 3 pptv and $\Delta^{17}\text{O}(\text{BrO}) = 35\text{‰}$, we find that summer average $\Delta^{17}\text{O}(\text{NO}_3^-)$ in our box model is increased to 23‰, which explains just over half of the summer measurement-model $\Delta^{17}\text{O}(\text{NO}_3^-)$ discrepancy. Varying $\Delta^{17}\text{O}(\text{BrO})$ over the full range suggested by previous authors (30 - 42‰) [*Morin et al.*, 2007] results in $\pm 1\text{‰}$ variations in box model average summer $\Delta^{17}\text{O}(\text{NO}_3^-)$. We use BrO concentrations at the high end of the range of observations reported for June (3 pptv) [*Huey et al.*, 2007], to calculate a maximum

contribution of bromine chemistry to $\Delta^{17}\text{O}(\text{NO}_3^-)$. However, additional measurements of BrO concentration in summer and characterization of $\Delta^{17}\text{O}(\text{BrO})$ are necessary to better constrain the impact of bromine chemistry on $\Delta^{17}\text{O}(\text{NO}_3^-)$.

3.7.4 Tropospheric Transport of Nitrate

Recent global modeling results suggest that higher summertime $\Delta^{17}\text{O}(\text{NO}_3^-)$ is produced over oceanic regions surrounding Greenland (21 - 27‰) than over the Greenland ice sheet (18‰) [Hastings and Alexander, 2006] due to increased importance of reaction X7 (see Table 3.1) over DMS-emitting oceanic regions. The similarity between summer snowpit $\Delta^{17}\text{O}(\text{NO}_3^-)$ at Summit (22 - 29‰) and global model summertime $\Delta^{17}\text{O}(\text{NO}_3^-)$ results for neighboring regions (21 - 27‰) suggests that regional transport of nitrate can largely explain the discrepancy between our snowpit measurements and box model results. Regional transport of nitrate is expected to be an important snowpack nitrate source at Summit, given the short lifetime of NO_x and Summit's location downwind of North American NO_x emission sources [Kahl *et al.*, 1997; Miller *et al.*, 2002]. Consistent with the seasonality of our snowpit measurement-box model discrepancy, the contrast between $\Delta^{17}\text{O}(\text{NO}_3^-)$ produced over Greenland versus surrounding oceans occurs only in summer [Hastings and Alexander, 2006], when differences between DMS concentrations over the oceans and land are most pronounced.

If regional transport of nitrate is the dominant cause of the discrepancy between our snowpit measurements and box model $\Delta^{17}\text{O}(\text{NO}_3^-)$, then nitrate sources expected to produce $\Delta^{17}\text{O}(\text{NO}_3^-)$ reflecting local oxidation chemistry, such as PAN decomposition in air and post-depositional processing (see also Figure 3.2), must be minor sources of

snowpack nitrate at Summit. Research on the importance of PAN chemistry for snowpack nitrate at Summit is not yet conclusive. An early estimate suggested thermal decomposition of PAN in air could account for the entire flux of nitrate to the snow at Summit [Munger *et al.*, 1999]. However, more recent ground-based measurements at Summit [Ford *et al.*, 2002] suggest that PAN concentrations are up to an order of magnitude lower than those used in the calculation of [Munger *et al.*, 1999]. While several studies suggest that PAN decomposition on snowgrains may also be important for snowpack nitrate concentrations [Bartels-Rausch *et al.*, 2002; Ford *et al.*, 2002; Dassau *et al.*, 2004], attempts to observe and quantify *in situ* decomposition of PAN on snow crystals have been inconclusive [Ford *et al.*, 2002]. Because the chemical mechanism for thermal decomposition of PAN on snowgrains is unknown, it is also unclear whether or not this chemistry would contribute to a local oxidation signal in $\Delta^{17}\text{O}(\text{NO}_3^-)$. Additional research is necessary to clarify both the mechanism and the contribution of PAN decomposition to snowpack nitrate at Summit.

The amount of snowpack nitrate that is post-depositionally processed can be estimated based on recent measurements of the vertical flux of snowpack nitrate photolysis products at Summit [Honrath *et al.*, 2002]. Based on observed snowpack nitrate concentrations of $1.2 \mu\text{M}$ and upward NO_x vertical fluxes of 2.5×10^{12} molecules $\text{m}^{-2} \text{s}^{-1}$, Honrath *et al.* [2002] calculate that 33 days would be required to release 100% of the nitrate in the top 1 cm of the surface snowpack. Assuming a constant accumulation rate of 0.2 cm/day at Summit [e.g., Dibb and Fehsenfeld, 2004] and no permanent loss of nitrate from the snowpack (i.e., all nitrate lost from the snowpack is re-deposited locally), this suggests post-depositional processing of 15% of snowpack nitrate. Further studies of

post-depositional processing of nitrate are needed to confirm this lone estimate made from the study of *Honrath et al.* [2002]. Due to the uncertain contributions of PAN chemistry and post-depositional processing to snowpack nitrate concentrations, dominance of a regional (rather than local) NO_x oxidation source of snowpack nitrate cannot be ruled out. A dominant snowpack nitrate source from regionally-transported nitrate would partially explain the summer measurement-model $\Delta^{17}\text{O}(\text{NO}_3^-)$ discrepancy.

3.8 Sensitivity of $\Delta^{17}\text{O}$ of Nitrate to Oxidation Chemistry

In this section, a box model sensitivity study (Figure 3.4) is used to explore the magnitude of changes in $\Delta^{17}\text{O}(\text{NO}_3^-)$ resulting from varying the importance of individual oxidation pathways of nitrate formation (see also Figure 3.1). Figure 3.4a shows that summer $\Delta^{17}\text{O}(\text{NO}_3^-)$ is uniquely sensitive to changes in the strength of NO oxidation by O_3 in NO_x cycling (i.e., partition factor *A*); equivalent forcing of NO_2 oxidation pathways (i.e., partition factors *B*, *C*, or *D*) have almost no effect on summer $\Delta^{17}\text{O}(\text{NO}_3^-)$. Summer $\Delta^{17}\text{O}(\text{NO}_3^-)$ is, thus, primarily determined by changes in the ratio of O_3 concentration to peroxy radical concentrations, $[\text{O}_3]/([\text{HO}_2]+[\text{RO}_2])$, which sets partition factor *A*. In contrast to summer, winter $\Delta^{17}\text{O}(\text{NO}_3^-)$ (Figure 3.4b) is sensitive to multiple NO_2 oxidation pathways that have opposing effects on $\Delta^{17}\text{O}(\text{NO}_3^-)$. While a factor 9 increase in the strength of nitrate formation by N_2O_5 hydrolysis decreases winter $\Delta^{17}\text{O}(\text{NO}_3^-)$ by 2‰, the same increase in strength of NO_3 oxidation by HC/DMS H-abstraction increases winter $\Delta^{17}\text{O}(\text{NO}_3^-)$ by 3‰. The maximum response of winter $\Delta^{17}\text{O}(\text{NO}_3^-)$ to the factor 9 forcing of any single oxidation pathway is less than half of that in summer (3‰ vs. 8‰). Thus, a factor of 9 change in abundances of total HCs and DMS impacts winter

$\Delta^{17}\text{O}(\text{NO}_3^-)$ half as much as a factor of 9 change in $[\text{O}_3]/([\text{HO}_2]+[\text{RO}_2])$ impacts summer $\Delta^{17}\text{O}(\text{NO}_3^-)$. Figure 3.4c demonstrates that changes in annual mean $\Delta^{17}\text{O}(\text{NO}_3^-)$ cannot be directly attributed to changes in any single oxidant or oxidation pathway. For example, the largest two annual mean $\Delta^{17}\text{O}(\text{NO}_3^-)$ responses to the factor 9 forcing of individual oxidation pathways differ by only 1‰ ($\Delta^{17}\text{O}(\text{NO}_3^-)$ responses to the factor of 9 forcing of NO oxidation by O_3 and NO_3 oxidation by DMS/HC hydrogen-abstraction are 3.5‰ and 2.4‰, respectively). These results support previous work showing that annual mean $\Delta^{17}\text{O}(\text{NO}_3^-)$ is more sensitive to O_3 concentration changes than changes in any other individual chemical species [Lyons, 2001; Michalski *et al.*, 2003], but demonstrate that quantitative interpretation of annual mean $\Delta^{17}\text{O}(\text{NO}_3^-)$ requires knowledge of additional species affecting multiple oxidation pathways (e.g., DMS, HCs, etc.).

The strong sensitivity of summer $\Delta^{17}\text{O}(\text{NO}_3^-)$ to partition factor A (i.e., $[\text{O}_3]/([\text{HO}_2]+[\text{RO}_2])$) reinforces the importance of O_3 , HO_2 , and RO_2 abundances for accurate modeling of $\Delta^{17}\text{O}(\text{NO}_3^-)$. In our box model, we use surface observations of O_3 at Summit and model input of $(\text{HO}_2+\text{RO}_2)$ that is within 10% of summer surface observations [Sjostedt *et al.*, 2007](see Section 4.0 and Table 3.3), limiting errors in $\Delta^{17}\text{O}(\text{NO}_3^-)$ results associated with the calculation of partition factor A . Note that, while GEOS-Chem-derived box model inputs of NO_2 , DMS, and HCs differ more strongly from reported observations (Table 3.3) (observations of NO_3 concentration at Summit are unavailable for model validation), $\Delta^{17}\text{O}(\text{NO}_3^-)$ in summer is insensitive to changes in oxidation paths affected by these species (e.g., NO_2 oxidation by OH and hydrogen-abstraction by HC/DMS, respectively)(see Table 3.2). Validation of wintertime GEOS-Chem-derived box model inputs for species to which winter $\Delta^{17}\text{O}(\text{NO}_3^-)$ is sensitive (e.g.,

DMS, HC, nitrate production via N_2O_5 hydrolysis) is not possible due to the lack of reported winter measurements. While maximum $\Delta^{17}\text{O}(\text{NO}_3^-)$ of measurements (33.7‰) in winter agrees well with results of the box model (33.0‰), validation of these model inputs is necessary to improve our understanding of controls on winter $\Delta^{17}\text{O}(\text{NO}_3^-)$.

The strong sensitivity of summer $\Delta^{17}\text{O}(\text{NO}_3^-)$ to the ratio of O_3 to peroxy radical concentrations also has several implications for the interpretation of $\Delta^{17}\text{O}(\text{NO}_3^-)$ in ice cores. First, the unique summer sensitivity to $[\text{O}_3]/([\text{HO}_2]+[\text{RO}_2])$ suggests that quantitative constraints on NO oxidants may be possible, if summer nitrate could be isolated. Currently, the isolation of summer nitrate in deep ice is problematic due to limits on seasonal dating of deep ice and diffusion of nitrate within the ice. Second, because annual mean $\Delta^{17}\text{O}(\text{NO}_3^-)$ is most sensitive to changes in $[\text{O}_3]/([\text{HO}_2]+[\text{RO}_2])$ in summer, if NO oxidation pathways vary considerably over time, annual mean $\Delta^{17}\text{O}(\text{NO}_3^-)$ in ice cores would reflect these changes more strongly than changes in other oxidation pathways (e.g., N_2O_5 hydrolysis, hydrogen abstraction by HC/DMS). As a result, measurements of ice core $\Delta^{17}\text{O}(\text{NO}_3^-)$ at annual or decadal resolution should not necessarily be interpreted as a reflection of the annual mean oxidative capacity of the atmosphere, as the signal may be dominated by changes in one season. Strong seasonality in the nitrate depositional flux to the snowpack could amplify or attenuate this effect. Neither nitrate concentrations in snow nor snow accumulation rates suggest a strong, consistent seasonal cycle in nitrate deposition in modern climate at Summit [Anklin *et al.*, 1998; Burkhardt *et al.*, 2004; Dibb and Fehsenfeld, 2004 and references therein; Hastings *et al.*, 2004; Dibb *et al.*, 2007]. However, a strong seasonality of nitrate deposition in the past would influence interpretation of ice core $\Delta^{17}\text{O}(\text{NO}_3^-)$.

3.9 Conclusions

We present the first measurements of seasonal variations in polar $\Delta^{17}\text{O}(\text{NO}_3^-)$ from snowpits at Summit, Greenland. We compare these measurements with results from an atmospheric photochemical box model to examine controls on snowpack $\Delta^{17}\text{O}(\text{NO}_3^-)$ and implications for ice core $\Delta^{17}\text{O}(\text{NO}_3^-)$ interpretation. Although measurements and box model results agree well in winter, summer snowpit measurements are consistently 2 - 7‰ higher than predicted by our box model. This indicates important influences on summer $\Delta^{17}\text{O}(\text{NO}_3^-)$ not accounted for in our box model. $\Delta^{17}\text{O}(\text{OH})$ may be higher than assumed in our box model during summer, as a result of reduced isotopic equilibration of OH with atmospheric water vapor under polar conditions. Tropospheric $\Delta^{17}\text{O}(\text{O}_3)$ in summer at Summit may be increased by vertical transport of stratospheric O_3 with higher $\Delta^{17}\text{O}$. Reactive bromine chemistry may contribute significantly to nitrate production in summer, resulting in higher $\Delta^{17}\text{O}(\text{NO}_3^-)$ than predicted by our box model, which does not include bromine chemistry. Lastly, tropospheric transport of nitrate with high summer $\Delta^{17}\text{O}(\text{NO}_3^-)$ from neighboring oceanic regions could also explain the high summer $\Delta^{17}\text{O}(\text{NO}_3^-)$ observed at Summit.

Our box model sensitivity study provides further guidance for interpretation of ice core $\Delta^{17}\text{O}(\text{NO}_3^-)$. Because annual mean $\Delta^{17}\text{O}(\text{NO}_3^-)$ is most sensitive to changes in the ratio of $[\text{O}_3]/([\text{HO}_2]+[\text{RO}_2])$ in summer, the interpretation of annual mean $\Delta^{17}\text{O}(\text{NO}_3^-)$ in ice cores must consider potential impacts of changes in seasonal oxidation chemistry, not only annual mean changes in the oxidative capacity of the atmosphere. For example, in glacial climate, when accumulation in Greenland may be strongest in summer [Krinner *et*

al., 1997; *Werner et al.*, 2000], this sensitivity of annual mean $\Delta^{17}\text{O}(\text{NO}_3^-)$ to summer oxidation chemistry would be amplified. The sensitivity of annual mean $\Delta^{17}\text{O}(\text{NO}_3^-)$ to concentrations of many species in our box model (e.g., HO_2 , DMS, HC, aerosols, etc.), also suggests that constraints on these species would be required in order to quantitatively reconstruct oxidant concentrations from ice core $\Delta^{17}\text{O}(\text{NO}_3^-)$. Quantitative reconstructions of all such species affecting $\Delta^{17}\text{O}(\text{NO}_3^-)$ are not available from ice cores. However, complementary information on oxidation chemistry, NO_x sources, and post-depositional processing is available from related ice core measurements, including $\Delta^{17}\text{O}(\text{SO}_4^{2-})$, $\delta^{15}\text{N}(\text{NO}_3^-)$, $\delta^{18}\text{O}(\text{NO}_3^-)$ [*Alexander et al.*, 2002, 2004; *Hastings et al.*, 2005]. Combining these ice core measurements may eventually permit a consistent, quantitative interpretation of paleoatmospheric oxidation chemistry.

Tables

Table 3.1: Box Model Reactions and Reaction Rate Constants

#	Reaction	Rate Constant	Reference
NO_x Cycling			
X1	NO + O ₃ → NO ₂ + O ₂	$k_1 = (3.0 \times 10^{-12}) \times e^{(-1500/T)}$	[Sander et al., 2006]
X2	NO + HO ₂ → NO ₂ + OH	$k_2 = (3.50 \times 10^{-12}) \times e^{(250/T)}$	[Sander et al., 2006]
X3^a	NO + RO ₂ → NO ₂ + RO	$k_3 = k_2$	[Sander et al., 2006]
NO₂ Oxidation to HNO₃			
X5^b	NO ₂ + OH → HNO ₃	$k_{5\text{low}} = (2.4 \times 10^{-30}) \times (T/300)^{-3.1}$ $k_{5\text{high}} = (2.5 \times 10^{-11}) \times (T/300)^0$ $F_c = 0.6$	[Sander et al., 2006]
X6^c	NO ₂ + O ₃ → NO ₃ + O ₂	$k_6 = (1.2 \times 10^{-13}) \times e^{(2450/T)}$	[Sander et al., 2006]
X7	NO ₃ + DMS → HNO ₃ + products	$k_7 = (1.9 \times 10^{-13}) \times e^{(500/T)}$	[Sander et al., 2006]
X8	NO ₃ + CH ₃ CHO → HNO ₃ + CH ₃ C(O)O ₂	$k_8 = (1.4 \times 10^{-12}) \times e^{(-1860/T)}$	[Atkinson et al., 2006]
X9	NO ₃ + ALK4 → HNO ₃ + (ALK4)O ₂	$k_9 = (2.8 \times 10^{-12}) \times e^{(-3280/T)}$	[Atkinson et al., 2006]
X10	NO ₃ + RCHO → HNO ₃ + (RCO)O ₂	$k_{10} = 6.5 \times 10^{-15}$	[Atkinson et al., 2006]
X11^{b,c}	NO ₃ + NO ₂ ↔ N ₂ O ₅	$k_{11\text{low}} = (2.0 \times 10^{-30}) \times (300/T)^{4.4}$ $k_{11\text{high}} = (1.4 \times 10^{-12}) \times (300/T)^{0.7}$ $F_c = 0.6$	[Sander et al., 2006]
X12^c	N ₂ O ₅ + H ₂ O → 2 HNO ₃	$k_{12} = \left(\frac{a}{D_g} + \frac{4}{v\gamma} \right)^{-1} A$	[Schwartz, 1987]

R represents hydrocarbon chain; DMS represents dimethylsulfide; ALK4 represents ≥ C4 alkanes; RCHO represents >C2 aldehydes

^aFor reaction X3, we use the same reaction rate constant as for reaction X2 because we assume $k_3[RO_2][NO] \approx 0.5 \times k_2[HO_2][NO]$

^bFor reactions X5 and X11, we report low and high pressure limits and F_c , used to calculate pressure and temperature dependent rates for termolecular reactions (see [Sander et al., 2006]).

^cReactions X6 and X11-12 are not directly calculated in our box model, but are derived from global chemical transport model calculations (see text and Table 3.2).

Table 3.2: Calculation of Partition Ratios in Box Model

Partition Factor	Formation Rate of Pathway	Calculation	Notes
A_{num}	$\frac{d[NO_2]_{O_3}}{dt}$	$= k_1[NO][O_3]$	-
A_{denom}	$\frac{d[NO_2]_{total}}{dt}$	$= k_1[NO][O_3] + k_2[NO][HO_2] + 0.5 k_2[NO][HO_2]$	$k_3[NO][RO_2] = 0.5 k_2[NO][HO_2]$
B_{num}	$\frac{d[HNO_3]_{OH}}{dt}$	$= k_5[NO_2][OH]$	-
C_{num}	$\frac{d[HNO_3]_{N_2O_5}}{dt}$	$= k_{12}[N_2O_5]$	<i>GEOS-Chem output</i>
D_{num}	$\frac{d[HNO_3]_{HC/DMS}}{dt}$	$= k_7[DMS][NO_3] + k_8[CH_2O][NO_3] + k_9[CH_3CHO][NO_3] + k_{10}[ALK4][NO_3]$	-
$B.C.D.$ denom	$\frac{d[HNO_3]_{total}}{dt}$	$B_{num} + C_{num} + D_{num}$	-

Subscript 'num' and 'denom' signify 'numerator' and 'denominator', respectively.

Table 3.3: Comparison of Box Model Inputs with Reported Observations

Species	Box Model Inputs	Observations	Location	References
O ₃ (ppbv) ^a	41.6-52.1	41.6-52.1	Summit, Greenland	www.esrl.noaa.gov/gmd/
Temperature (K) ^a	234-264	233-261	Summit, Greenland	K. Schrott, ETH Zurich pers. comm.
OH (molec/cm ³) ^b	4 × 10 ⁶	4 × 10 ⁶ 6.4 × 10 ⁶	Summit, Greenland	<i>Yang et al.</i> , 2002; <i>Sjostedt et al.</i> , 2007
NO (pptv) ^b	5.9	24.7 [0.8-83]	Summit, Greenland	<i>Dibb et al.</i> , 2002; <i>Ford et al.</i> , 2002; <i>Yang et al.</i> , 2002
NO ₂ (pptv) ^b	8.4	32.7 [7.9-55.4]	Summit, Greenland	<i>Dibb et al.</i> , 2002; <i>Ford et al.</i> , 2002; <i>Yang et al.</i> , 2002
(HO ₂ +RO ₂) (molec/cm ³) ^{b†}	2.0 × 10 ⁸	2.2 × 10 ⁸	Summit, Greenland	<i>Sjostedt et al.</i> , 2007
DMS (pptv) ^c	9.5	[D.L. – 1.5]	Summit, Greenland	D. R. Blake, UC Irvine pers. comm.
CH ₃ CHO (pptv) ^d	104	166 [26-459]	Alert, Canada	<i>Boudries et al.</i> , 2002
> C2 aldehydes (pptv) ^{d††}	9.3	18 [D.L.- 110]	Alert, Canada	<i>Boudries et al.</i> , 2002
≥ C4 alkanes (pptv) ^{e††}	127	[21-790]	North Atlantic	<i>Hopkins et al.</i> , 2002

Reported observations and corresponding box model inputs indicated as:

^a range of monthly means over the year 2004, ^b summer mean, ^c June mean, ^d April mean, ^e August mean.

Range of individual measurements indicated in brackets, "D.L." indicates detection limit.

[†] Reported box model input (HO₂+RO₂) reflects assumption RO₂ = ½ HO₂

^{††} Sum of observed C3-C4 aldehydes (*Boudries et al.*, 2002, Table 2); sum of observed C4-C7 alkanes (*Hopkins et al.*, 2002 Table 1)

Figures

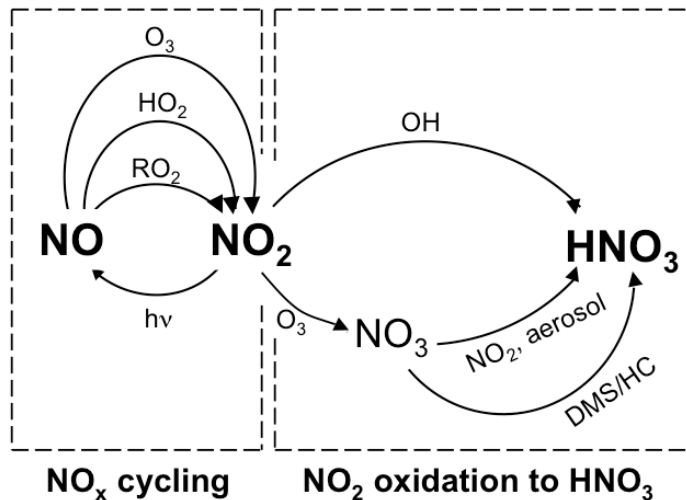


Figure 3.1: Chemistry of nitrate formation in box model calculations. Two oxidation steps are included: NO_x cycling and NO_2 oxidation to HNO_3 . The three oxidation pathways in NO_x cycling are oxidation by O_3 , HO_2 , and RO_2 . The three main oxidation pathways in NO_2 oxidation to HNO_3 are: (1) oxidation via OH ; (2) oxidation by O_3 to NO_3 , reaction of NO_3 with NO_2 , and subsequent hydrolysis of N_2O_5 on water vapor molecules and/or aerosols; and (3) oxidation by O_3 to NO_3 , and abstraction of a hydrogen atom from dimethylsulfide or a hydrocarbon.

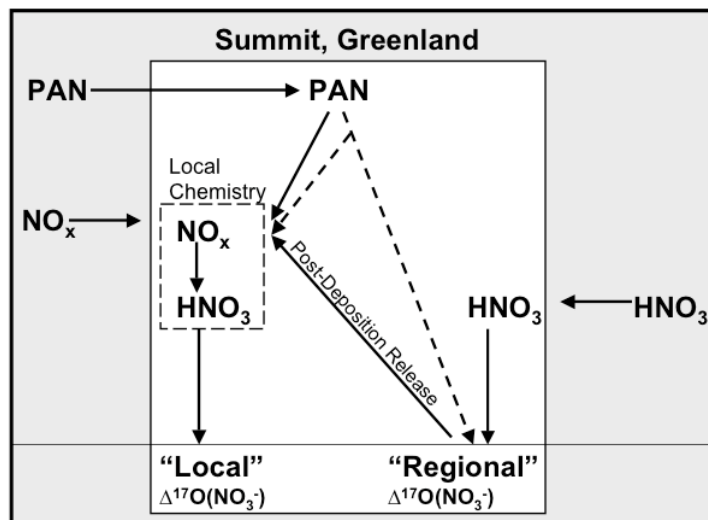


Figure 3.2: Local versus regional oxidation chemistry reflected in $\Delta^{17}\text{O}$ of nitrate. The pathway shown on the right demonstrates that transport of nitrate produced in another region will result in $\Delta^{17}\text{O}(\text{NO}_3^-)$ reflecting oxidation conditions outside the Summit area. The pathway shown on the left demonstrates that NO_x oxidation by local oxidants over Summit will result in $\Delta^{17}\text{O}(\text{NO}_3^-)$ reflecting local oxidation chemistry. Sources of NO_x to the local atmosphere that contribute to this pathway include transport of NO_x , thermal decomposition of peroxyacetyl nitrate (PAN) in ambient air, and post-depositional release of NO_x from snowpack nitrate. It has been suggested that PAN decomposition may also occur on snowgrains; however, the chemical mechanism, and hence the impact of this process on $\Delta^{17}\text{O}(\text{NO}_3^-)$, remains unknown (dotted arrows).

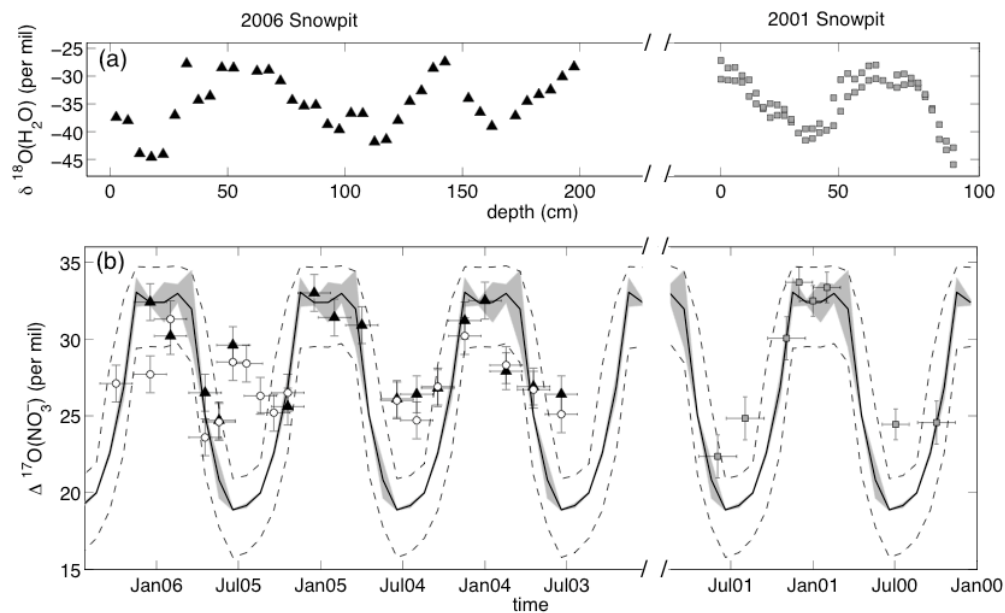


Figure 3.3: (a) 2001 and 2006 snowpit $\delta^{18}\text{O}$ of water versus depth, and (b) 2001 and 2006 snowpit and box model $\Delta^{17}\text{O}$ of nitrate versus time. (The alignment of time and depth on x-axes is meant to provide a visual aid, not a direct correspondence; $\delta^{18}\text{O}$ of water for the 2001 snowpit is reproduced from *Hastings et al.* [2004]) Points indicate measurements of $\delta^{18}\text{O}$ of water and $\Delta^{17}\text{O}$ of nitrate, while the solid line indicates modeled $\Delta^{17}\text{O}$ of nitrate. Gray squares represent measurements for the 2001 snowpit, while black triangles and white circles represent measurements for the 2006 snowpit taken 1 m laterally apart. Vertical error bars indicate the 2σ error of measurements. Horizontal error bars in panel (b) encompass potential dating errors. Model predictions were obtained using a box model for Summit, Greenland, as described in the text. The box model output for $\Delta^{17}\text{O}$ of nitrate in 2004 are replicated here over 2000-2001 and 2003-2006 to provide a visual comparison with snowpit data. The shaded area estimates box model interannual variability, calculated from the 2σ deviation of box model output for years 2001 and 2004. The dashed lines represent the 2σ model error, estimated by propagating uncertainties in reaction rates used.

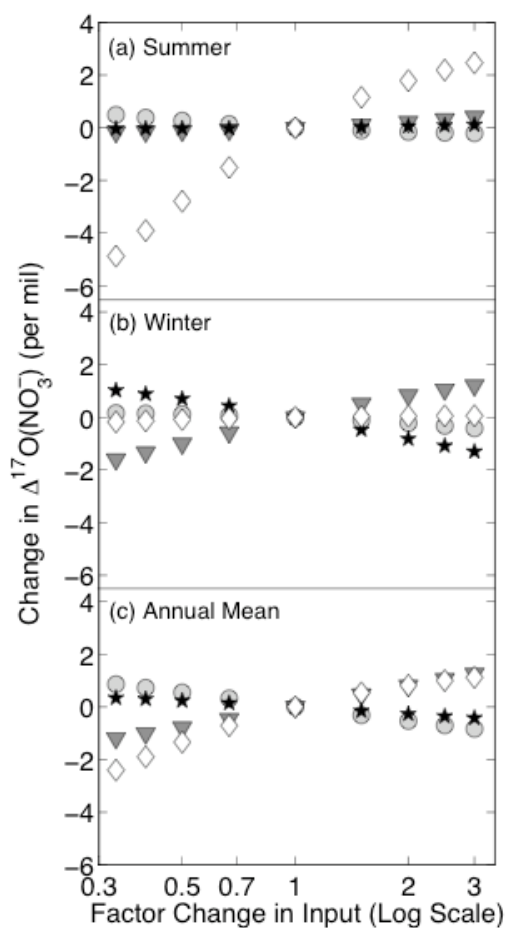


Figure 3.4: Sensitivity of $\Delta^{17}\text{O}(\text{NO}_3^-)$ to various oxidation pathways. We plot the magnitude of change in $\Delta^{17}\text{O}(\text{NO}_3^-)$ resulting from separately forcing the strengths of individual oxidation pathways: NO oxidation to NO_2 by O_3 (white diamond), NO_2 oxidation to HNO_3 by OH (light gray circle), NO_2 oxidation to HNO_3 by H-abstraction from DMS and HCs (dark gray triangle), and NO_2 oxidation to HNO_3 by N_2O_5 hydrolysis (black star). We force each path by factors of 3, 2.5, 2, 1.5, $2/3$, $1/2$, $2/5$, and $1/3$. We show (a) summertime average (June, July, August) $\Delta^{17}\text{O}(\text{NO}_3^-)$, (b) wintertime average (December, January, February) $\Delta^{17}\text{O}(\text{NO}_3^-)$, and (c) annual average $\Delta^{17}\text{O}(\text{NO}_3^-)$.

Chapter 4

Sulfate Sources and Oxidation Chemistry Over the Past ~230 Years from Sulfur and Oxygen Isotopes of Sulfate in a West Antarctic Ice Core

4.1 Summary

The sulfur and oxygen isotopic composition of sulfate in polar ice cores provide information about past changes in atmospheric sulfate sources and formation pathways. We present decadal-scale mean ice core measurements of $\Delta^{17}\text{O}$, $\delta^{34}\text{S}$, $\Delta^{33}\text{S}$, and $\Delta^{36}\text{S}$ of sulfate over the past 230 years from the West Antarctic Ice Sheet (WAIS) Divide deep ice core drill site (WDC05-A). The low mean $\delta^{34}\text{S}$ of non-sea salt sulfate at WAIS Divide ($6.0 \pm 0.2\text{‰}$) relative to East Antarctic coastal and plateau sites likely reflects a combination of stronger influence of volcanogenic and/or stratospheric sulfate with low $\delta^{34}\text{S}$ and the influence of frost flowers on the sea salt sulfate-to-sodium ratio. $\Delta^{33}\text{S}$ and $\Delta^{36}\text{S}$ measurements are all within analytical uncertainty of zero, but do not contradict a contribution of stratospheric sources to background sulfate deposition at WAIS Divide. $\Delta^{17}\text{O}$ of non-sea salt sulfate shows a small but significant increase between the late 1700s ($1.8 \pm 0.2\text{‰}$) and late 1800s ($2.6 \pm 0.2\text{‰}$), but the influence of stratospheric-scale volcanic events on $\Delta^{17}\text{O}$ in the early 1800s remains uncertain. The lack of change in $\Delta^{17}\text{O}$ of non-sea salt sulfate from the mid-1800s to early 2000s ($2.4\text{--}2.6 \pm 0.2\text{‰}$) is consistent with atmospheric chemistry model estimates indicating preindustrial to industrial increases in O_3 as high as 50% and decreases in OH of 20% in the southern polar troposphere, as long as H_2O_2 concentrations also increase by over 50%. An increase in atmospheric H_2O_2 in the southern polar region during the past century is qualitatively supported by H_2O_2 concentration increases in West Antarctic ice cores.

4.2 Introduction

Atmospheric oxidants (e.g., O₃, OH, H₂O₂) are the primary sink for most reduced trace gases that contribute to air pollution and climate change (e.g., CO, CH₄). The abundance of atmospheric oxidants thus limits the atmospheric residence time of reduced trace gases. Global chemical transport and climate models of past atmospheric oxidation chemistry suggest that recent increases in anthropogenic emissions due to biomass burning and fossil fuel combustion have altered the global abundances of tropospheric oxidants [*Martinerie et al.*, 1995; *Wang and Jacob*, 1998; *Mickley et al.*, 1999; *Lelieveld and Dentener*, 2000; *Grenfell et al.*, 2001; *Hauglustaine and Brasseur*, 2001; *Lelieveld et al.*, 2002; *Shindell et al.*, 2003; *Lamarque et al.*, 2005]. While these models agree on the sign of preindustrial to industrial change in O₃ concentration (25% to over 60% increase), estimates of changes in OH concentration vary in both sign and magnitude (+6% to -33%). Improved quantitative constraints on past changes in atmospheric oxidation chemistry are necessary to improve global atmospheric chemistry and climate model predictions of future changes in response to additional increases in anthropogenic emissions.

The oxygen isotope anomaly ($\Delta^{17}\text{O} \approx \delta^{17}\text{O} - (0.52 \times \delta^{18}\text{O})$ where $\delta^x\text{O} = ((^x\text{O}/^{16}\text{O})_{\text{sample}} / (^x\text{O}/^{16}\text{O})_{\text{standard}}) - 1$, with $x = 17$ or 18 and Vienna Standard Mean Ocean Water (V-SMOW) is the standard) of sulfate in ice cores shows promise for empirical validation of model-calculated paleoatmospheric oxidation chemistry [*Alexander et al.*, 2002; *Alexander et al.*, 2004]. The $\Delta^{17}\text{O}$ of sulfate ($\Delta^{17}\text{O}(\text{SO}_4^{2-})$) reflects the relative importance of different oxidants (e.g., O₃, OH, H₂O₂) in the production of sulfate because the oxidants transfer different $\Delta^{17}\text{O}$ to oxidation products [*Savarino et al.*, 2000]. Ice

core records of $\Delta^{17}\text{O}(\text{SO}_4^{2-})$ and $\Delta^{17}\text{O}(\text{NO}_3^-)$ over the past three centuries from Site A, Greenland show a strong perturbation attributed to high levels of biomass burning in North America in the late 1800s/early 1900s, with a weaker perturbation due to increasing fossil fuel burning emissions during the 20th century [Alexander *et al.*, 2004]. Global climate and chemical transport models suggest that oxidation chemistry of the southern hemisphere has also been perturbed on this timescale, with O_3 increasing by 10-50% and OH decreasing by 0-20% in the southern polar low to mid-troposphere (>600 mb; 60 – 90°S) due to increases in NO_x (= NO+NO₂), CO, and CH₄ concentrations since the preindustrial period [Wang and Jacob, 1998; Mickley *et al.*, 1999; Shindell *et al.*, 2003]. However, no observational record from the southern hemisphere has yet been available to validate these model estimates.

Sulfur isotope data provide information complementary to $\Delta^{17}\text{O}(\text{SO}_4^{2-})$ concerning the sources of sulfate (e.g., sea salt, marine biogenic, terrigenous and biogenic continental, and volcanogenic emissions). Sulfur isotopes are reported as $\delta^x\text{S}(\text{‰}) = \left(\frac{(^x\text{S}/^{32}\text{S})_{\text{sample}}}{(^x\text{S}/^{32}\text{S})_{\text{standard}}} - 1 \right) \times 1000$, where $x = 33, 34$, or 36 and Canyon Diablo Triolite (CDT) is the standard. $\delta^{34}\text{S}$ analysis has been widely used to examine partitioning between various tropospheric sources of sulfate, which produce sulfate with different $\delta^{34}\text{S}$ [Nielsen, 1974; Rees *et al.*, 1978; Calhoun *et al.*, 1991; Nielsen *et al.*, 1991; McArdle and Liss, 1995; Patris *et al.*, 2000a]. Measurements of $\Delta^{33}\text{S}$ (= $\delta^{33}\text{S} - 1000 \times (1 + \delta^{34}\text{S}/1000)^{0.515} - 1$ (‰)) and $\Delta^{36}\text{S}$ (= $\delta^{36}\text{S} - 1000 \times (1 + \delta^{34}\text{S}/1000)^{0.190} - 1$ (‰)) can be used to investigate the importance of stratospheric sources of sulfate, since only sulfate of stratospheric origin is expected to have non-zero $\Delta^{33}\text{S}$ and $\Delta^{36}\text{S}$ in the present day [Farquhar *et al.*, 2000; Farquhar *et al.*, 2001].

Here, we present the first ice core measurements of the complete isotopic composition of sulfate ($\Delta^{17}\text{O}$, $\delta^{34}\text{S}$, $\Delta^{33}\text{S}$, $\Delta^{36}\text{S}$) spanning the preindustrial-industrial transition (late 1700s to present) from the West Antarctic Ice Sheet (WAIS) Divide ($79^{\circ}28.1'\text{S}$ $112^{\circ}5.2'\text{W}$). The isotopic composition of sulfate is expected to be preserved during burial in the polar icepack, enabling ice core measurements to be used to reconstruct paleoatmospheric conditions [Lloyd, 1968; Patris *et al.*, 2000a; Alexander *et al.*, 2002, 2003]. We use sulfur isotopes of sulfate to estimate relative sulfate source contributions in West Antarctica and examine differences relative to East Antarctica. We interpret ice core $\Delta^{17}\text{O}(\text{SO}_4^{2-})$ quantitatively using the partitioning between tropospheric sulfate formation pathways at WAIS Divide extracted from a global chemical transport model for the present day [Alexander *et al.*, 2009b]. We then examine whether ice core $\Delta^{17}\text{O}(\text{SO}_4^{2-})$ changes are consistent with reported tropospheric oxidant abundance changes from model simulations of the preindustrial atmosphere.

4.3 Controls on Isotopic Composition of Atmospheric Sulfate

Atmospheric $\Delta^{17}\text{O}(\text{SO}_4^{2-})$ reflects the composition of its precursor SO_2 , which is in isotopic equilibrium with water vapor ($\Delta^{17}\text{O} = 0\text{‰}$), and the transfer of isotopically anomalous oxygen atoms ($\Delta^{17}\text{O} > 0\text{‰}$) from oxidants during SO_2 oxidation to sulfate [Savarino *et al.*, 2000]. Due to the large $\Delta^{17}\text{O}$ of tropospheric ozone (25-35‰) [Schueler *et al.*, 1990; Krankowsky *et al.*, 1995; Johnston and Thiemens, 1997; Krankowsky *et al.*, 2000; Lyons, 2001], SO_2 oxidation by ozone on cloud water droplets or aerosols is expected to produce large tropospheric $\Delta^{17}\text{O}(\text{SO}_4^{2-})$ of 6.3-8.8‰, following the observation that ozone transfers one-quarter of its $\Delta^{17}\text{O}$ signature to sulfate during SO_2

oxidation [Savarino *et al.*, 2000]. The transfer of $\Delta^{17}\text{O}$ from O_3 to sulfate found by this early laboratory study [Savarino *et al.*, 2000] may be an underestimate since it did not examine the potential for preferential transfer of the terminal oxygen atom of ozone (i.e., O-O-Q) that is enriched in $\Delta^{17}\text{O}$ [Bhattacharya *et al.*, 2008], which occurs in other O_3 oxidation processes (e.g., $\text{NO}+\text{O}_3$ [Savarino *et al.*, 2008]). In-cloud SO_2 oxidation by H_2O_2 is expected to produce $\Delta^{17}\text{O}(\text{SO}_4^{2-})$ of 0.5-1‰, based on the $\Delta^{17}\text{O}$ of tropospheric H_2O_2 (1-2‰) and the observed transfer of one-half the $\Delta^{17}\text{O}$ signature of H_2O_2 during SO_2 oxidation [Savarino and Thiemens, 1999; Savarino *et al.*, 2000]. By contrast, due to rapid oxygen isotope exchange between OH and water vapor [Dubey *et al.*, 1997; Lyons, 2001], gas-phase SO_2 oxidation by OH is expected to produce $\Delta^{17}\text{O}(\text{SO}_4^{2-}) = 0\text{‰}$ throughout most of the troposphere, although it has been suggested that $\Delta^{17}\text{O}$ of OH may be non-zero in the dry polar atmosphere [Morin *et al.*, 2007]. Partitioning between the dominant tropospheric sulfate production pathways is controlled by oxidant abundances, cloud liquid water content, which affects the relative importance of gas- and aqueous-phase reactions, and pH, which affects the partitioning of dissolved SO_2 as SO_3^{2-} with which O_3 reacts most rapidly [Chameides, 1984; Calvert *et al.*, 1985]. Sulfate produced in the stratosphere is expected to reflect gas-phase SO_2 oxidation by stratospheric OH [Alexander *et al.*, 2002; Savarino *et al.*, 2003a], which has non-zero $\Delta^{17}\text{O}$ (2-45‰) [Lyons, 2001; Liang *et al.*, 2006; Zahn *et al.*, 2006]. However, some episodic stratospheric-scale volcanic events cause stratospheric SO_2 injection large enough to titrate stratospheric OH, leading to sulfate formation via a different oxidation pathway producing $\Delta^{17}\text{O}(\text{SO}_4^{2-}) = 0\text{‰}$ [Savarino *et al.*, 2003a]. Atmospheric transport and deposition processes fractionate oxygen isotopes of sulfate according to mass-dependent

relationships ($\delta^{17}\text{O} \approx 0.52 \times \delta^{18}\text{O}$) [Matsuhisa *et al.*, 1978], such that $\Delta^{17}\text{O}(\text{SO}_4^{2-})$ values are conserved.

Atmospheric $\delta^{34}\text{S}$ of sulfate reflects the relative contributions of different sources of sulfate [Calhoun *et al.*, 1991; McArdle *et al.*, 1998; Patris *et al.*, 2000a; Alexander *et al.*, 2003; Pruett *et al.*, 2004; Jonsell *et al.*, 2005] because different tropospheric sulfur sources display different ranges of $\delta^{34}\text{S}$ (Figure 4.1). While $\delta^{34}\text{S}$ of sea salt sulfate is well-constrained to 21‰ [Rees *et al.*, 1978], and estimates of $\delta^{34}\text{S}$ of marine biogenic sources fall within a small range (14-22‰) [Calhoun *et al.*, 1991; McArdle *et al.*, 1998; Patris *et al.*, 2000b], the range of possible $\delta^{34}\text{S}$ from tropospheric- and stratospheric-scale volcanism is comparatively large (-6 to +17‰) [Nielsen *et al.*, 1991; Baroni *et al.*, 2008] (Figure 4.1). Terrigenous continental material also displays a large range of $\delta^{34}\text{S}$ values (0-20‰) [Nielsen *et al.*, 1991]. Background (non-volcanic) sulfate from the lower stratospheric reservoir has been estimated to have $\delta^{34}\text{S}$ of 2.6‰ [Castleman *et al.*, 1973], although values as low as -24‰ have been observed higher in the stratosphere [Castleman *et al.*, 1974]. The influence of sulfur isotope fractionation in different sulfur oxidation pathways [Saltzman *et al.*, 1983; Tanaka *et al.*, 1994] and Rayleigh fractionation during transport must also be considered in order to deduce tropospheric sulfur source partitioning from $\delta^{34}\text{S}$.

Sulfur isotope anomalies of sulfate reflect the influence of stratospheric sources of sulfate. Unlike $\delta^{34}\text{S}$, $\Delta^{33}\text{S}$ and $\Delta^{36}\text{S}$ are conserved during atmospheric transport, deposition, and oxidation processes, which fractionate sulfur isotopes following mass-dependent relationships ($\delta^{33}\text{S} = 1000 \times (1 + \delta^{34}\text{S}/1000)^{0.515} - 1$ and $\delta^{36}\text{S} = 1000 \times (1 + \delta^{34}\text{S}/1000)^{0.190} - 1$). Non-zero sulfur isotope anomalies are produced during UV

photolysis of SO₂ at wavelengths less than 310 nm, which occur only above the tropopause [Farquhar *et al.*, 2000; Farquhar *et al.*, 2001]. Studies of ice core sulfate [Alexander *et al.*, 2003; Savarino *et al.*, 2003b; Baroni *et al.*, 2008], atmospheric sulfate aerosols [Romero & Thiemens, 2003; Mather *et al.*, 2006], and sulfate in terrestrial gypsum deposits [Bindeman *et al.*, 2007] reinforce the interpretation of $\Delta^{33}\text{S}$ as a tracer for stratospheric sulfur sources, although the utility of $\Delta^{36}\text{S}$ as a stratospheric tracer is limited by large analytical uncertainties [Alexander *et al.*, 2003; Baroni *et al.*, 2008].

4.4 Methods

Isotopic and major ion concentration measurements were made on a 70-meter ice core drilled at WAIS Divide during the summer 2005 field campaign, WDC05-A (78° 55' S, 114° 13' W). Cores were shipped frozen to the U.S. National Ice Core Laboratory (NICL) in Colorado, where core allocations for sulfate isotope and major ion analyses were cut with a bandsaw in a clean lab at -22°C. To avoid analysis of contaminants, only sections of ice taken from the inner portion of the core were used for isotopic analysis of sulfate and major ions. Inner core sections were kept frozen until analysis.

Analysis of major trace elements of WDC05-A was performed at the Desert Research Institute following methods adapted from *McConnell* [2002], in which an ice core melter is linked with a continuous-flow analysis system (CFA) to provide real-time measurements of major elements with high depth-resolution (centimeter-scale). Sulfur, sodium, calcium, magnesium, and a range of other elements are measured with two Thermo-Finnegan Element2 high-resolution inductively coupled plasma mass spectrometers (HR-ICP-MS) operating in parallel. The depth-age relationship for the 70-

meter core (“WDC05-A:1”) is derived from sodium and total sulfur concentrations and has uncertainty of ± 1 year [Banta *et al.*, 2008; Mischler *et al.*, 2009]. Total sulfur concentrations of WDC05-A were used to determine the volume of ice needed to achieve ~ 5 μmol of sulfate per sample for isotopic analysis. We assume dissolved sulfate is $\sim 70\%$ of total sulfur at WAIS Divide following comparisons between ion chromatographic (IC) and ICPMS duplicate measurements of a nearby WAIS Divide ice core (WDC05-Q, 79°28.05’S, 112°5.14’W) (personal communication J. Cole-Dai). Analytical uncertainties of sodium, sulfur, calcium, and magnesium measurements are $\pm 5\%$ (1σ).

For isotopic analysis of sulfate, sample silver sulfate was prepared following methods described by [Kunasek *et al.*, 2008] and isotope analysis of silver sulfate was performed following the methods of [Savarino *et al.*, 2001]. At the University of Washington, ice was melted and combined in clean 4 L beakers, then evaporated to ~ 50 mL in a class 100 clean hood in order to concentrate sulfate. Concentrated samples were then pumped through an automated system for separation of anions by ion chromatography (IonPac® AS19 separation column (4 x 250 mm); 7-15 mM KOH) and conversion of sulfate to silver form (Ag_2SO_4) by cation exchange (AMMS® III membrane (4 mm); 2.5 mM Ag_2SO_4 regenerant) [i.e., Kunasek *et al.*, 2008]. Silver sulfate fractions were dried and shipped to University of California - San Diego, where they were transferred to and dried in quartz boats. In a continuous-flow system [i.e., Savarino *et al.*, 2001], the Ag_2SO_4 was pyrolyzed to release O_2 and SO_2 , which are then trapped separately. The SO_2 is further converted to SF_6 , following established procedures [Farquhar *et al.*, 2000]. The three oxygen isotopologues of O_2 and four sulfur

isotopologues of SF₆ were then analyzed using Finnegan MAT 251 and 252 isotope ratio mass spectrometers (IRMS), respectively.

The contribution of sea salt (ss) and non-sea salt (nss) sulfate were determined from Na⁺ and SO₄²⁻ concentrations following $[\text{SO}_4^{2-}]_{\text{total}} = [\text{SO}_4^{2-}]_{\text{nss}} + k[\text{Na}^+]$, where k is the sulfate-to-sodium ratio of sea salt. (Hereafter the subscripts “_{nss}” and “_{ss}” refer to non-sea salt and sea salt sulfate, respectively.) We calculate the sea salt contribution using $k = 0.25$, following the majority of previous sulfur isotope studies in Antarctica [Alexander *et al.*, 2002, 2003; Patris *et al.*, 2000a; Pruett *et al.*, 2004]. We also estimate a minimum sea salt contribution using the lowest estimated coastal Antarctic k value of 0.07 [Wagenbach *et al.*, 1998], which reflects a strong contribution of frost flowers with depleted k to total sea salt deposition. Isotopic values are corrected for the influence of sea salt by mass balance, assuming $\Delta^{17}\text{O}(\text{SO}_4^{2-})_{\text{ss}} = 0\text{‰}$ [Alexander *et al.*, 2002] and $\delta^{34}\text{S}_{\text{ss}} = 21\text{‰}$ [Rees *et al.*, 1978]. We also estimate the sulfate contribution of terrigenous continental material (“_{terr}”) (e.g., from crustal CaSO₄ and MgSO₄) using non-sea salt calcium and non-sea salt magnesium concentrations following $[\text{SO}_4^{2-}]_{\text{terr}} = m[\text{Ca}^{2+}]_{\text{nss}}$ and $[\text{SO}_4^{2-}]_{\text{terr}} = n[\text{Mg}^{2+}]_{\text{nss}}$, where m and n are the average sulfate-to-calcium and sulfate-to-magnesium ratios in crustal material (~0.18 and 0.24, respectively) [e.g., Patris *et al.*, 2002]. Non-sea salt concentrations of magnesium and calcium are determined using known ratios of calcium-to-sodium (0.038) and magnesium-to-sodium (0.12) in seawater, as described in Legrand *et al.* [1997].

Ice core $\Delta^{17}\text{O}(\text{SO}_4^{2-})_{\text{nss}}$ is interpreted using the fractional contribution of different atmospheric sulfate production pathways (e.g., oxidation by OH, H₂O₂, O₃) calculated using a global chemical transport model of the present day (1989-1991) described by

Alexander et al. [2009b] (GEOS-Chem, www-as.harvard.edu/chemistry/trop/geos/). The model bulk cloud water pH is set to 5.0, at the high end of the range found in marine stratocumulus clouds (3.3-5.0 [*Faloona, 2009*]), since the remote southern polar region is expected to be impacted minimally by anthropogenic emissions that acidify precipitation. The global model results at the WAIS Divide site include the influence of tropospheric transport. In addition to the three dominant SO₂ oxidation pathways described in Section 4.3, the global model also considers SO₂ oxidation by O₃ on sea salt aerosols [*Alexander et al., 2005*] and by O₂ catalyzed by transition metals (Fe(III), Mn(II)) in calculating sulfate oxidation pathway partitioning [*Alexander et al., 2009b*].

4.5 Ice Core Observations and Model Results

Ice core measurements of multi-decadal mean sulfur and oxygen isotopes are shown in Table 4.1 and Figure 4.2, along with sodium and sulfate concentrations. Each sample represents 27-44 years of snow accumulation. Total sulfur measurements (Figure 4.2a) show a strong (56%) increase in the early 1800s sample, which spans two stratospheric-scale volcanic eruptions recorded in other Antarctic ice cores: an unknown volcanic eruption in 1810 and Mt. Tambora in 1815 [*Dai et al., 1991; ColeDai et al., 1997*]. The contribution of sea salt sulfate to total sulfate (not shown) derived from sulfur and sodium measurements (Figure 4.2a) depends strongly on k (14-21% for $k = 0.25$ and 4-6% for $k = 0.07$), but varies little temporally ($\pm 1\%$) with the exception of the early 1800s, where the stratospheric-scale volcanic influence reduces the contribution of sea salt (5% and 2% for $k = 0.25$ and 0.07, respectively). The contribution of terrigenous continental material to total sulfate (not shown) is $<2\%$ throughout the ice core record

whether non-sea salt calcium or non-sea salt magnesium is used as the conservative tracer. Raw $\delta^{34}\text{S}$ measurements vary between 5.5-9.3‰ (mean 6.8‰), with a maximum in the late-1800s/early-1900s and relative minima during the early 1800s stratospheric-scale volcanic influence and the late 1900s (Figure 4.2b). $\delta^{34}\text{S}_{\text{nss}}$ shows similar temporal structure (Figure 4.2c), but the absolute values depend strongly on k (mean 3.1‰ for $k = 0.25$ versus mean 5.9‰ for $k = 0.07$). $\Delta^{33}\text{S}$ and $\Delta^{36}\text{S}$ measurements (Figure 4.2d-4.2e) are all within 2σ analytical uncertainty of zero, consistent with mass-dependent chemical processes. Due to the large analytical uncertainties of the $\Delta^{36}\text{S}$ measurement and consequent ambiguities in its use as a stratospheric sulfur source tracer [Baroni *et al.*, 2008], we focus on $\Delta^{33}\text{S}$ measurements in our discussion. Both raw $\Delta^{17}\text{O}(\text{SO}_4^{2-})$ measurements (Figure 4.2f) and corrected $\Delta^{17}\text{O}(\text{SO}_4^{2-})_{\text{nss}}$ (Figure 4.2g) show small but significant changes during the ice core record, with lower $\Delta^{17}\text{O}(\text{SO}_4^{2-})_{\text{nss}}$ in the late 1700s (2.2 and 1.8‰ for $k = 0.25$ and 0.07, respectively) and consistent higher $\Delta^{17}\text{O}(\text{SO}_4^{2-})_{\text{nss}}$ from the late 1800s to 2005 (mean $\Delta^{17}\text{O}(\text{SO}_4^{2-})_{\text{nss}} = 3.0$ and 2.5‰ for $k = 0.25$ and 0.07 respectively from 1880-2005). The global model of the present day finds that sulfate reaching WAIS Divide is predominantly produced by in-cloud SO_2 oxidation by H_2O_2 (68%), with in-cloud SO_2 oxidation by O_3 and gas-phase SO_2 oxidation by OH comprising the bulk of the remaining sulfate production (16% and 12%, respectively). SO_2 oxidation by O_3 on sea salt aerosols and by O_2 with transition metal catalysis are minor contributors to total sulfate reaching WAIS Divide (<1%, <4%, respectively) in the model, as is primary sulfate from anthropogenic emissions (<1%).

4.6 Sulfur Isotopes and Source Partitioning

4.6.1 $\delta^{34}\text{S}$ and Sulfur Sources

Figure 4.1 summarizes spatial differences in ice core $\delta^{34}\text{S}_{\text{nss}}$ throughout the Antarctic, including the findings of the present study. The range of ice core $\delta^{34}\text{S}_{\text{nss}}$ (1.2-6.2‰, $k = 0.25$) from WAIS Divide is consistent with recent measurements of another West Antarctic ice core from the RIDSA campaign (-0.7 to +6.8‰, $k = 0.25$)(78.73°S, 116.33°W) [Pruett *et al.*, 2004] (Figure 4.1), confirming that West Antarctic background $\delta^{34}\text{S}_{\text{nss}}$ is significantly lower than reported ice core measurements from both East Antarctic coastal and plateau sites (minimum $\delta^{34}\text{S}_{\text{nss}} = 11$ ‰) [Patris *et al.*, 2000a; Alexander *et al.*, 2003; Jonsell *et al.*, 2005; Baroni *et al.*, 2008] (Figure 4.1). The fact that $\delta^{34}\text{S}_{\text{nss}}$ is lower at the inland WAIS ice core sites than either coastal or inland sites in East Antarctica suggests that Antarctic $\delta^{34}\text{S}_{\text{nss}}$ spatial variability is not simply a function of distance from the oceanic source region. Following previous authors [Jonsell *et al.*, 2005], we thus infer that spatial variability in fractionation during atmospheric transport (i.e., Rayleigh fractionation) and sulfate oxidation, which primarily reflect distance from the coast, are not the dominant processes responsible for the low $\delta^{34}\text{S}_{\text{nss}}$ at WAIS Divide. We thus suggest instead that the lower $\delta^{34}\text{S}_{\text{nss}}$ values of West relative to East Antarctica is due to a relatively stronger contribution of sulfur sources with low $\delta^{34}\text{S}$, such as local Antarctic tropospheric volcanism and/or background stratospheric influence, as also suggested by Pruett *et al.* [2004]. Although the influence of a continental sulfate source may also help explain the low $\delta^{34}\text{S}_{\text{nss}}$ at WAIS, our estimate based on ice core non-sea salt calcium and non-sea salt magnesium concentrations suggests this contribution is negligible (<2%).

A large difference in volcanic and/or stratospheric sulfate contributions between West and East Antarctica is possible given differences in meteorology and topography. Of the 26 Antarctic region volcanoes listed by the Smithsonian volcano database (<http://www.volcano.si.edu/world/>) as active within the Holocene, all are within or bordering on the western hemisphere in proximity to regions of cyclogenesis that impact West Antarctica [King & Turner, 1997; Simmonds *et al.*, 2003; Carrasco *et al.*, 2003]. Due to the lower mean elevation of West versus East Antarctica, cyclone activity penetrates further into West Antarctica [King & Turner, 1997], potentially leading to a greater contribution of volcanogenic sources to sulfate deposition in this region. However, only a few Antarctic volcanoes are known to be currently active (i.e., Mt. Erebus, Deception Island, and Buckle Island), and most studies suggest a minor contribution of volcanic sources to sulfate deposition in Antarctica (max 10-30%) [Radke, 1982; Rose *et al.*, 1985; Zreda-Gostynska *et al.*, 1997; Minkin *et al.*, 1998], although these studies suggest that large spatial heterogeneity is possible. The greater influence of cyclone activity on West relative to East Antarctica may also lead to greater entrainment of stratospheric air in the troposphere, due to tropopause folding associated with strong cyclone activity [Danielsen, 1968; Holton *et al.*, 1985; Stohl *et al.*, 2003]. However, because Antarctic cyclones also entrain marine air from the oceanic regions in which they originate, the net influence of cyclonic activity in West Antarctica on the contribution of stratospheric sources to sulfate deposition is ambiguous. Most studies of sulfur source attribution in East Antarctica are consistent with negligible influence of stratospheric sources [Patris *et al.*, 2000a; Alexander *et al.*, 2003], but a study in coastal East and West

Antarctica could not rule out a stratospheric sulfur contribution as high as 10-33%

[*Minkin et al.*, 1998].

We can estimate whether volcanogenic and stratospheric sulfur source contributions are a reasonable explanation for the low $^{34}\text{S}_{\text{nss}}$ at WAIS Divide, using the following quantitative representation of sulfur source $\delta^{34}\text{S}$ signature mixing [e.g., *Patris et al.*, 2000a]:

$$\delta^{34}S_{\text{total}} = \delta^{34}_{\text{ss}} + \delta^{34}_{\text{nss}} = f_{\text{ss}} \delta^{34}_{\text{ss}} + f_{\text{mb}} \delta^{34}_{\text{mb}} + f_{\text{v}} \delta^{34}_{\text{v}} + f_{\text{s}} \delta^{34}_{\text{s}} \quad (1)$$

where f and δ^{34} are the fractional contribution and corresponding $\delta^{34}\text{S}$ of each sulfur source, including sea salt (ss), non-sea salt (nss), marine biogenic (mb), volcanic (v) and stratospheric (s). Mean background $\delta^{34}\text{S}_{\text{nss}}$ in the WAIS ice core is 3.7‰ ($k = 0.25$), when the data point of the early 1800s (1810-1837) is omitted due to the known stratospheric-scale volcanic influence during this time [*Dai et al.*, 1991; *Cole-Dai et al.*, 1997]. Assuming marine biogenic $\delta^{34}\text{S}$ of 18.6‰ [*Patris et al.*, 2000a] and a low range of -6 to 0‰ to represent both volcanic and stratospheric source $\delta^{34}\text{S}$ signatures [*Baroni et al.*, 2008], this mean background ice core $\delta^{34}\text{S}_{\text{nss}}$ value suggests that the combination of volcanic and stratospheric sulfur sources contributes at least 60-80% of West Antarctic surface sulfate deposition. Thus, contributions of stratospheric and volcanic sources of sulfur higher than those estimated in previous Antarctic studies (i.e., ~33% stratospheric, ~30% volcanic) [*Radke*, 1982; *Rose et al.*, 1985; *Minkin et al.*, 1998] are necessary to explain the low $\delta^{34}\text{S}_{\text{nss}}$ of West relative to East Antarctica through differences in sulfur source contributions alone.

Another factor that may contribute to the low $\delta^{34}\text{S}_{\text{nss}}$ of West Antarctica is the calculation of the sea salt fraction. It has been suggested that frost flowers formed on sea ice, not the open ocean surface, are the dominant source of sea salt across the Antarctic continent [Wolff *et al.*, 2003]. Processing of sea salt during frost flower production depletes sulfur relative to sodium abundances, potentially leading to an underestimate of non-sea salt sulfate concentrations if k of open ocean water is assumed (i.e., $k = 0.25$) [Wagenbach *et al.*, 1998; Rankin *et al.*, 2002]. This effect is most noticeable at coastal locations, where unrealistic negative non-sea salt concentrations are frequently found unless very low k is used (e.g., 0.07, 0.09 [Wagenbach *et al.*, 1998; Jonsell *et al.*, 2005]) to reflect the influence of sulfate-depletion in frost flowers. Using a low k of 0.07 instead of the classical open ocean value ($k = 0.25$) results in an increase of over 3‰ in mean background ice core $\delta^{34}\text{S}_{\text{nss}}$ (see Table 4.1, Figure 4.1; again, data point of 1810-1837 omitted). Using the higher mean background $\delta^{34}\text{S}_{\text{nss}}$ ($k = 0.07$) in equation 1 and following similar assumptions as above ($\delta^{34}_{\text{mb}} = 18.6\text{‰}$, $\delta^{34}_{\text{v}} = \delta^{34}_{\text{s}} = -6$ to 0‰), the calculated minimum contribution of volcanic and stratospheric sulfur sources to background West Antarctic sulfate deposition is reduced to 49-65%. A depletion of heavy isotopes during frost flower formation, resulting in a reduced sea salt $\delta^{34}\text{S}$ source signature, would further reduce the calculated contribution of volcanic and stratospheric sources, but has not yet been investigated. The low West Antarctic $\delta^{34}\text{S}$ can thus be explained through a combination of frost flower influence on sea salt composition and strong stratospheric and volcanogenic sulfur sources near the maximum of previous coastal and East Antarctic source attribution studies (i.e., maximum ~30% stratospheric, ~30% volcanic) [Radke, 1982; Rose *et al.*, 1985; Minkin *et al.*, 1998]. Refinements to $\delta^{34}\text{S}$

source signature characterization (e.g., $\delta^{34}\text{S}$ of frost flowers) and/or additional independent estimates of sulfate source attribution (e.g., using aerosol ^{10}Be or ^{35}S [Minkin *et al.*, 1998; Lee & Thiemens, 2001]) are critical for improving quantitative sulfate source attribution at WAIS Divide. Temporal changes in ice core $\delta^{34}\text{S}_{\text{nss}}$ at WAIS Divide (Figure 4.2) are thus best interpreted qualitatively, with higher (lower) $\delta^{34}\text{S}_{\text{nss}}$ reflecting greater marine biogenic (stratospheric and/or volcanic) influence.

4.6.2 $\Delta^{33}\text{S}$ and Stratospheric Sulfur Sources

Ice core $\Delta^{33}\text{S}$ measurements of background sulfate at WAIS are all within analytical uncertainty of zero ($\pm 0.2\text{‰}$) (Figure 4.2d & 4.2e), indicating no detectable stratospheric influence on sulfate deposited at WAIS Divide. This finding is identical to previous background $\Delta^{33}\text{S}$ measurements in East Antarctica [Alexander *et al.*, 2003; Savarino *et al.*, 2003b; Baroni *et al.*, 2007; Baroni *et al.*, 2008] and consistent with other Antarctic background sulfate source attribution studies that suggest dominance of tropospheric sulfate sources [Legrand and Mayewski, 1997; Bergin *et al.*, 1998; Minikin *et al.*, 1998]. However, the lack of significant perturbation to the WAIS ice core $\Delta^{33}\text{S}$ record during the early 1800s period of known stratospheric-scale volcanic influence necessitates explanation. Assuming that 36% of the sulfate in the early 1800s sample is from episodic stratospheric-scale volcanism, if 30% of the remaining 64% of background sulfate is also of stratospheric origin, as suggested by our ice core $\delta^{34}\text{S}_{\text{nss}}$ analysis (Section 4.6.1), then stratospheric sources may contribute a total of up to 55% to sulfate of this sample (i.e., 36% episodic stratospheric-scale volcanic, 19% background stratospheric, 45% background tropospheric). In fact, despite the dominance (>60%) of

stratospheric-scale volcanogenic sulfate in ice core $\Delta^{33}\text{S}$ samples in a recent East Antarctic study [Baroni *et al.*, 2008], only half of the eight stratospheric-scale volcanic events identified displayed significant non-zero $\Delta^{33}\text{S}$ before background sulfate contributions were corrected. This may be explained by considering that a stratospheric-scale volcanic event increases both tropospheric and stratospheric SO_2 . Our results along with the findings of Baroni *et al.* [2008] suggest that background measurements of ice core $\Delta^{33}\text{S}$ within analytical uncertainty of zero cannot yet be used to rule out significant contributions of stratospheric sources (e.g., approaching 60%). The lack of significant non-zero $\Delta^{33}\text{S}$ throughout the WAIS ice core records, including the early 1800s sample, thus does not contradict a contribution of stratospheric sources to background sulfate deposited at WAIS Divide, as suggested by our ice core $\delta^{34}\text{S}_{\text{nss}}$ analysis (e.g., 25-30%)(Section 4.6.1).

4.7 Oxygen Isotopes and Oxidation Chemistry

4.7.1 Ice Core Variations in $\Delta^{17}\text{O}$ of Sulfate

The robustness of the increasing trend in WAIS ice core $\Delta^{17}\text{O}(\text{SO}_4^{2-})_{\text{nss}}$ between the late 1700s and late 1800s is weak due to the influence of stratospheric-scale volcanism in the early 1800s (1810-1837 sample). Previous work indicates that stratospheric-scale volcanic $\Delta^{17}\text{O}(\text{SO}_4^{2-})$ signatures can vary greatly, with relatively small amounts of stratospheric SO_2 injection resulting in high $\Delta^{17}\text{O}(\text{SO}_4^{2-})$ (e.g., Pinatubo 1991 eruption: $\Delta^{17}\text{O}(\text{SO}_4^{2-}) = 4.3\text{‰}$) due to the dominance of stratospheric SO_2 oxidation by OH with high $\Delta^{17}\text{O}$, and relatively large amounts of stratospheric SO_2 injection resulting in dominant stratospheric SO_2 oxidation by secondary oxidation pathways with low $\Delta^{17}\text{O}$

after OH is titrated (e.g., 1259 eruption of unknown origin: $\Delta^{17}\text{O}(\text{SO}_4^{2-}) = 0.7\text{‰}$) [Savarino *et al.*, 2003a]. Because only these two stratospheric-scale volcanic eruptions have been measured for ice core $\Delta^{17}\text{O}(\text{SO}_4^{2-})$ signatures, a reliable empirical relationship between stratospheric SO_2 injection amount and a stratospheric-scale volcanic $\Delta^{17}\text{O}(\text{SO}_4^{2-})$ cannot yet be determined. The influence of the two early 1800s stratospheric-scale volcanic eruptions (1815 Tambora eruption and 1810 eruption of unknown origin) on ice core $\Delta^{17}\text{O}(\text{SO}_4^{2-})_{\text{nss}}$ of the early 1800s sample thus cannot be strongly constrained. The perceived trend of increasing $\Delta^{17}\text{O}(\text{SO}_4^{2-})_{\text{nss}}$ between the late 1700s and late 1800s is thus driven by only one data point (late 1700s). Several independent records, including terrestrial charcoal records [Marlon *et al.*, 2009] and ice core $\delta^{13}\text{C}\text{H}$ [Ferretti *et al.*, 2005], suggest a Holocene minimum in global biomass burning in the late 1600s and 1700s, followed by an increase into the late 1800s. The low ice core $\Delta^{17}\text{O}(\text{SO}_4^{2-})_{\text{nss}}$ in the late 1700s (2.2 and 1.8‰ for $k = 0.25$ and 0.07) is coincident with the minimum of the global biomass burning records for the past 2,000 years; however, extending the ice core record of $\Delta^{17}\text{O}(\text{SO}_4^{2-})_{\text{nss}}$ further back in time is necessary for clarifying and quantifying the relationship between these events. In the model-based interpretation that follows, we thus focus on the ice core $\Delta^{17}\text{O}(\text{SO}_4^{2-})_{\text{nss}}$ record from the mid-1800s to early 2000s, which corresponds to the period examined by most model studies of preindustrial to industrial change in atmospheric chemistry.

4.7.2 Model Interpretation of Ice Core $\Delta^{17}\text{O}$ of Sulfate (1837-2005)

Here, we examine whether the lack of change in ice core $\Delta^{17}\text{O}(\text{SO}_4^{2-})_{\text{nss}}$ from 1837-2005 is consistent with model estimates of preindustrial to industrial changes in

tropospheric oxidant concentrations in the southern polar region. Previous chemical transport and climate model studies have found preindustrial to industrial increases of 10-50% for O₃ and decreases of 0-20% for OH (i.e., $([X]_{\text{PD}} - [X]_{\text{PI}}) / [X]_{\text{PI}}$ for $X = \text{O}_3$ or OH) [Wang and Jacob, 1998; Mickley et al., 1999; Shindell et al., 2003] in the lower to middle troposphere (600-1000 mb) of the southern polar region (60-90°S). A more recent model simulation that generally agrees with these earlier literature values of preindustrial to industrial changes in O₃ and OH in the lower to middle polar troposphere (20-28% increase in O₃; 8-20% decrease in OH) suggests that H₂O₂ increases by 40-52% from the preindustrial to the industrial in this region [Sofen et al., in prep.]. An increase in atmospheric H₂O₂ in the southern polar region during the past century is qualitatively supported by ice core H₂O₂ concentration increases observed at high accumulation sites near the WAIS Divide, although additional work is needed to quantify an atmospheric H₂O₂ change from these records [Frey et al., 2006]. We calculate the change in tropospheric $\Delta^{17}\text{O}(\text{SO}_4^{2-})_{\text{nss}}$ associated with these model predictions of preindustrial to industrial change in tropospheric oxidant concentrations and compare this with the ice core $\Delta^{17}\text{O}(\text{SO}_4^{2-})_{\text{nss}}$ record from 1837-2005.

4.7.2.1 Assumptions in Calculation of $\Delta^{17}\text{O}(\text{SO}_4^{2-})_{\text{nss}}$ Change

In our calculation of preindustrial to industrial change in tropospheric $\Delta^{17}\text{O}(\text{SO}_4^{2-})_{\text{nss}}$, we assume no significant change in cloud water pH consistent with the lack of change in WAIS ice core records of sulfate (see Figure 4.2a), the dominant control on cloud water pH, and preliminary measurements of mineral acidity in East Antarctic ice cores (personal communication, D. Pasteris). We also assume negligible preindustrial to

industrial changes in cloud liquid water abundance in the southern polar region. Although recent warming (since 1957) in West Antarctica has been significant ($>0.1^\circ\text{C}/\text{decade}$) [Steig *et al.*, 2009], the overall trend over the last two centuries is much smaller ($\sim 0.2^\circ/\text{century}$) and may not be statistically significant [Schneider *et al.*, 2006; Schneider and Steig, 2008]. We do not examine the influence of stratospheric sulfate formation in our calculation of preindustrial to industrial change in $\Delta^{17}\text{O}(\text{SO}_4^{2-})_{\text{nss}}$ because of uncertainties in both the contribution of stratospheric sulfate sources at WAIS (see Section 4.6.1-4.6.2) and the $\Delta^{17}\text{O}(\text{SO}_4^{2-})_{\text{nss}}$ of background stratospheric sulfate sources, which has never been constrained by measurements. Our analysis thus addresses whether the lack of change in ice core $\Delta^{17}\text{O}(\text{SO}_4^{2-})_{\text{nss}}$ is consistent with model estimates of changes in tropospheric oxidants alone.

4.7.2.2 Calculation of Preindustrial to Industrial Tropospheric $\Delta^{17}\text{O}(\text{SO}_4^{2-})_{\text{nss}}$ Change

Results from the global model for the contributions of various tropospheric SO_2 oxidation pathways to sulfate production at WAIS uphold previous interpretation of background tropospheric $\Delta^{17}\text{O}(\text{SO}_4^{2-})_{\text{nss}}$ in Antarctica [Alexander *et al.*, 2002; Savarino *et al.*, 2003a] as largely controlled by the transfer of isotopic signatures from the three dominant tropospheric SO_2 oxidation pathways: gas-phase oxidation by OH and in-cloud oxidation by O_3 and H_2O_2 . Other tropospheric formation pathways contribute minimally to sulfate deposited at this location ($<4\%$ total). We can thus interpret tropospheric $\Delta^{17}\text{O}(\text{SO}_4^{2-})_{\text{nss}}$ following a simple isotope mass balance:

$$\Delta^{17}\text{O}(\text{SO}_4^{2-})_{\text{nss}} = (f_{\text{OH}} \times \Delta^{17}\text{O}_{\text{OH}}) + (f_{\text{H}_2\text{O}_2} \times \Delta^{17}\text{O}_{\text{H}_2\text{O}_2}) + (f_{\text{O}_3} \times \Delta^{17}\text{O}_{\text{O}_3}) \quad (2)$$

where f_{OH} , $f_{H_2O_2}$, and f_{O_3} represent the fractional contributions of sulfate production by each oxidant, and $\Delta^{17}O_{OH}$, $\Delta^{17}O_{H_2O_2}$, and $\Delta^{17}O_{O_3}$ represent the signatures of sulfate produced by each oxidant. We assume $\Delta^{17}O_{OH}$, $\Delta^{17}O_{H_2O_2}$, and $\Delta^{17}O_{O_3}$ values of 0‰, 0.9‰, and 8.8‰ respectively, following previous model studies [Alexander *et al.*, 2005, 2009b]. Using the normalized fractional contribution of the three dominant tropospheric oxidation pathways (f_{OH} , $f_{H_2O_2}$, and $f_{O_3} = 12\%$, 71% , and 17%) derived from the global model for WAIS Divide for the present day [Alexander *et al.*, 2009b], we calculate tropospheric $\Delta^{17}O(SO_4^{2-})_{nss} = 2.1\%$ for the present day following equation 2. The estimated present day tropospheric $\Delta^{17}O(SO_4^{2-})_{nss}$ is lower than ice core $\Delta^{17}O(SO_4^{2-})_{nss}$ measurements of the industrial period (3.0 and 2.5‰ for $k = 0.25$ and 0.07 , respectively). The use of a low k value, to reflect the potentially important influence of frost flowers on the WAIS sea salt budget, reduces but does not eliminate the difference between calculated tropospheric and ice core $\Delta^{17}O(SO_4^{2-})_{nss}$ in the industrial period. The influence of a background stratospheric sulfate contribution with high $\Delta^{17}O(SO_4^{2-})$ may explain part or all of the difference between calculated tropospheric $\Delta^{17}O(SO_4^{2-})_{nss}$ and ice core $\Delta^{17}O(SO_4^{2-})_{nss}$ measurements of the industrial period. Uncertainties in the relative contributions and isotopic signatures of different sulfate formation pathways (i.e., f_{OH} , $f_{H_2O_2}$, f_{O_3} , $\Delta^{17}O_{OH}$, $\Delta^{17}O_{H_2O_2}$, and $\Delta^{17}O_{O_3}$) may also contribute to the difference between our calculated tropospheric $\Delta^{17}O(SO_4^{2-})_{nss}$ and ice core $\Delta^{17}O(SO_4^{2-})_{nss}$ measurements of the industrial period, but impact our calculation of preindustrial to industrial $\Delta^{17}O(SO_4^{2-})_{nss}$ change minimally, as detailed later in Section 4.7.2.3.

We estimate the preindustrial sulfate contribution by each oxidant (f_x , $x = OH$, H_2O_2 , O_3) by scaling the baseline industrial (present-day) f_x extracted from the global

model ($f_{H_2O_2}$, f_{O_3} , f_{OH} of 71%, 17%, 12%) by the ratio of preindustrial to industrial abundance for each oxidant, as long as all f_x values are re-normalized:

$$f_{x,PI} = \frac{f_{x,PD} \times r_x}{\sum (f_{x,PD} \times r_x)} \quad (3)$$

where r_x is the ratio of preindustrial (PI) to present day (PD) abundances of oxidants ($r_x = [X]_{PI}/[X]_{PD}$). In this approach, we treat f_{OH} , $f_{H_2O_2}$, and f_{O_3} as equivalent to the sulfate production rate by each oxidant normalized to the total sulfate production rate in the industrial period, thereby inherently assuming that the lifetimes of sulfate produced by different oxidants are similar, consistent with results from previous global model studies [Alexander *et al.*, 2005, 2009b]. We then make use of the fact that the sulfate production rate by each oxidant is linearly related to the oxidant abundance. The mean preindustrial to industrial tropospheric oxidant changes ($[X]_{PD}-[X]_{PI} / [X]_{PI}$) estimated for the model of Sofen *et al.* [in prep.] correspond to preindustrial to industrial oxidant concentration ratios ($r_x = [X]_{PI}/[X]_{PD}$) of 0.68, 0.80, and 1.17 for $r_{H_2O_2}$, r_{O_3} , r_{OH} , respectively. Using these preindustrial to industrial oxidant ratios and estimating preindustrial f_x and $\Delta^{17}O(SO_4^{2-})_{nss}$ via equations 3 and 2 results in estimated preindustrial tropospheric $\Delta^{17}O(SO_4^{2-})_{nss}$ that differs negligibly (<0.01‰) from the calculated present day value (2.1‰).

The calculated tropospheric $\Delta^{17}O(SO_4^{2-})_{nss}$ does not differ between preindustrial and industrial, despite significant changes in tropospheric oxidant abundances, due to the counterbalancing influence of different oxidant changes on $\Delta^{17}O(SO_4^{2-})_{nss}$. The contribution of H_2O_2 to sulfate production is lower in the preindustrial relative to the industrial, while contributions of O_3 and OH to sulfate production are higher in the preindustrial relative to the industrial. The relative contribution of O_3 to sulfate production in the preindustrial is slightly higher than in the industrial (18% versus 17%),

despite lower preindustrial O₃ abundances, due to the substantially lower contribution of H₂O₂ to sulfate production in the preindustrial relative to the industrial (63% versus 71%). The slightly higher sulfate production by O₃ in the preindustrial would elevate preindustrial $\Delta^{17}\text{O}(\text{SO}_4^{2-})_{\text{nss}}$ relative to the industrial, but is offset by the combination of higher sulfate production by OH and lower production by H₂O₂ in the preindustrial, which would reduce preindustrial $\Delta^{17}\text{O}(\text{SO}_4^{2-})_{\text{nss}}$ relative to the industrial. Our model-based calculation of preindustrial to industrial tropospheric $\Delta^{17}\text{O}(\text{SO}_4^{2-})_{\text{nss}}$ changes thus indicates that preindustrial to industrial model oxidant concentration changes of *Sofen et al.* [in prep] are independently consistent with the lack of change observed in the ice core $\Delta^{17}\text{O}(\text{SO}_4^{2-})_{\text{nss}}$ record. No temporal changes in other atmospheric conditions (e.g., stratospheric sulfate contribution or isotopic signature, tropospheric cloud water pH or cloud liquid water abundance) are necessary to reconcile these tropospheric model oxidant changes with the ice core $\Delta^{17}\text{O}(\text{SO}_4^{2-})_{\text{nss}}$ record.

We can use the same calculation (equations 2 and 3) to estimate H₂O₂ changes necessary for reported model preindustrial to industrial O₃ and OH changes in the lower atmosphere (< 600 mb) of the southern polar region [*Wang and Jacob, 1998; Mickley et al., 1999; Shindell et al., 2003*] to be consistent with deviations of tropospheric $\Delta^{17}\text{O}(\text{SO}_4^{2-})_{\text{nss}}$ within analytical uncertainty ($\pm 0.2\text{‰}$) over this time period. We estimate that deviations of tropospheric $\Delta^{17}\text{O}(\text{SO}_4^{2-})_{\text{nss}}$ within analytical uncertainty are consistent with the minimum reported preindustrial to industrial O₃ increase of 10% and OH decrease of 10% in the lower atmosphere (> 600 mb) of the southern polar region [i.e., *Shindell et al., 2003*] only if H₂O₂ changes remain between -9% and +49%. The maximum reported preindustrial to industrial O₃ increase of 50% and OH decrease of

20% in the southern polar region [Mickley *et al.*, 1999] is consistent with deviations of tropospheric $\Delta^{17}\text{O}(\text{SO}_4^{2-})_{\text{nss}}$ within analytical uncertainty only if H_2O_2 increases between 51-170%. Tropospheric $\Delta^{17}\text{O}(\text{SO}_4^{2-})_{\text{nss}}$ may have changed by greater than $\pm 0.2\text{‰}$ from preindustrial to industrial and still be consistent with the ice core $\Delta^{17}\text{O}(\text{SO}_4^{2-})_{\text{nss}}$ record, if there is a significant background stratospheric sulfate source at WAIS Divide that does not vary temporally. A significant background stratospheric source would reduce the sensitivity of ice core $\Delta^{17}\text{O}(\text{SO}_4^{2-})_{\text{nss}}$ to changes in tropospheric $\Delta^{17}\text{O}(\text{SO}_4^{2-})_{\text{nss}}$. Our estimated ranges of preindustrial to industrial tropospheric H_2O_2 changes necessary to reconcile tropospheric model O_3 and OH changes with deviations of ice core $\Delta^{17}\text{O}(\text{SO}_4^{2-})_{\text{nss}}$ within analytical uncertainty ($<\pm 0.2\text{‰}$) are therefore conservative.

4.7.2.3 Uncertainties in Calculation of $\Delta^{17}\text{O}(\text{SO}_4^{2-})_{\text{nss}}$ Change

In Section 4.7.2.2, we focus on the calculated preindustrial to industrial change in tropospheric $\Delta^{17}\text{O}(\text{SO}_4^{2-})_{\text{nss}}$, rather than the magnitude of $\Delta^{17}\text{O}(\text{SO}_4^{2-})_{\text{nss}}$ at each time, because the change in $\Delta^{17}\text{O}(\text{SO}_4^{2-})_{\text{nss}}$ is less sensitive to uncertainties in the boundary conditions of our calculation (i.e., f_{OH} , $f_{\text{H}_2\text{O}_2}$, f_{O_3} , $\Delta^{17}\text{O}_{\text{OH}}$, $\Delta^{17}\text{O}_{\text{H}_2\text{O}_2}$, and $\Delta^{17}\text{O}_{\text{O}_3}$ in equation 2). Uncertainties in these boundary conditions may partially contribute to the difference between calculated tropospheric $\Delta^{17}\text{O}(\text{SO}_4^{2-})_{\text{nss}}$ and ice core $\Delta^{17}\text{O}(\text{SO}_4^{2-})_{\text{nss}}$ measurements of the industrial period. Uncertainties of $\pm 4\%$ in the model-derived relative contributions of sulfate formation by O_3 , OH, and/or H_2O_2 (i.e., f_{OH} , $f_{\text{H}_2\text{O}_2}$, and f_{O_3}) can explain the difference (0.4‰ , $k = 0.07$) between calculated tropospheric $\Delta^{17}\text{O}(\text{SO}_4^{2-})_{\text{nss}}$ and ice core $\Delta^{17}\text{O}(\text{SO}_4^{2-})_{\text{nss}}$ of the industrial period. Increasing the $\Delta^{17}\text{O}$ transferred to sulfate by O_3 and/or OH in our calculation (i.e., $\Delta^{17}\text{O}_{\text{OH}} = 0\text{‰}$ and/or

$\Delta^{17}O_{O_3} = 8.8\text{‰}$) by 1-3‰ can also reconcile the difference (0.4-0.9‰ for $k = 0.07$ -0.25 respectively) between calculated tropospheric $\Delta^{17}O(\text{SO}_4^{2-})_{\text{nss}}$ and ice core $\Delta^{17}O(\text{SO}_4^{2-})_{\text{nss}}$ and is consistent with previous work suggesting these values are underestimates (see Section 4.3). Neither of these changes to our boundary conditions results in a significant ($>\pm 0.2\text{‰}$) calculated preindustrial to industrial tropospheric $\Delta^{17}O(\text{SO}_4^{2-})_{\text{nss}}$ change associated with the model results of *Sofen et al.* [in prep.], nor do they alter the sign of the bounds we estimate in order for preindustrial to industrial H_2O_2 changes associated with reported model O_3 and OH changes to be consistent with tropospheric $\Delta^{17}O(\text{SO}_4^{2-})_{\text{nss}}$ changes of less than $\pm 0.2\text{‰}$. Estimated bounds for preindustrial to industrial H_2O_2 changes associated with reported model O_3 and OH changes are altered by a maximum of 8% by uncertainties of $\pm 4\%$ in the relative contributions of sulfate formation by O_3 , OH, and/or H_2O_2 . The calculation of bounds for preindustrial to industrial H_2O_2 changes associated with reported model O_3 and OH changes should be revisited if new constraints become available concerning polar $\Delta^{17}O$ of sulfate produced by O_3 and or OH.

4.8 Conclusions

We have presented the first ice core record of the complete isotopic composition of sulfate from WAIS Divide, Antarctica spanning the preindustrial to industrial time period (~1775-2005). Sulfate concentrations show no trend over the WAIS Divide ice core record, although a strong spike is apparent in the early 1800s sample due to two stratospheric-scale volcanic eruptions during this time (1815 Tambora eruption and 1810 eruption of unknown origin). Mean $\delta^{34}\text{S}_{\text{nss}}$ values from the WAIS Divide ice core are significantly lower than both inland and coastal East Antarctic ice core measurements of

late Holocene age, consistent with other West Antarctic observations [Pruett *et al.*, 2004]. Because the observed pattern of spatial variability in Antarctic $\delta^{34}\text{S}_{\text{nss}}$ does not follow a spatial pattern similar to that expected for either variations in sulfate transport pathways or oxidation chemistry, we rule these out as dominant causes of the relatively low $\delta^{34}\text{S}_{\text{nss}}$ at WAIS Divide, following previous authors [Jonsell *et al.*, 2005]. The sulfate contribution of terrigenous continental material at WAIS Divide is estimated to be low (<2%) and cannot account for the low ice core $\delta^{34}\text{S}_{\text{nss}}$. We thus suggest the low $\delta^{34}\text{S}_{\text{nss}}$ in West Antarctica reflects a combination of stronger influence of volcanogenic and stratospheric sulfate with low $\delta^{34}\text{S}$ in West relative to East Antarctica and the influence of frost flowers on the sea salt sulfate-to-sodium ratio (i.e., k). A low sulfate-to-sodium ratio, reflecting frost flower influence, also helps explain differences between $\Delta^{17}\text{O}(\text{SO}_4^{2-})_{\text{nss}}$ of the WAIS ice core and $\Delta^{17}\text{O}(\text{SO}_4^{2-})_{\text{nss}}$ calculated based on global chemical transport model results [Alexander *et al.*, 2009b], reinforcing this explanation of the low $\delta^{34}\text{S}$ values at WAIS. $\Delta^{33}\text{S}$ remains within analytical uncertainty of zero throughout the WAIS Divide ice core record, consistent with previous East Antarctic ice core $\Delta^{33}\text{S}$ measurements [Alexander *et al.*, 2003]. However, the lack of significant non-zero $\Delta^{33}\text{S}$ throughout the WAIS ice core records does not contradict a contribution of stratospheric sources for background sulfate deposited at WAIS Divide, as suggested by our ice core $\delta^{34}\text{S}_{\text{nss}}$ analysis.

Ice core $\Delta^{17}\text{O}(\text{SO}_4^{2-})_{\text{nss}}$ at WAIS Divide shows no significant changes ($\pm 0.2\text{‰}$) throughout the late 1800s to the early 2000s. This contrasts with the ice core $\Delta^{17}\text{O}(\text{SO}_4^{2-})_{\text{nss}}$ record from Greenland, which shows a strong perturbation during this time (2‰) [Alexander *et al.*, 2004], consistent with a stronger influence of anthropogenic activity on

northern hemisphere oxidant abundances. Data extracted from a previously published global chemical transport model study [Alexander *et al.*, 2009b] indicates that tropospheric $\Delta^{17}\text{O}(\text{SO}_4^{2-})_{\text{nss}}$ at WAIS Divide can be interpreted following a simple mixing of three primary tropospheric sulfate production pathways: SO_2 oxidation by OH, H_2O_2 , and O_3 . Using this mixing relationship, we show that the lack of significant change in ice core $\Delta^{17}\text{O}(\text{SO}_4^{2-})_{\text{nss}}$ between the mid-1800s and early-2000s is consistent with preindustrial to industrial increases in tropospheric O_3 and H_2O_2 and a decrease in OH suggested by recent global chemical transport modeling work [Sofen *et al.*, in prep.]. We also estimate that maximum atmospheric chemistry model estimates of preindustrial-industrial O_3 concentration increases (50%) and OH decreases (20%) in the southern polar region [Mickley *et al.*, 1999] are consistent with changes in tropospheric $\Delta^{17}\text{O}(\text{SO}_4^{2-})_{\text{nss}}$ within analytical uncertainty only if H_2O_2 also increases by over 50%. An increase in atmospheric H_2O_2 in the southern polar region during the past century is qualitatively supported by ice core H_2O_2 concentration increases in West Antarctica, but additional work is needed to quantify atmospheric H_2O_2 concentration changes from these records [Frey *et al.*, 2006]. Future atmospheric model studies of preindustrial to industrial change can use Antarctic ice core $\Delta^{17}\text{O}(\text{SO}_4^{2-})_{\text{nss}}$ measurements as constraints for relative changes in tropospheric oxidant concentrations following the simple mixing relationship described here.

Tables

Table 4.1: Raw and Non-Sea Salt $\delta^{34}\text{S}$ and $\Delta^{17}\text{O}$ of Sulfate from WAIS Divide

Start Year	End Year	$\delta^{34}\text{S}$	$\Delta^{17}\text{O}$	$k = 0.25$			$k = 0.07$		
				f_{ss}	$\delta^{34}\text{S}_{\text{nss}}$	$\Delta^{17}\text{O}_{\text{nss}}$	f_{ss}	$\delta^{34}\text{S}_{\text{nss}}$	$\Delta^{17}\text{O}_{\text{nss}}$
		(‰)	(‰)	(%)	(‰)	(‰)	(%)	(‰)	(‰)
2005	1978	5.5	2.4	19.4	1.8	2.9	5.4	4.6	2.5
1978	1951	7.2	2.2	21.5	3.4	2.8	6.0	6.3	2.4
1924	1880	9.3	2.3	20.7	6.2	3.0	5.8	8.6	2.5
1880	1837	8.0	2.5	21.5	4.4	3.1	6.0	7.2	2.6
1837	1810	4.0	2.3	14.3	1.2	2.6	4.0	3.3	2.4
1810	1774	6.6	1.7	20.6	2.9	2.2	5.8	5.7	1.8

Figures

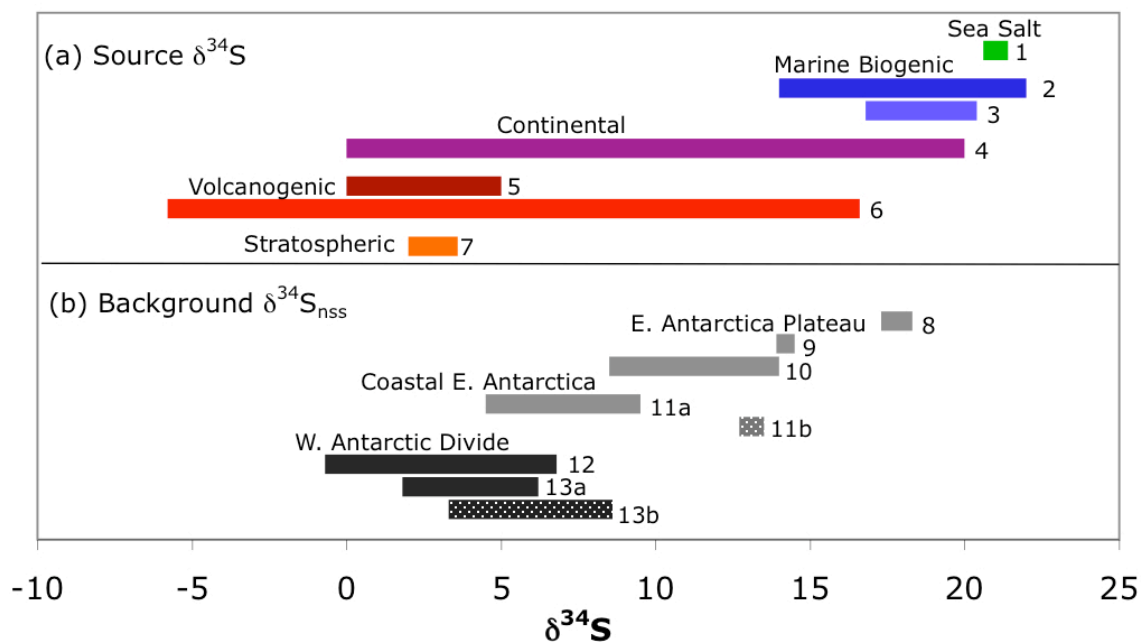


Figure 4.1: (a) Literature summary of reported $\delta^{34}\text{S}$ ranges of sulfur sources including (1) sea salt [Rees *et al.*, 1978], (2) marine biogenic theoretical range [Calhoun *et al.*, 1991], (3) marine biogenic at South Pole, Antarctica [Patris *et al.*, 2000a], (4) continental [Nielsen *et al.*, 1991], (5) volcanogenic [Nielsen *et al.*, 1991], (6) volcanogenic at South Pole and Dome C, Antarctica [Baroni *et al.*, 2007, 2008], (7) background stratospheric [Castleman *et al.*, 1973]. Where source signature estimates are derived from a single measurement, the range indicates 2σ analytical uncertainties. (b) Summary of measured background $\delta^{34}\text{S}_{\text{nss}}$ ranges from Antarctic ice core studies including measurements from (8) South Pole [Patris *et al.*, 2000a], (9) Vostok and Dome C [Alexander *et al.*, 2003], (10) Dome A [Jonsell *et al.*, 2005], (11a) coastal East Antarctica [Jonsell *et al.*, 2005], (12) West Antarctic RIDSA core site [Pruett *et al.*, 2004], (13a) WAIS Divide (this study). All studies report $\delta^{34}\text{S}_{\text{nss}}$ based on $k = 0.25$ (see text for k definition). Dotted bars reflect the calculation of $\delta^{34}\text{S}_{\text{nss}}$ based on different k , including (11b) $k = 0.09$ in coastal Antarctica [Jonsell *et al.*, 2005] and (13b) $k = 0.07$ in this study.

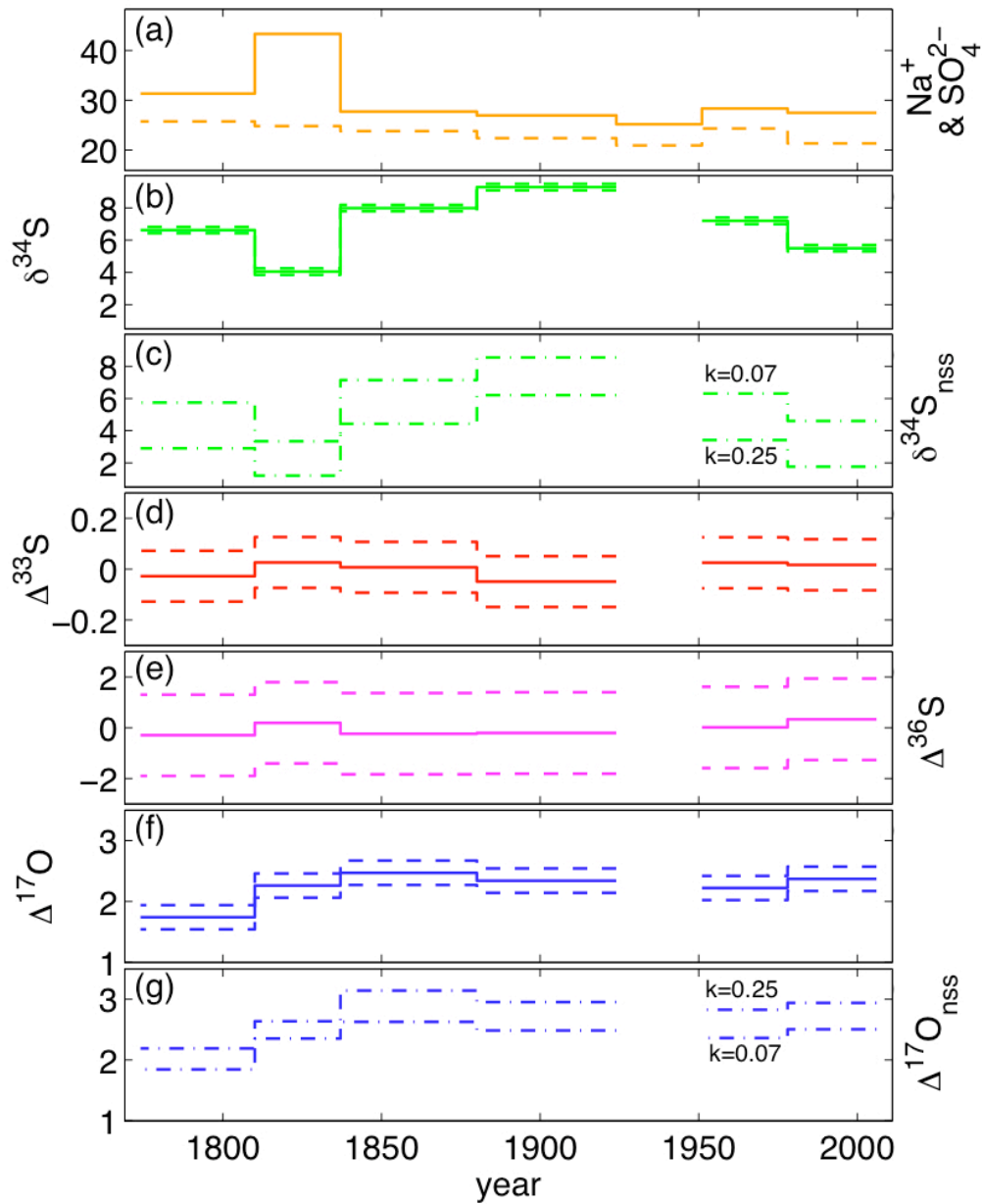


Figure 4.2: Timeseries of WAIS Divide ice core measurements including: (a) concentration of sulfate (orange) and sodium (orange dash); (b) $\delta^{34}\text{S}$ (green solid); (c) upper and lower estimates of $\delta^{34}\text{S}_{\text{nss}}$ (blue dash dot); (d) $\Delta^{33}\text{S}$ (red); (e) $\Delta^{36}\text{S}$ (magenta); (f) $\Delta^{17}\text{O}(\text{SO}_4^{2-})$ (blue solid); (g) upper and lower estimates of $\Delta^{17}\text{O}(\text{SO}_4^{2-})_{\text{nss}}$ (blue dash dot). Concentrations are in ppb and isotopic ratios are shown as ‰. 2σ errors for $\delta^{34}\text{S}$, $\Delta^{33}\text{S}$, $\Delta^{36}\text{S}$, and $\Delta^{17}\text{O}$ measurements are shown as dashed lines (0.2, 0.1, 1.6, 0.2‰, respectively). Values of $k = 0.25$ and 0.07 are used to estimate range of sea salt sulfate correction (see text). See text for description of timescale WDC05A:1.

Chapter 5

Conclusions

5.1 Summary of Findings and Implications

This dissertation presents improvements in both the measurement and interpretation of ice core $\Delta^{17}\text{O}(\text{NO}_3^-)$ and $\Delta^{17}\text{O}(\text{SO}_4^{2-})$, as well as providing new records of past temporal changes from $\Delta^{17}\text{O}(\text{NO}_3^-)$ and $\Delta^{17}\text{O}(\text{SO}_4^{2-})$ measurements in polar snow and ice. In brief, we have improved methods for $\Delta^{17}\text{O}(\text{NO}_3^-)$ and $\Delta^{17}\text{O}(\text{SO}_4^{2-})$ analysis by automating steps and reducing sample sizes; we have provided the first record of the seasonal cycle of $\Delta^{17}\text{O}(\text{NO}_3^-)$ at Summit, Greenland and used an atmospheric photochemical box model to interpret the observed range; we have used the atmospheric photochemical box model to explore the sensitivity of $\Delta^{17}\text{O}(\text{NO}_3^-)$ to changes in atmospheric chemical formation pathways; and we have provided the first record of ice core $\Delta^{17}\text{O}(\text{SO}_4^{2-})$ spanning the preindustrial-industrial transition in the Southern Hemisphere. These studies uphold previous interpretation of atmospheric $\Delta^{17}\text{O}(\text{NO}_3^-)$ and $\Delta^{17}\text{O}(\text{SO}_4^{2-})$ but improve quantitative interpretation of $\Delta^{17}\text{O}(\text{NO}_3^-)$ in Greenland and $\Delta^{17}\text{O}(\text{SO}_4^{2-})$ in Antarctica. Below, we summarize the findings of each study and elaborate on their importance to the scientific community.

In Chapter 2, we present new automated methods for the analysis of $\Delta^{17}\text{O}(\text{NO}_3^-)$ and $\Delta^{17}\text{O}(\text{SO}_4^{2-})$ at micromole levels, using pyrolysis of silver salts (AgNO_3 and Ag_2SO_4) in a continuous flow isotope ratio mass spectrometer system. Improvements include the automation of sample anion separation and conversion to silver salts (AgNO_3 and Ag_2SO_4) using an ion chromatography and cation exchange system with a fraction

collector (IC-CX-FC), and the automation of silver salt pyrolysis and isotopic analysis of O_2 using a continuous-flow system coupling a thermocouple elemental analyzer and an isotope ratio mass spectrometer (TCEA-IRMS) with He as the carrier gas. We also describe a system that has been further modified with a gas bench to cryofocus sample O_2 prior to isotopic analysis (TCEA-GB-IRMS), enabling determination of submicromole samples for $\Delta^{17}O(NO_3^-)$. Because $\Delta^{17}O(NO_3^-)$ and $\Delta^{17}O(SO_4^{2-})$ provide complementary information about atmospheric oxidation chemistry [Alexander *et al.*, 2004; Patris *et al.*, 2007], these streamlined methods for simultaneous analysis of $\Delta^{17}O(NO_3^-)$ and $\Delta^{17}O(SO_4^{2-})$ will greatly improve the efficiency of atmospheric and ice core measurement campaigns. Additionally, the reductions in sample size requirements will improve the temporal resolution of ice core analyses.

In Chapter 3, we present the first measurements of seasonal changes in snow $\Delta^{17}O(NO_3^-)$ from Summit, Greenland and interpret the observed range using an atmospheric photochemical box model. The seasonal range of $\Delta^{17}O(NO_3^-)$ in snowpits is similar to that observed at mid-latitudes [Michalski *et al.*, 2003], although the model predicts a larger range due to strong seasonal changes in local (Greenland) oxidant abundances following changes in incident radiation. The higher than expected summer $\Delta^{17}O(NO_3^-)$ values suggest the influence of one or more processes not included in the box model, including most notably tropospheric transport of nitrate with high $\Delta^{17}O(NO_3^-)$ from surrounding regions and/or higher than expected production of nitrate by reactive bromine chemistry (e.g., BrO) that imparts high $\Delta^{17}O(NO_3^-)$. A subsequent global chemical transport modeling study of $\Delta^{17}O(NO_3^-)$ [Alexander *et al.*, 2009a] confirmed that ~40% of the discrepancy between snowpit measurements and box model $\Delta^{17}O(NO_3^-)$

in mid-summer (July) is explained by tropospheric transport. The measurements of snow $\Delta^{17}\text{O}(\text{NO}_3^-)$ in the present day (2003-2005) provide critical constraints for the future interpretation of deep ice core $\Delta^{17}\text{O}(\text{NO}_3^-)$ measurements over glacial-interglacial climate changes. Additionally, the measurement-model comparison of the $\Delta^{17}\text{O}(\text{NO}_3^-)$ seasonal cycle provides the atmospheric chemistry modeling community new insights on the importance of secondary processes for nitrate production in polar regions.

We also employ the atmospheric photochemical box model to quantify the relative importance of various controls on $\Delta^{17}\text{O}(\text{NO}_3^-)$. In examining the sensitivity of $\Delta^{17}\text{O}(\text{NO}_3^-)$ to changes in individual nitrate production pathways, we find that annual mean $\Delta^{17}\text{O}(\text{NO}_3^-)$ is primarily determined by the relative importance of oxidants in NO_x cycling (e.g., $[\text{O}_3]$ versus $[\text{HO}_2+\text{RO}_2]$) rather than in NO_2 oxidation to nitrate. The importance of oxidation in NO_x cycling for determining $\Delta^{17}\text{O}(\text{NO}_3^-)$ was also later demonstrated at the global scale [*Alexander et al.*, 2009a]. A second critical finding of these sensitivity studies is that annual mean $\Delta^{17}\text{O}(\text{NO}_3^-)$ is not uniquely sensitive to oxidant abundances, but rather that a variety of other species (e.g., DMS, HC, aerosol) have non-negligible influence on the partitioning between oxidation pathways in nitrate production. In light of this, we suggest that ice core $\Delta^{17}\text{O}(\text{NO}_3^-)$ is best interpreted in conjunction with several other chemical and isotopic ice core measurements (e.g., $\Delta^{17}\text{O}(\text{SO}_4^{2-})$, $\delta^{15}\text{N}(\text{NO}_3^-)$, MSA, dust, etc.) that provide complementary information concerning atmospheric nitrate sources, atmospheric oxidants, and partitioning between homogeneous and heterogeneous oxidation.

In Chapter 4, we present the first measurements of the complete isotopic composition of sulfate ($\Delta^{17}\text{O}$, $\delta^{34}\text{S}$, $\Delta^{33}\text{S}$, $\Delta^{36}\text{S}$) from a West Antarctic ice core spanning

the preindustrial-industrial transition (~1775-2005). The low $\delta^{34}\text{S}_{\text{nss}}$ in the West Antarctic ice core likely reflects a combination of stronger influence of volcanogenic and stratospheric sulfate with low $\delta^{34}\text{S}$ in West relative to East Antarctica and the influence of frost flowers on the sea salt sulfate-to-sodium ratio (i.e., k). A low sulfate-to-sodium ratio, reflecting frost flower influence, also helps explain differences between $\Delta^{17}\text{O}(\text{SO}_4^{2-})_{\text{nss}}$ of the WAIS ice core and $\Delta^{17}\text{O}(\text{SO}_4^{2-})_{\text{nss}}$ calculated based on global chemical transport model results [Alexander *et al.*, 2009b]. $\Delta^{33}\text{S}$ remains within analytical uncertainty of zero throughout the WAIS Divide ice core record, but does not contradict a contribution of stratospheric sources to background sulfate deposited at WAIS Divide. Our analysis demonstrates that the interpretation of the isotopes of sulfate would be greatly improved by stronger constraints on Antarctic sea salt composition, reinforcing this recent focus of the Antarctic sulfate science community [Wagenbach *et al.*, 1998; Wolff *et al.*, 2003; Jourdain *et al.*, 2008]. It also highlights the need for further studies to quantify the influence of stratospheric and volcanogenic sources on sulfate deposition in West Antarctica in the present day.

Ice core reconstructions of atmospheric $\Delta^{17}\text{O}(\text{SO}_4^{2-})_{\text{nss}}$ at WAIS Divide show no significant changes ($\pm 0.2\%$) throughout the late 1800s to the early 2000s, in contrast to a Greenland ice core $\Delta^{17}\text{O}(\text{SO}_4^{2-})_{\text{nss}}$ record, which shows a strong perturbation during this time (2%) [Alexander *et al.*, 2004]. This difference between Northern and Southern Hemisphere records is broadly consistent with a stronger influence of anthropogenic activity on Northern Hemisphere oxidant abundances. By extracting data from a previously published global chemical transport model study [Alexander *et al.*, 2009b], we show that tropospheric $\Delta^{17}\text{O}(\text{SO}_4^{2-})$ from WAIS Divide can be interpreted following a

simple mixing of three primary sulfate production pathways: SO₂ oxidation by OH, H₂O₂, and O₃. Using this mixing relationship, we show that the lack of significant change in ice core $\Delta^{17}\text{O}(\text{SO}_4^{2-})_{\text{nss}}$ between the mid-1800s and early-2000s is consistent with preindustrial to industrial increases in tropospheric O₃ and H₂O₂ and a decrease in OH suggested by recent global chemical transport modeling work [Sofen *et al.*, in prep.]. We also constrain preindustrial-industrial changes in H₂O₂ that are necessary for published preindustrial-industrial changes in O₃ to be consistent with ice core $\Delta^{17}\text{O}(\text{SO}_4^{2-})_{\text{nss}}$ measurements from WAIS Divide. In the future, models of past changes in tropospheric oxidation chemistry (e.g., preindustrial-industrial and glacial-interglacial) must report abundances of all three primary SO₂ oxidants (OH, O₃, and H₂O₂) in order to use Antarctic ice core $\Delta^{17}\text{O}(\text{SO}_4^{2-})$ measurements as a constraint.

5.2 Further Research

The most compelling directions of further research for the use of ice core $\Delta^{17}\text{O}(\text{NO}_3^-)$ and $\Delta^{17}\text{O}(\text{SO}_4^{2-})$ in paleoatmospheric reconstructions of oxidation chemistry include: (1) additional improvements in methods for ice core analysis of $\Delta^{17}\text{O}(\text{NO}_3^-)$ and $\Delta^{17}\text{O}(\text{SO}_4^{2-})$, (2) improvements in atmospheric modeling of $\Delta^{17}\text{O}(\text{NO}_3^-)$ and $\Delta^{17}\text{O}(\text{SO}_4^{2-})$, and (3) future ice core $\Delta^{17}\text{O}(\text{NO}_3^-)$ and $\Delta^{17}\text{O}(\text{SO}_4^{2-})$ measurement campaigns.

The analytical methods presented here improve the simultaneous analysis of $\Delta^{17}\text{O}(\text{SO}_4^{2-})$ and $\Delta^{17}\text{O}(\text{NO}_3^-)$, by automating both sample preparation and isotopic analysis, and by reducing sample size limits of $\Delta^{17}\text{O}(\text{NO}_3^-)$ analysis to submicromole levels. The TCEA-GB-IRMS is also ready to be tested for application to $\Delta^{17}\text{O}(\text{SO}_4^{2-})$ analysis of submicromole sample sizes, which we expect to be successful based on

similarities between the $\Delta^{17}\text{O}(\text{NO}_3^-)$ and $\Delta^{17}\text{O}(\text{SO}_4^{2-})$ analytical methods. The possible influence of memory effects and/or isotopic exchange between samples and quartz capsules on submicromole $\Delta^{17}\text{O}(\text{SO}_4^{2-})$ analysis must also be investigated in detail, although these effects are expected to be negligible. The TCEA-GB-IRMS system may also be further refined by improving gas-tight seals on the TCEA autosampler and pyrolysis tube to reduce the cryofocusing blank. Such refinements may further improve the precision, accuracy, and size limits of submicromole analysis of both $\Delta^{17}\text{O}(\text{NO}_3^-)$ and $\Delta^{17}\text{O}(\text{SO}_4^{2-})$.

Improved modeling of $\Delta^{17}\text{O}(\text{NO}_3^-)$ and $\Delta^{17}\text{O}(\text{SO}_4^{2-})$ is also critical for using ice core $\Delta^{17}\text{O}(\text{NO}_3^-)$ and $\Delta^{17}\text{O}(\text{SO}_4^{2-})$ measurements to quantify temporal changes in oxidation chemistry in the past. As described briefly in Chapters 3 and 4 (Sections 3.7.1, 4.7.2), uncertainties in $\Delta^{17}\text{O}$ of atmospheric oxidants and/or the transfer of $\Delta^{17}\text{O}$ during oxidation produce important uncertainties in modeling of atmospheric and ice core $\Delta^{17}\text{O}(\text{NO}_3^-)$ and $\Delta^{17}\text{O}(\text{SO}_4^{2-})$. Most modeling studies [Michalski *et al.*, 2003; Alexander *et al.*, 2005, 2009a, 2009b; Kunasek *et al.*, 2008] assume $\Delta^{17}\text{O}(\text{OH})$ is zero throughout the troposphere, due to rapid isotopic exchange with atmospheric water vapor ($\Delta^{17}\text{O}(\text{H}_2\text{O}) = 0\text{‰}$) [Dubey *et al.*, 1997]. However, low water vapor abundances in dry polar regions are suggested to lead to reduced isotopic exchange between OH and H_2O , resulting in OH partially retaining non-zero $\Delta^{17}\text{O}$ from its sources (e.g., photolysis of O_3) [Morin *et al.*, 2007]. Most modeling studies of $\Delta^{17}\text{O}(\text{NO}_3^-)$ and $\Delta^{17}\text{O}(\text{SO}_4^{2-})$ also assume uniform $\Delta^{17}\text{O}(\text{O}_3) = 35\text{‰}$ throughout the troposphere, consistent with $\Delta^{17}\text{O}(\text{O}_3)$ model results [e.g., Lyons *et al.*, 2001] and the upper range of tropospheric measurements [Schueler *et al.*, 1990; Krankowsky *et al.*, 1995, 2000; Johnston and Thiemens, 1997].

However, tropospheric $\Delta^{17}\text{O}(\text{O}_3)$ measurements display a considerable range (mean 25-35‰ at different locations) [*Schueler et al.*, 1990; *Krankowsky et al.*, 1995, 2000; *Johnston and Thiemens*, 1997] relative to the small spatial variations expected in the troposphere ($< \pm 3\%$ [*Alexander et al.*, 2002]) based on the pressure- and temperature-dependence of $\Delta^{17}\text{O}(\text{O}_3)$ [*Morton et al.*, 1990; *Thiemens and Jackson*, 1990]. The recent discovery that terminal oxygen atoms of O_3 (i.e., O-O-Q) that are enriched in $\Delta^{17}\text{O}$ [*Bhattacharya et al.*, 2008] are preferentially transferred during an O_3 oxidation reaction ($\text{NO}+\text{O}_3$) [*Savarino et al.*, 2008] also demands further investigation of isotope transfer in other O_3 oxidation reactions (e.g., $\text{SO}_3^{2-}+\text{O}_3$, NO_2+O_3). Preferential terminal oxygen atom transfer from O_3 would result in elevation of $\Delta^{17}\text{O}$ in oxidation products above values expected based on statistically equivalent transfer of the $\Delta^{17}\text{O}$ anomaly from all oxygen atoms of O_3 . Improved laboratory measurements of $\Delta^{17}\text{O}$ of oxidants and the transfer of $\Delta^{17}\text{O}$ during oxidation reactions of O_3 will improve the use of $\Delta^{17}\text{O}(\text{NO}_3^-)$ and $\Delta^{17}\text{O}(\text{SO}_4^{2-})$ for quantifying partitioning between atmospheric oxidation pathways in nitrate and sulfate production.

The atmospheric chemistry modeling approaches presented here may also be improved. The rudimentary photochemical box modeling and isotopic signature mixing approaches used to interpret $\Delta^{17}\text{O}(\text{NO}_3^-)$ and $\Delta^{17}\text{O}(\text{SO}_4^{2-})$ in Chapters 3 and 4 provide a broad understanding of controls on $\Delta^{17}\text{O}(\text{NO}_3^-)$ and $\Delta^{17}\text{O}(\text{SO}_4^{2-})$. However, these approaches have several limitations. First, the model approaches do not include fully-coupled atmospheric oxidation chemistry. In other words, a change in abundance of one oxidant species does not alter the abundances of other oxidant species, despite the fact that oxidant species are inextricably linked through photochemical cycling [*Jacob*, 1999].

Secondly, in the studies of the photochemical box model of $\Delta^{17}\text{O}(\text{NO}_3^-)$ (Chapter 3), an arbitrary range of perturbations (i.e., up to factor of 3) was employed to examine the sensitivity of $\Delta^{17}\text{O}(\text{NO}_3^-)$ to the atmospheric species influencing nitrate formation. However, some atmospheric species are expected to exhibit wider ranges of variability than others, and the variability depends on the timescale studied (e.g., O_3 varies little seasonally, while OH varies strongly). A more sophisticated model approach for quantitative interpretation of ice core $\Delta^{17}\text{O}(\text{NO}_3^-)$ and $\Delta^{17}\text{O}(\text{SO}_4^{2-})$ would include fully-coupled chemistry, atmospheric transport, and perturbations to the atmospheric chemical system driven by well-constrained atmospheric emissions for the time period studied. $\Delta^{17}\text{O}(\text{NO}_3^-)$ and $\Delta^{17}\text{O}(\text{SO}_4^{2-})$ calculations have recently been incorporated into the global chemical transport model GEOS-Chem [*Alexander et al.*, 2005, 2009a, 2009b], and studies are currently underway to examine preindustrial-industrial and glacial-interglacial perturbations to atmospheric chemistry using these models.

Finally, improvements in ice core reconstructions of past atmospheric oxidation chemistry cannot be made without acquiring new ice core datasets of $\Delta^{17}\text{O}(\text{NO}_3^-)$ and $\Delta^{17}\text{O}(\text{SO}_4^{2-})$. A clear area of further research discussed in Chapter 4 is the extension of the WAIS ice core record further into the past (before 1775 A.D.). Extending this record may improve our interpretation of the reduced Southern Hemisphere $\Delta^{17}\text{O}(\text{SO}_4^{2-})$ in the late 1700s, providing new insights on whether oxidant abundances were constant throughout the preindustrial Holocene. Another gap in the study of ice core oxidation chemistry reconstructions is the lack of any published ice core $\Delta^{17}\text{O}(\text{NO}_3^-)$ record spanning the glacial-interglacial climate transition. Also, there is no ice core record of either $\Delta^{17}\text{O}(\text{NO}_3^-)$ or $\Delta^{17}\text{O}(\text{SO}_4^{2-})$ over the glacial-interglacial climate transition from the

Northern Hemisphere. Future ice core measurement campaigns should aim to provide simultaneous measurements of $\Delta^{17}\text{O}(\text{NO}_3^-)$ and $\Delta^{17}\text{O}(\text{SO}_4^{2-})$, as they offer complementary information about atmospheric oxidation chemistry. Additionally, ice core $\Delta^{17}\text{O}(\text{NO}_3^-)$ and $\Delta^{17}\text{O}(\text{SO}_4^{2-})$ should be interpreted along with complementary ice core measurements that indicate changes in nitrate and sulfate oxidation unrelated to atmospheric oxidant abundances (e.g., MSA, pH; see Sections 3.8 and 4.7.2).

The automation and reduction of sample size limits for $\Delta^{17}\text{O}(\text{NO}_3^-)$ and $\Delta^{17}\text{O}(\text{SO}_4^{2-})$ analysis will facilitate widespread application of these measurements to atmospheric and ice core campaigns. New atmospheric and ice core measurements and improvements in modeling of $\Delta^{17}\text{O}(\text{NO}_3^-)$ and $\Delta^{17}\text{O}(\text{SO}_4^{2-})$ will strengthen our quantitative understanding of the relationship between these isotopic tracers and atmospheric oxidant abundances. Improvements in the quantitative interpretation of atmospheric oxidant abundances from atmospheric and ice core $\Delta^{17}\text{O}(\text{NO}_3^-)$ and $\Delta^{17}\text{O}(\text{SO}_4^{2-})$ measurements will allow these tracers to be more widely applied as constraints or validation for oxidation chemistry in climate and atmospheric chemistry models of the past and present.

REFERENCES

- Alexander, B., J. Savarino, N. I. Barkov, R. J. Delmas, and M. H. Thiemens (2002), Climate driven changes in the oxidation pathways of atmospheric sulfur, *Geophys. Res. Lett.*, 29(14), p.1685, doi:10.1029/2002GL014879.
- Alexander, B., M. H. Thiemens, J. Farquhar, A. J. Kaufman, J. Savarino, and R. J. Delmas (2003), East Antarctic ice core sulfur isotope measurements over a complete glacial-interglacial cycle, *J. Geophys. Res.-Atmos.*, 108(D24), p.4786, doi:10.1029/2003JD003513.
- Alexander, B., J. Savarino, K. J. Kreutz, and M. H. Thiemens (2004), Impact of preindustrial biomass-burning emissions on the oxidation pathways of tropospheric sulfur and nitrogen, *J. Geophys. Res.-Atmos.*, 109(D08303), doi:10.1029/2003JD004218.
- Alexander, B., R. J. Park, D. J. Jacob, Q. B. Li, R. M. Yantosca, J. Savarino, C. C. W. Lee, and M. H. Thiemens (2005), Sulfate formation in sea-salt aerosols: Constraints from oxygen isotopes, *J. Geophys. Res.-Atmos.*, 110(D10), doi:10.1029/2004JD005659.
- Alexander, B., M. G. Hastings, D. J. Allman, J. Dachs, J. A. Thornton, and S. A. Kunasek (2009a), Quantifying atmospheric nitrate formation pathways based on a global model of the oxygen isotopic composition ($\delta^{17}\text{O}$) of atmospheric nitrate, *Atmos. Chem. Phys.*, 9(14), 5043-5056.
- Alexander, B., R. J. Park, D. J. Jacob, and S. L. Gong (2009b), Transition metal-catalyzed oxidation of atmospheric sulfur: Global implications for the sulfur budget, *J. Geophys. Res.-Atmos.*, 114(D02309), doi:10.1029/2008JD010486.
- Anklin, M., R. C. Bales, E. Mosley-Thompson, and K. Steffen (1998), Annual accumulation at two sites in northwest Greenland during recent centuries, *J. Geophys. Res.-Atmos.*, 103(D22), 28775-28783.
- Atkinson, R., R. A. Cox, J. N. Crowley, R. F. J. Hampson, R. G. Hynes, M. E. Jenkin, J. A. Kerr, M. J. Rossi, and J. Troe (2006), Summary of Evaluated Kinetic and Photochemical Data for Atmospheric Chemistry, Section II. Organic Reactions, International Union of Pure and Applied Chemistry (IUPAC), <http://www.iupac-kinetic.ch.cam.ac.uk/>, accessed June 2006.
- Banta, J. R., J. R. McConnell, M. M. Frey, R. C. Bales, and K. Taylor (2008), Spatial and temporal variability in snow accumulation at the West Antarctic Ice Sheet Divide over recent centuries, *J. Geophys. Res.-Atmos.*, 113(D23), doi:10.1029/2008JD010235.

- Bao, H. M., and M. H. Thiemens (2000), Generation of O-2 from BaSO₄ using a CO₂-laser fluorination system for simultaneous analysis of delta O-18 and delta O-17, *Anal. Chem.*, 72(17), 4029-4032.
- Baroni, M., M. H. Thiemens, R. J. Delmas, and J. Savarino (2007), Mass-independent sulfur isotopic compositions in stratospheric volcanic eruptions, *Science*, 315(5808), 84-87.
- Baroni, M., J. Savarino, J. H. Cole-Dai, V. K. Rai, and M. H. Thiemens (2008), Anomalous sulfur isotope compositions of volcanic sulfate over the last millennium in Antarctic ice cores, *J. Geophys. Res.-Atmos.*, 113(D20), doi:10.1029/2008JD010185.
- Bartels-Rausch, T., B. Eichler, P. Zimmermann, H. W. Gaggeler, and M. Ammann (2002), The adsorption enthalpy of nitrogen oxides on crystalline ice, *Atmos. Chem. Phys.*, 2, 235-247.
- Bekki, S. (1995), Oxidation of Volcanic SO₂ - a Sink for Stratospheric OH and H₂O, *Geophys. Res. Lett.*, 22(8), 913-916.
- Bergin, M. H., E. A. Meyerson, J. E. Dibb, and P. A. Mayewski (1998), Relationship between continuous aerosol measurements and firn core chemistry over a 10-year period at the South Pole, *Geophys. Res. Lett.*, 25(8), 1189-1192.
- Bhattacharya, S. K., A. Pandey, and J. Savarino (2008), Determination of intramolecular isotope distribution of ozone by oxidation reaction with silver metal, *J. Geophys. Res.-Atmos.*, 113(D3), doi: 10.1029/2006JD008309.
- Bindeman, I. N., J. M. Eiler, B. A. Wing, and J. Farquhar (2007), Rare sulfur and triple oxygen isotope geochemistry of volcanogenic sulfate aerosols, *Geochim. Cosmochim. Acta*, 71(9), 2326-2343.
- Böhlke, J. K., S. J. Mroczkowski, and T. B. Coplen (2003), Oxygen isotopes in nitrate: new reference materials for O-18 : O-17 : O-16 measurements and observations on nitrate-water equilibration, *Rapid Commun. Mass Spectrom.*, 17(16), 1835-1846.
- Boudries, H., J. W. Bottenheim, C. Guimbaud, A. M. Grannas, P. B. Shepson, S. Houdier, S. Perrier, and F. Dominé (2002), Distribution and trends of oxygenated hydrocarbons in the high Arctic derived from measurements in the atmospheric boundary layer and interstitial snow air during the ALERT2000 field campaign, *Atmos. Environ.*, 36(15-16), 2573-2583.
- Brenninkmeijer, C. A. M., C. Janssen, J. Kaiser, T. Rockmann, T. S. Rhee, and S. S. Assonov (2003), Isotope effects in the chemistry of atmospheric trace compounds, *Chem. Rev.*, 103(12), 5125-5161.

- Brook, E. J. (2005), Tiny bubbles tell all, *Science*, 310(5752), 1285-1287.
- Burkhart, J. F., M. Hutterli, R. C. Bales, and J. R. McConnell (2004), Seasonal accumulation timing and preservation of nitrate in firn at Summit, Greenland, *J. Geophys. Res.-Atmos.*, 109(D19302), doi:10.1029/2004JD004658.
- Calhoun, J. A., T. S. Bates, and R. J. Charlson (1991), Sulfur Isotope Measurements of Submicrometer Sulfate Aerosol-Particles over the Pacific-Ocean, *Geophys. Res. Lett.*, 18(10), 1877-1880.
- Calvert, J. G., and S. E. Lindberg (2003), A modeling study of the mechanism of the halogen-ozone-mercury homogeneous reactions in the troposphere during the polar spring, *Atmos. Environ.*, 37(32), 4467-4481.
- Calvert, J. G., A. Lazrus, G. L. Kok, B. G. Heikes, J. G. Walega, J. Lind, and C. A. Cantrell (1985), Chemical Mechanisms of Acid Generation in the Troposphere, *Nature*, 317(6032), 27-35.
- Carrasco, J. F., D. H. Bromwich, and A. J. Monaghan (2003), Distribution and characteristics of mesoscale cyclones in the Antarctic: Ross Sea eastward to the Weddell Sea, *Monthly Weather Review*, 131(2), 289-301.
- Casciotti, K. L., D. M. Sigman, M. G. Hastings, J. K. Bohlke, and A. Hilkert (2002), Measurement of the oxygen isotopic composition of nitrate in seawater and freshwater using the denitrifier method, *Anal. Chem.*, 74(19), 4905-4912.
- Castleman, A. W.-J., H. R. Munkelwitz, and B. Manowitz (1973), Contribution of Volcanic Sulfur-Compounds to Stratospheric Aerosol Layer, *Nature*, 244(5415), 345-346.
- Castleman, A. W., H. R. Munkelwitz and B. Manowitz (1974), Isotopic studies of the sulfur component of the stratospheric aerosol layer, *Tellus*, 26B(1-2), 222-234.
- Chameides, W. L. (1984), The Photochemistry of a Remote Marine Stratiform Cloud, *J. Geophys. Res.-Atmos.*, 89(ND3), 4739-4755.
- Chappellaz, J. A., I. Y. Fung, and A. M. Thompson (1993), The Atmospheric CH₄ Increase since the Last Glacial Maximum, *Tellus Ser. B-Chem. Phys. Meteorol.*, 45(3), 228-241.
- Cliff, S. S., and M. H. Thiemens (1997), The O-18/O-16 and O-17/O-16 ratios in atmospheric nitrous oxide: A mass-independent anomaly, *Science*, 278, 1774-1776.
- Cole-Dai, J., E. MosleyThompson, and L. G. Thompson (1997), Annually resolved southern hemisphere volcanic history from two Antarctic ice cores, *J. Geophys. Res.-Atmos.*, 102(D14), 16761-16771.

- Craig, H. (1961), Standard for Reporting Concentrations of Deuterium and Oxygen-18 in Natural Waters, *Science*, *133*, p.1833.
- Dai, J., E. Mosleythompson, and L. G. Thompson (1991), Ice Core Evidence for an Explosive Tropical Volcanic-Eruption 6 Years Preceding Tambora, *J. Geophys. Res.-Atmos.*, *96*(D9), 17361-17366.
- Danielsen, E.F. (1968), Stratospheric-tropospheric exchange based upon radioactivity, ozone, and potential vorticity, *J. Atmos. Sci.*, *25*(3), 502-518.
- Dassau, T. M., A. L. Sumner, S. L. Koeniger, P. B. Shepson, J. Yang, R. E. Honrath, N. J. Cullen, K. Steffen, H. W. Jacobi, M. Frey, and R. C. Bales (2002), Investigation of the role of the snowpack on atmospheric formaldehyde chemistry at Summit, Greenland, *J. Geophys. Res.-Atmos.*, *107*(D19), p.4394, doi:10.1029/2002JD002182.
- Dassau, T. M., P. B. Shepson, J. W. Bottenheim, and K. M. Ford (2004), Peroxyacetyl nitrate photochemistry and interactions with the Arctic surface, *J. Geophys. Res.-Atmos.*, *109*(D18302), doi:10.1029/2004JD004562.
- Davidson, C. I., J. R. Harrington, M. J. Stephenson, M. J. Small, F. P. Boscoe, and R. E. Gandley (1989), Seasonal-Variations in Sulfate, Nitrate and Chloride in the Greenland Ice-Sheet - Relation to Atmospheric Concentrations, *Atmos. Environ.*, *23*(11), 2483-2493.
- Dibb, J. E. (2007), Vertical mixing above Summit, Greenland: Insights into seasonal and high frequency variability from the radionuclide tracers Be-7 and Pb-210, *Atmos. Environ.*, *41*(24), 5020-5030.
- Dibb, J. E., and M. Fahnstock (2004), Snow accumulation, surface height change, and firn densification at Summit, Greenland: Insights from 2 years of in situ observation, *J. Geophys. Res.-Atmos.*, *109*(D24113), doi:10.1029/2003JD004300.
- Dibb, J. E., M. Arsenault, M. C. Peterson, and R. E. Honrath (2002), Fast nitrogen oxide photochemistry in Summit, Greenland snow, *Atmos. Environ.*, *36*(15-16), 2501-2511.
- Dibb, J. E., S. I. Whitlow, and M. Arsenault (2007), Seasonal variations in the soluble ion content of snow at Summit. Greenland: Constraints from three years of daily surface snow samples, *Atmos. Environ.*, *41*(24), 5007-5019.
- Dubey, M. K., R. Mohrschladt, N. M. Donahue, and J. G. Anderson (1997), Isotope specific kinetics of hydroxyl radical (OH) with water (H₂O): Testing models of reactivity and atmospheric fractionation, *J. Phys. Chem. A*, *101*(8), 1494-1500.
- Evans, M. J., and D. J. Jacob (2005), Impact of new laboratory studies of N₂O₅ hydrolysis on global model budgets of tropospheric nitrogen oxides, ozone, and OH, *Geophys. Res. Lett.*, *32*(9), p.L0913, doi:10.1029/2005GL022469.

- Evans, M. J., D. J. Jacob, E. Atlas, C. A. Cantrell, F. Eisele, F. Flocke, A. Fried, R. L. Mauldin, B. A. Ridley, B. Wert, R. Talbot, D. Blake, B. Heikes, J. Snow, J. Walega, A. J. Weinheimer, and J. Dibb (2003), Coupled evolution of BrO_x-ClO_x-HO_x-NO_x chemistry during bromine-catalyzed ozone depletion events in the arctic boundary layer, *J. Geophys. Res.-Atmos.*, *108*(D4), doi:10.1029/2002JD002732.
- Falouna, I. (2009), Sulfur processing in the marine atmospheric boundary layer: A review and critical assessment of modeling uncertainties, *Atmos. Environ.*, *43*(18), 2841–2854.
- Farquhar, J., J. Savarino, T. L. Jackson, and M. H. Thiemens (2000), Evidence of atmospheric sulphur in the martian regolith from sulphur isotopes in meteorites, *Nature*, *404*, 50-52.
- Farquhar, J., J. Savarino, S. Airieau, and M. H. Thiemens (2001), Observation of wavelength-sensitive mass-independent sulfur isotope effects during SO₂ photolysis: Implications for the early atmosphere, *J. Geophys. Res.-Planets*, *106*(E12), 32829-32839.
- Ferretti, D. F., J. B. Miller, J. W. C. White, D. M. Etheridge, K. R. Lassey, D. C. Lowe, C. M. M. Meure, M. F. Dreier, C. M. Trudinger, T. D. van Ommen, and R. L. Langenfelds (2005), Unexpected changes to the global methane budget over the past 2000 years, *Science*, *309*(5741), 1714-1717.
- Fischer, H., M. Behrens, M. Bock, U. Richter, J. Schmitt, L. Loulergue, J. Chappellaz, R. Spahni, T. Blunier, M. Leuenberger, and T. F. Stocker (2008), Changing boreal methane sources and constant biomass burning during the last termination, *Nature*, *452*(7189), 864-867.
- Ford, K. M., B. M. Campbell, P. B. Shepson, S. B. Bertman, R. E. Honrath, M. Peterson, and J. E. Dibb (2002), Studies of Peroxyacetyl nitrate (PAN) and its interaction with the snowpack at Summit, Greenland, *J. Geophys. Res.-Atmos.*, *107*(D10), p.4102, doi:10.1029/2001JD000547.
- Frey M. M., R. C. Bales, J. R. McConnell (2006), Climate sensitivity of the century-scale hydrogen peroxide (H₂O₂) record preserved in 23 ice cores from West Antarctica, *J. Geophys. Res.-Atmos.*, *111*(D21301), doi:10.1029/2005JD006816.
- Gane, M. P., N. A. Williams, and J. R. Sodeau (2001), A reflection-absorption infrared spectroscopy (RAIRS) investigation of the low-temperature heterogeneous hydrolysis of bromine nitrate, *J. Phys. Chem. A*, *105*(16), 4002-4009.
- Grannas, A. M., P. B. Shepson, C. Guimbaud, A. L. Sumner, M. Albert, W. Simpson, F. Domine, H. Boudries, J. Bottenheim, H. J. Beine, R. Honrath, and X. L. Zhou (2002),

A study of photochemical and physical processes affecting carbonyl compounds in the Arctic atmospheric boundary layer, *Atmos. Environ.*, 36(15-16), 2733-2742.

Grannas, A. M., A. E. Jones, J. Dibb, M. Ammann, C. Anastasio, H. J. Beine, M. Bergin, J. Bottenheim, C. S. Boxe, G. Carver, G. Chen, J. H. Crawford, F. Domine, M. M. Frey, M. I. Guzman, D. E. Heard, D. Helmig, M. R. Hoffmann, R. E. Honrath, L. G. Huey, M. Hutterli, H. W. Jacobi, P. Klan, B. Lefer, J. McConnell, J. Plane, R. Sander, J. Savarino, P. B. Shepson, W. R. Simpson, J. R. Sodeau, R. von Glasow, R. Weller, E. W. Wolff, and T. Zhu (2007), An overview of snow photochemistry: evidence, mechanisms and impacts, *Atmos. Chem. Phys.*, 7, 4329-4373.

Grenfell, J. L., D. T. Shindell, D. Koch, and D. Rind (2001), Chemistry-climate interactions in the Goddard Institute for Space Studies general circulation model 2. New insights into modeling the preindustrial atmosphere, *J. Geophys. Res.-Atmos.*, 106(D24), 33435-33451.

Guo, S., G. J. S. Bluth, W. I. Rose, I. M. Watson, and A. J. Prata (2004), Re-evaluation of SO₂ release of the 15 June 1991 Pinatubo eruption using ultraviolet and infrared satellite sensors, *Geochem. Geophys. Geosyst.*, 5, 31.

Hanson, D. R., A. R. Ravishankara, and E. R. Lovejoy (1996), Reaction of BrONO₂ with H₂O on submicron sulfuric acid aerosol and the implications for the lower stratosphere, *J. Geophys. Res.-Atmos.*, 101(D4), 9063-9069.

Hastings, M. G., and B. Alexander (2006), First global modeling of the isotopic composition of atmospheric nitrate, *Eos Transactions, AGU*, 87, Fall Meet. Suppl., Abstract B12A-01.

Hastings, M. G., E. J. Steig, and D. M. Sigman (2004), Seasonal variations in N and O isotopes of nitrate in snow at Summit, Greenland: Implications for the study of nitrate in snow and ice cores, *J. Geophys. Res.-Atmos.*, 109(D20306), doi:10.1029/2004JD004991.

Hastings, M. G., D. M. Sigman, and E. J. Steig (2005), Glacial/interglacial changes in the isotopes of nitrate from the Greenland Ice Sheet Project 2 (GISP2) ice core, *Glob. Biogeochem. Cycle*, 19(4).

Hauglustaine, D. A., and G. P. Brasseur (2001), Evolution of tropospheric ozone under anthropogenic activities and associated radiative forcing of climate, *J. Geophys. Res.-Atmos.*, 106(D23), 32337-32360.

Helmig, D., S. J. Oltmans, T. O. Morse, and J. E. Dibb (2007), What is causing high ozone at Summit, Greenland?, *Atmos. Environ.*, 41(24), 5031-5043.

Holton, J. R., P. H. Haynes, M. E. McIntyre, A. R. Douglass, R. B. Rood, and L. Pfister (1995), Stratosphere-Troposphere Exchange, *Rev. Geophys.*, 33(4), 403-439.

- Honrath, R. E., M. C. Peterson, S. Guo, J. E. Dibb, P. B. Shepson, and B. Campbell (1999), Evidence of NO_x production within or upon ice particles in the Greenland snowpack, *Geophys. Res. Lett.*, *26*(6), 695-698.
- Honrath, R. E., S. Guo, M. C. Peterson, M. P. Dziobak, J. E. Dibb, and M. A. Arsenault (2000), Photochemical production of gas phase NO_x from ice crystal NO₃, *J. Geophys. Res.-Atmos.*, *105*(D19), 24183-24190.
- Honrath, R. E., Y. Lu, M. C. Peterson, J. E. Dibb, M. A. Arsenault, N. J. Cullen, and K. Steffen (2002), Vertical fluxes of NO_x, HONO, and HNO₃ above the snowpack at Summit, Greenland, *Atmos. Environ.*, *36*(15-16), 2629-2640.
- Hopkins, J. R., I. D. Jones, A. C. Lewis, J. B. McQuaid, and P. W. Seakins (2002), Non-methane hydrocarbons in the Arctic boundary layer, *Atmos. Environ.*, *36*(20), 3217-3229.
- Huey, L. G., J. Dibb, J. Stutz, S. Brooks, R. von Glasow, B. Lefer, G. Chen, S. Kim, and D. Tanner (2007), Observations of Halogens at Summit, Greenland, *Eos Transactions, AGU*, *88*, Fall. Meet. Suppl., Abstract A42B-05.
- Hutterli, M. A., J. R. McConnell, R. C. Bales, and R. W. Stewart (2003), Sensitivity of hydrogen peroxide (H₂O₂) and formaldehyde (HCHO) preservation in snow to changing environmental conditions: Implications for ice core records, *J. Geophys. Res.-Atmos.*, *108* (D1), p.4023, doi:10.1029/2002JD002528.
- Jacob, D. J. (1999), *Introduction to Atmospheric Chemistry*, Princeton University Press, Princeton.
- Janssen, C. (2005), Intramolecular isotope distribution in heavy ozone ((OOO)-O-16-O-18-O-16 and (OOO)-O-16-O-16-O-18), *J. Geophys. Res.-Atmos.*, *110*(D8), doi: 10.1029/2004JD005479.
- Johnston, J. C., and M. H. Thiemens (1997), The isotopic composition of tropospheric ozone in three environments, *J. Geophys. Res.-Atmos.*, *102*(D21), 25395-25404.
- Jonsell, U., M. E. Hansson, C. M. Morth, and P. Torssander (2005), Sulfur isotopic signals in two shallow ice cores from Dronning Maud Land, Antarctica, *Tellus Ser. B-Chem. Phys. Meteorol.*, *57*(4), 341-350.
- Jourdain, B., S. Preunkert, O. Cerri, H. Castebrunet, R. Udisti, and M. Legrand (2008), Year-round record of size-segregated aerosol composition in central Antarctica (Concordia station): Implications for the degree of fractionation of sea-salt particles, *J. Geophys. Res.-Atmos.*, *113*(D14308), doi:10.1029/2007JD009584.

- Jouzel, J., R. B. Alley, K. M. Cuffey, W. Dansgaard, P. Grootes, G. Hoffmann, S. J. Johnsen, R. D. Koster, D. Peel, C. A. Shuman, M. Stievenard, M. Stuiver, and J. White (1997), Validity of the temperature reconstruction from water isotopes in ice cores, *J. Geophys. Res.-Oceans*, 102(C12), 26471-26487.
- Kahl, J. D. W., D. A. Martinez, H. Kuhns, C. I. Davidson, J. L. Jaffrezo, and J. M. Harris (1997), Air mass trajectories to Summit, Greenland: A 44-year climatology and some episodic events, *J. Geophys. Res.-Oceans*, 102(C12), 26861-26875.
- Kaiser, J., M. G. Hastings, B. Z. Houlton, T. Rockmann, and D. M. Sigman (2007), Triple oxygen isotope analysis of nitrate using the denitrifier method and thermal decomposition of N₂O, *Anal. Chem.*, 79(2), 599-607.
- Kaplan, J. O. (2002), Wetlands at the Last Glacial Maximum: Distribution and methane emissions, *Geophysical Research Letters*, 29(6), 1079, doi:10.1029/2001GL013366.
- Kaplan, J. O., G. Folberth, and D. A. Hauglustaine (2006), Role of methane and biogenic volatile organic compound sources in late glacial and Holocene fluctuations of atmospheric methane concentrations, *Glob. Biogeochem. Cycle*, 20(2).
- Karol, I. L., V. A. Frolkis, and A. A. Kiselev (1995), Radiative-Photochemical Modeling of the Annually Averaged Composition and Temperature of the Global Atmosphere During the Last Glacial and Interglacial Periods, *J. Geophys. Res.-Atmos.*, 100(D4), 7291-7301.
- King, J. C. and J. Turner (1997), *Antarctic Meteorology and Climatology*, Cambridge Atmospheric and Space Science Series, Cambridge University Press, Cambridge.
- Krankowsky, D., F. Bartecki, G. G. Klees, K. Mauersberger, K. Schellenbach, and J. Stehr (1995), Measurement of Heavy Isotope Enrichment in Tropospheric Ozone, *Geophys. Res. Lett.*, 22(13), 1713-1716.
- Krankowsky, D., P. Lammerzahl, and K. Mauersberger (2000), Isotopic measurements of stratospheric ozone, *Geophys. Res. Lett.*, 27(17), 2593-2595.
- Krinner, G., C. Genthon, and J. Jouzel (1997), GCM analysis of local influences on ice core delta signals, *Geophys. Res. Lett.*, 24(22), 2825-2828.
- Kunasek, S. A., B. Alexander, E. J. Steig, M. G. Hastings, D. J. Gleason, and J. C. Jarvis (2008), Measurements and modeling of $\Delta^{17}\text{O}$ of nitrate in snowpits from Summit, Greenland, *J. Geophys. Res.-Atmos.*, 113(D24302), doi:10.1029/2008JD010103.
- Lamarque, J. F., P. Hess, L. Emmons, L. Buja, W. Washington, and C. Granier (2005), Tropospheric ozone evolution between 1890 and 1990, *J. Geophys. Res.-Atmos.*, 110(D08304), doi:10.1029/2004JD005537.

- Lawrence, M. G., P. Jockel, and R. von Kuhlmann (2001), What does the global mean OH concentration tell us?, *Atmos. Chem. Phys.*, *1*, 37-49.
- Lee, C.W., and M. Thiemens (2001), The $\delta^{17}\text{O}$ and $\delta^{18}\text{O}$ measurements of atmospheric sulfate from a coastal and high alpine region: A mass-independent isotopic anomaly, *J. Geophys. Res.-Atmos.*, *106*(D15), 17359-17373.
- Legrand, M., and P. Mayewski (1997), Glaciochemistry of polar ice cores: A review, *Rev. Geophys.*, *35*(3), 219-243.
- Legrand, M., C. Hammer, M. De Angelis, J. Savarino, R. Delmas, H. Clausen, and S. Johnsen (1997), Sulfur-containing species (methanesulfonate and SO_4) over the last climatic cycle in the Greenland Ice Core Project (central Greenland) ice core, *J. Geophys. Res.-Oceans*, *102*(C12), 26663-26679.
- Lelieveld, J., and F. J. Dentener (2000), What controls tropospheric ozone?, *J. Geophys. Res.-Atmos.*, *105*(D3), 3531-3551.
- Lelieveld, J., W. Peters, F. J. Dentener, and M. C. Krol (2002), Stability of tropospheric hydroxyl chemistry, *J. Geophys. Res.-Atmos.*, *107*(D23), p.4715, doi:10.1029/2002JD002272.
- Levy, H., P. S. Kasibhatla, W. J. Moxim, A. A. Klonecki, A. I. Hirsch, S. J. Oltmans, and W. L. Chameides (1997), The global impact of human activity on tropospheric ozone, *Geophys. Res. Lett.*, *24*(7), 791-794.
- Levy, H., W. J. Moxim, A. A. Klonecki, and P. S. Kasibhatla (1999), Simulated tropospheric NO_x: Its evaluation, global distribution and individual source contributions, *J. Geophys. Res.-Atmos.*, *104*(D21), 26279-26306.
- Lloyd, R. M. (1968), Oxygen isotope behavior in the sulfate-water system, *J. Geophys. Res.-Atmos.*, *73*(18), 6099-6110.
- Liang, M. C., F. W. Irion, J. D. Weibel, C. E. Miller, G. A. Blake, and Y. L. Yung (2006), Isotopic composition of stratospheric ozone, *J. Geophys. Res.-Atmos.*, *111*(D2), doi: doi: 10.1029/2005JD006342.
- Loulergue, L., A. Schilt, R. Spahni, V. Masson-Delmotte, T. Blunier, B. Lemieux, J. M. Barnola, D. Raynaud, T. F. Stocker, and J. Chappellaz (2008), Orbital and millennial-scale features of atmospheric CH₄ over the past 800,000 years, *Nature*, *453*(7193), 383-386.
- Lyons, J. R. (2001), Transfer of mass-independent fractionation in ozone to other oxygen-containing radicals in the atmosphere, *Geophys. Res. Lett.*, *28*(17), 3231-3234.

- Madronich, S. and S. Flocke (1997), Theoretical estimation of biologically effective UV radiation at the Earth's surface, in *Solar Ultraviolet Radiation - Modeling, Measurements & Effects*, NATO ASI Series I: Global Environmental Change, edited by C. S. Zerefos and A. F. Bais, Vol. 52, 23-48, Springer-Verlag, Berlin.
- Marlon, J. R., P. J. Bartlein, C. Carcaillet, D. G. Gavin, S. P. Harrison, P. E. Higuera, F. Joos, M. J. Power, and I. C. Prentice (2009), Climate and human influences on global biomass burning over the past two millennia, *Nature Geoscience*, *1*, 697-702.
- Martinerie, P., G. P. Brasseur, and C. Granier (1995), The Chemical-Composition of Ancient Atmospheres - a Model Study Constrained by Ice Core Data, *J. Geophys. Res.-Atmos.*, *100*(D7), 14291-14304.
- Mather, T. A., J. R. McCabe, V. K. Rai, M. H. Thiemens, D. M. Pyle, T. H. E. Heaton, H. J. Sloane, and G. R. Fern (2006), Oxygen and sulfur isotopic composition of volcanic sulfate aerosol at the point of emission, *J. Geophys. Res.-Atmos.*, *111*(D18), doi:10.1029/2005JD006584.
- Matsuhisa, Y., J. R. Goldsmith, and R. N. Clayton (1978), Mechanisms of Hydrothermal Crystallization of Quartz at 250-Degrees-C and 15 Kbar, *Geochim. Cosmochim. Acta*, *42*(2), p.173.
- Mauersberger, K., D. Krankowsky, and C. Janssen (2003), Oxygen isotope processes and transfer reactions, *Space Sci. Rev.*, *106*(1-4), 265-279.
- McArdle, N. C., and P. S. Liss (1995), Isotopes and Atmospheric Sulfur, *Atmos. Environ.*, *29*(18), 2553-2556.
- McArdle, N., P. Liss, and P. Dennis (1998), An isotopic study of atmospheric sulphur at three sites in Wales and at Mace Head, Eire, *J. Geophys. Res.-Atmos.*, *103*(D23), 31079-31094.
- McCabe, J. R., C. S. Boxe, A. J. Colussi, M. R. Hoffmann, and M. H. Thiemens (2005), Oxygen isotopic fractionation in the photochemistry of nitrate in water and ice, *J. Geophys. Res.-Atmos.*, *110*(D15), doi: 10.1029/2004JD005484.
- McCabe, J. R., J. Savarino, B. Alexander, S. L. Gong, and M. H. Thiemens (2006), Isotopic constraints on non-photochemical sulfate production in the Arctic winter, *Geophysical Research Letters*, *33*(L05810), doi:10.1029/2005GL025164.
- McCabe, J. R., M. H. Thiemens, and J. Savarino (2007), A record of ozone variability in South Pole Antarctic snow: Role of nitrate oxygen isotopes, *J. Geophys. Res.-Atmos.*, *112*(D12303), doi:10.1029/2006JD007822.

- McConnell, J. R. (2002), Continuous ice-core chemical analyses using inductively Coupled Plasma Mass Spectrometry, *Environ. Sci. Technol.*, *36*(1), 7-11.
- McNamara, J. P., and I. H. Hillier (2001), Mechanism of the hydrolysis of halogen nitrates in small water clusters studied by electronic structure methods, *J. Phys. Chem. A*, *105*(29), 7011-7024.
- Michalski, G., J. Savarino, J. K. Bohlke, and M. Thiemens (2002), Determination of the total oxygen isotopic composition of nitrate and the calibration of a Delta O-17 nitrate reference material, *Anal. Chem.*, *74*(19), 4989-4993.
- Michalski, G., Z. Scott, M. Kabling, and M. H. Thiemens (2003), First measurements and modeling of $\Delta^{17}\text{O}$ in atmospheric nitrate *Geophys. Res. Lett.*, *30*(16), p.1870, doi:10.1029/2003GL017015.
- Mickley, L. J., P. P. Murti, D. J. Jacob, J. A. Logan, D. M. Koch, and D. Rind (1999), Radiative forcing from tropospheric ozone calculated with a unified chemistry-climate model, *J. Geophys. Res.-Atmos.*, *104*(D23), 30153-30172.
- Miller, J. E., J. D. W. Kahl, F. Heller, and J. M. Harris (2002), A three-dimensional residence-time analysis of potential summertime atmospheric transport to Summit, Greenland, *Ann. Glaciol.*, *35*, 403-408.
- Minikin, A., M. Legrand, J. Hall, D. Wagenbach, C. Kleefeld, E. Wolff, E. C. Pasteur, and F. Ducroz (1998), Sulfur-containing species (sulfate and methanesulfonate) in coastal Antarctic aerosol and precipitation, *J. Geophys. Res.-Atmos.*, *103*(D9), 10975-10990.
- Mischler, J. A., T. A. Sowers, R. B. Alley, M. Battle, J. R. McConnell, L. Mitchell, T. Popp, E. Sofen, and M. K. Spencer 26 (*in press.*), Carbon and hydrogen isotopic composition of methane over the last 1000 years, *Global Biogeochem. Cycles*, doi:10.1029/2009GB003460.
- Monaghan, A. J., D. H. Bromwich, R. L. Fogt, S. H. Wang, P. A. Mayewski, D. A. Dixon, A. Ekaykin, M. Frezzotti, I. Goodwin, E. Isaksson, S. D. Kaspari, V. I. Morgan, H. Oerter, T. D. Van Ommen, C. J. Van der Veen, and J. H. Wen (2006), Insignificant change in Antarctic snowfall since the International Geophysical Year, *Science*, *313*(5788), 827-831.
- Morin, S., J. Savarino, S. Bekki, S. Gong, and J. W. Bottenheim (2007), Signature of Arctic surface ozone depletion events in the isotope anomaly (Delta O-17) of atmospheric nitrate, *Atmos. Chem. Phys.*, *7*, 1451-1469.
- Morton, J., J. Barnes, B. Schueler, and K. Mauersberger (1990), Laboratory studies of heavy ozone, *J. Geophys. Res.-Atmos.*, *95*(D1), 901 – 907.

- Munger, J. W., D. J. Jacob, S. M. Fan, A. S. Colman, and J. E. Dibb (1999), Concentrations and snow-atmosphere fluxes of reactive nitrogen at Summit, Greenland, *J. Geophys. Res.-Atmos.*, *104*(D11), 13721-13734.
- Nielsen, H. (1974), Isotopic Composition of Major Contributors to Atmospheric Sulfur, *Tellus*, *26*(1-2), 213-221.
- Nielsen, H., J. Pilot, L. N. Grinenko, V. A. Grinenko, A. Y. Lein, J. W. Smith, and R. G., Pankina (1991), Lithospheric sources of sulphur, in *Stable Isotopes: Natural and Anthropogenic Sulphur in the Environment*, edited by H. R. Krouse and V. A. Grinenko, 65-132, John Wiley, New York.
- Patris, N., R. J. Delmas, and J. Jouzel (2000a), Isotopic signatures of sulfur in shallow Antarctic ice cores, *J. Geophys. Res.-Atmos.*, *105*(D6), 7071-7078.
- Patris, N., N. Mihalopoulos, E. D. Baboukas, and J. Jouzel (2000b), Isotopic composition of sulfur in size-resolved marine aerosols above the Atlantic Ocean, *J. Geophys. Res.-Atmos.*, *105*(D11), 14449-14457.
- Patris N., R. J. Delmas, M. Legrand, M. De Angelis, F. A. Ferron, M. Stiévenard, and J. Jouzel (2002), First sulfur isotope measurements in central Greenland ice cores along the preindustrial and industrial periods, *J. Geophys. Res.-Atmos.*, *107*(D11), doi:10.1029/2001JD000672.
- Patris, N., S. S. Cliff, P. K. Quinn, M. Kasem, and M. H. Thiemens (2007), Isotopic analysis of aerosol sulfate and nitrate during ITCT-2k2: Determination of different formation pathways as a function of particle size, *J. Geophys. Res.-Atmos.*, *112*(D23301), doi:10.1029/2005JD006214.
- Peterson, M. C., and R. E. Honrath (2001), Observations of rapid photochemical destruction of ozone in snowpack interstitial air, *Geophysical Research Letters*, *28*(3), 511-514.
- Prinn, R. G. (2003), The cleansing capacity of the atmosphere, *Annu. Rev. Environ. Resour.*, *28*, 29-57.
- Pruett, L. E., K. J. Kreutz, M. Wadleigh, P. A. Mayewski, and A. Kurbatov (2004), Sulfur isotopic measurements from a West Antarctic ice core: implications for sulfate source and transport, *Annals of Glaciology*, *39*, 161-168, doi:10.3189/172756404781814339.
- Radke, L. F. (1982), Sulfur and Sulfate from Mt Erebus, *Nature*, *299*(5885), 710-712.
- Rankin, A. M., E. W. Wolff, and S. Martin (2002), Frost flowers: Implications for tropospheric chemistry and ice core interpretation, *J. Geophys. Res.-Atmos.*, *107*(D23), 4683, doi:10.1029/2002JD002492.

- Rees, C. E., W. J. Jenkins, and J. Monster (1978), Sulfur Isotopic Composition of Ocean Water Sulfate, *Geochim. Cosmochim. Acta*, 42(4), 377-381.
- Revesz, K., and J. K. Bohlke (2002), Comparison of delta O-18 measurements in nitrate by different combustion techniques, *Anal. Chem.*, 74(20), 5410-5413.
- Ridley, B. A., and J. J. Orlando (2003), Active nitrogen in surface ozone depletion events at alert during spring 1998, *J. Atmos. Chem.*, 44(1), 1-22.
- Romero A. B., M. H. Thiemens (2003), Mass-independent sulfur isotopic compositions in present-day sulfate aerosols, *J. Geophys. Res.-Atmos.*, 108(D16), doi:10.1029/2003JD003660, 2003.
- Rose, W. I., R. L. Chuan, and P. R. Kyle (1985), Rate of sulphur dioxide emission from Erebus volcano, Antarctica, December 1983, *Nature*, 316(6030), 710-712.
- Saltzman, E. S., G. W. Brass, and D. A. Price (1983), The Mechanism of Sulfate Aerosol Formation - Chemical and Sulfur Isotopic Evidence, *Geophys. Res. Lett.*, 10(7), 513-516.
- Sander, R., Y. Rudich, R. von Glasow, and P. J. Crutzen (1999), The role of BrNO₃ in marine tropospheric chemistry: A model study, *Geophys. Res. Lett.*, 26(18), 2857-2860.
- Sander, S. P., R. R. Friedl, A. R. Ravishankara, D. M. Golden, C. E. Kolb, M. J. Kurylo, M. J. Molina, G. K. Moortgat, H. Keller-Rudek, B. J. Finlayson-Pitts, P. H. Wine, R. E. Huie, and V. L. Orkin (2006), Chemical Kinetics and Photochemical Data for Use in Atmospheric Studies, NASA Jet Propulsion Lab, report number 06-2, Pasadena, California.
- Savarino, J., and M. H. Thiemens (1999), Mass-independent oxygen isotope (O-16, O-17, O-18) fractionation found in H-x, O-x reactions, *J. Phys. Chem. A*, 103(46), 9221-9229.
- Savarino, J., C. C. W. Lee, and M. H. Thiemens (2000), Laboratory oxygen isotopic study of sulfur (IV) oxidation: Origin of the mass-independent oxygen isotopic anomaly in atmospheric sulfates and sulfate mineral deposits on Earth, *J. Geophys. Res.-Atmos.*, 105(D23), 29079-29088.
- Savarino, J., B. Alexander, V. Darmohusodo, and M. H. Thiemens (2001), Sulfur and oxygen isotope analysis of sulfate at micromole levels using a pyrolysis technique in a continuous flow system, *Anal. Chem.*, 73(18), 4457-4462.
- Savarino, J., S. Bekki, J. H. Cole-Dai, and M. H. Thiemens (2003a), Evidence from sulfate mass independent oxygen isotopic compositions of dramatic changes in

- atmospheric oxidation following massive volcanic eruptions, *J. Geophys. Res.-Atmos.*, *108*(D21), 4671, doi:10.1029/2003JD003737.
- Savarino, J., A. Romero, J. Cole-Dai, S. Bekki, and M. H. Thiemens (2003b), UV induced mass-independent sulfur isotope fractionation in stratospheric volcanic sulfate, *Geophys. Res. Lett.*, *30*(21), Article Number 2131.
- Savarino, J., J. Kaiser, S. Morin, D. M. Sigman, and M. H. Thiemens (2007), Nitrogen and oxygen isotopic constraints on the origin of atmospheric nitrate in coastal Antarctica, *Atmos. Chem. Phys.*, *7*(8), 1925-1945.
- Savarino, J., S. K. Bhattacharya, S. Morin, M. Baroni, and J. F. Doussin (2008), The NO + O₃ reaction: A triple oxygen isotope perspective on the reaction dynamics and atmospheric implications for the transfer of the ozone isotope anomaly, *J. Chem. Phys.*, *128*(19), doi: 10.1063/1.2917581.
- Schneider, D. P., and E. J. Steig (2008), Ice cores record significant 1940s Antarctic warmth related to tropical climate variability, *Proceedings of the National Academy of Sciences of the United States of America*, *105*(34), 12154-12158.
- Schneider, D. P., E. J. Steig, T. D. van Ommen, D. A. Dixon, P. A. Mayewski, J. M. Jones, and C. M. Bitz (2006), Antarctic temperatures over the past two centuries from ice cores, *Geophys. Res. Lett.*, *33*(16), doi:10.1029/2006GL027057.
- Schueler, B., J. Morton, and K. Mauersberger (1990), Measurement of Isotopic Abundances in Collected Stratospheric Ozone Samples, *Geophys. Res. Lett.*, *17*(9), 1295-1298.
- Schwartz, S. E. (1987), Aqueous-Phase Reactions in Clouds, in *The Chemistry of Acid Rain: Sources and Atmospheric Processes*, edited by G. E. G. Russell W. Johnson, American Chemical Society, Washington, D.C., 1987.
- Shindell, D. T., G. Faluvegi, and N. Bell (2003), Preindustrial-to-present-day radiative forcing by tropospheric ozone from improved simulations with the GISS chemistry-climate GCM, *Atmos. Chem. Phys.*, *3*, 1675-1702.
- Sigg, A., and A. Neftel (1991), Evidence for a 50-Percent Increase in H₂O₂ over the Past 200 Years from a Greenland Ice Core, *Nature*, *351*, 557-559.
- Simmonds, I., K. Keay, and E. P. Lim (2003), Synoptic activity in the seas around Antarctica, *Monthly Weather Review*, *131*(2), 272-288.
- Sjostedt, S. J., L. G. Huey, D. J. Tanner, J. Peischl, G. Chen, J. E. Dibb, B. Lefer, M. A. Hutterli, A. J. Beyersdorf, N. J. Blake, D. R. Blake, D. Sueper, T. Ryerson, J. Burkhardt, and A. Stohl (2007), Observations of hydroxyl and the sum of peroxy

- radicals at Summit, Greenland during summer 2003, *Atmos. Environ.*, *41*(24), 5122-5137.
- Spivakovsky, C. M., J. A. Logan, S. A. Montzka, Y. J. Balkanski, M. Foreman-Fowler, D. B. A. Jones, L. W. Horowitz, A. C. Fusco, C. A. M. Brenninkmeijer, M. J. Prather, S. C. Wofsy, and M. B. McElroy (2000), Three-dimensional climatological distribution of tropospheric OH: Update and evaluation, *J. Geophys. Res.-Atmos.*, *105*(D7), 8931-8980.
- Staffelbach, T., A. Neftel, B. Stauffer, and D. Jacob (1991), A Record of the Atmospheric Methane Sink from Formaldehyde in Polar Ice Cores, *Nature*, *349*, 603-605.
- Steig, E. J., D. P. Schneider, S. D. Rutherford, M. E. Mann, J. C. Comiso, and D. T. Shindell (2009), Warming of the Antarctic ice-sheet surface since the 1957 International Geophysical Year, *Nature*, *457*(7228), 459-462.
- Stohl, A., P. Bonasoni, P. Cristofanelli, W. Collins, J. Feichter, A. Frank, C. Forster, E. Gerasopoulos, H. Gaggeler, P. James, T. Kentarchos, H. Kromp-Kolb, B. Kruger, C. Land, J. Meloen, A. Papayannis, A. Priller, P. Seibert, M. Sprenger, G. J. Roelofs, H. E. Scheel, C. Schnabel, P. Siegmund, L. Tobler, T. Trickl, H. Wernli, V. Wirth, P. Zanis, and C. Zerefos (2003), Stratosphere-troposphere exchange: A review, and what we have learned from STACCATO, *J. Geophys. Res.-Atmos.*, *108*(D12), doi:10.1029/2002JD002490.
- Stroud, C., S. Madronich, E. Atlas, B. Ridley, F. Flocke, A. Weinheimer, B. Talbot, A. Fried, B. Wert, R. Shetter, B. Lefer, M. Coffey, B. Heikes, and D. Blake (2003), Photochemistry in the arctic free troposphere: NO_x budget and the role of odd nitrogen reservoir recycling, *Atmos. Environ.*, *37*(24), 3351-3364.
- Tanaka, N., D. M. Rye, Y. Xiao, and A. C. Lasaga (1994), Use of Stable Sulfur Isotope Systematics for Evaluating Oxidation Reaction Pathways and in-Cloud Scavenging of Sulfur-Dioxide in the Atmosphere, *Geophys. Res. Lett.*, *21*(14), 1519-1522.
- Thiemens, M. H. (1999), Atmosphere science - Mass-independent isotope effects in planetary atmospheres and the early solar system, *Science*, *283*(5400), 341-345
- Thiemens, M. H. (2006), History and applications of mass-independent isotope effects, *Annual Review of Earth and Planetary Sciences*, *34*, 217-262.
- Thiemens, M. H., and J. E. Heidenreich (1983), The Mass-Independent Fractionation of Oxygen - a Novel Isotope Effect and Its Possible Cosmochemical Implications, *Science*, *219*, 1073-1075.
- Thiemens, M. H., and T. Jackson (1990), Pressure dependency for heavy isotope enhancement in ozone formation, *Geophys. Res. Lett.*, *17*(6), 717 – 719.

- Thompson, A. M., J. A. Chappellaz, I. Y. Fung, and T. L. Kucsera (1993), The Atmospheric CH₄ Increase since the Last Glacial Maximum .2. Interactions with Oxidants, *Tellus Ser. B-Chem. Phys. Meteorol.*, 45(3), 242-257.
- Valdes, P. J., D. J. Beerling, and C. E. Johnson (2005), The ice age methane budget, *Geophys. Res. Lett.*, 32(2), 2.
- van den Ende, D., and S. Stolte (1984), The Influence of the Orientation of the NO Molecule Upon the Chemi-Luminescent Reaction $\text{NO} + \text{O}_3 \rightarrow \text{NO}_2^* + \text{O}_2$, *Chem. Phys.*, 89, 121-139.
- Volz, A., and D. Kley (1988), Evaluation of the Montsouris Series of Ozone Measurements Made in the 19th-Century, *Nature*, 332, 240-242.
- Wagenbach, D., F. Ducroz, R. Mulvaney, L. Keck, A. Minikin, M. Legrand, J. S. Hall, and E. W. Wolff (1998), Sea-salt aerosol in coastal Antarctic regions, *J. Geophys. Res.-Atmos.*, 103(D9), 10961-10974.
- Wagner, T., and U. Platt (1998), Satellite mapping of enhanced BrO concentrations in the troposphere, *Nature*, 395, 486-490.
- Wang, Y. H., and D. J. Jacob (1998), Anthropogenic forcing on tropospheric ozone and OH since preindustrial times, *J. Geophys. Res.-Atmos.*, 103(D23), 31123-31135.
- Werner, M., U. Mikolajewicz, M. Heimann, and G. Hoffmann (2000), Borehole versus isotope temperatures on Greenland: Seasonality does matter, *Geophys. Res. Lett.*, 27(5), 723-726.
- Whitlow, S., P. A. Mayewski, and J. E. Dibb (1992), A Comparison of Major Chemical-Species Seasonal Concentration and Accumulation at the South-Pole and Summit, Greenland, *Atmos. Environ. Part A*, 26(11), 2045-2054.
- Wolff, E. W., A. M. Rankin, and R. Rothlisberger (2003), An ice core indicator of Antarctic sea ice production?, *Geophys. Res. Lett.*, 30(22), doi:10.1029/2003GL018454.
- Yang, J., R. E. Honrath, M. C. Peterson, J. E. Dibb, A. L. Sumner, P. B. Shepson, M. Frey, H. W. Jacobi, A. Swanson, and N. Blake (2002), Impacts of snowpack emissions on deduced levels of OH and peroxy radicals at Summit, Greenland, *Atmos. Environ.*, 36(15-16), 2523-2534.
- Yang, Q. Z., P. A. Mayewski, S. Whitlow, M. Twickler, M. Morrison, R. Talbot, J. Dibb, and E. Linder (1995), Global Perspective of Nitrate Flux in Ice Cores, *J. Geophys. Res.-Atmos.*, 100(D3), 5113-5121.

- Zahn, A., P. Franz, C. Bechtel, J. U. Grooss, and T. Rockmann (2006), Modelling the budget of middle atmospheric water vapour isotopes, *Atmos. Chem. Phys.*, 6, 2073-2090.
- Zhou, X. L., H. J. Beine, R. E. Honrath, J. D. Fuentes, W. Simpson, P. B. Shepson, and J. W. Bottenheim (2001), Snowpack photochemical production of HONO: a major source of OH in the Arctic boundary layer in springtime, *Geophys. Res. Lett.*, 28(21), 4087-4090.
- Zielinski, G. A. (1995), Stratospheric Loading and Optical Depth Estimates of Explosive Volcanism over the Last 2100 Years Derived from the Greenland-Ice-Sheet-Project-2 Ice Core, *J. Geophys. Res.-Atmos.*, 100(D10), 20937-20955.
- ZredaGostynska, G., P. R. Kyle, D. Finnegan, and K. M. Prestbo (1997), Volcanic gas emissions from Mount Erebus and their impact on the Antarctic environment, *J. Geophys. Res.-Solid Earth*, 102(B7), 15039-15055.

VITA

Shelley Anne Kunasek

Personal**Birth:** 20 January 1980**Citizenship:** United States of America and Canada**Education****B.A. Chemistry (2001)**
Pomona College, Claremont, California**Ph.D. Earth and Space Sciences (2009)**
University of Washington, Seattle, Washington**Publications**

- Alexander, B., M. G. Hastings, D. J. Allman, J. Dachs, J. A. Thornton, and **S. A. Kunasek** (2009), Quantifying atmospheric nitrate formation pathways based on a global model of the oxygen isotopic composition ($\Delta^{17}\text{O}$) of atmospheric nitrate, *Atmos. Chem. Phys.*, 9(14), 5043-5056.
- Jarvis J. C., M. G. Hastings, E. J. Steig, **S. A. Kunasek** (2009), Isotopic ratios in gas-phase HNO_3 and snow nitrate at Summit, Greenland, *J. Geophys. Res.-Atmos.*, 114(D17301), doi:10.1029/2009JD012134.
- Kunasek, S. A.**, B. Alexander, E. J. Steig, M. G. Hastings, D. J. Gleason, and J. C. Jarvis (2008), Measurements and modeling of $\Delta^{17}\text{O}$ of nitrate in snowpits from Summit, Greenland, *J. Geophys. Res.-Atmos.*, 113(D24302), doi:10.1029/2008JD010103.
- Jarvis J. C., E. J. Steig, M. G. Hastings, **S. A. Kunasek** (2008), Influence of local photochemistry on isotopes of nitrate in Greenland snow, *Geophys. Res. Lett.*, 35(L21804), doi:10.1029/2008GL035551.